

Universidade do Minho  
Escola de Engenharia

Ana Mafalda Meneses Costa | Development of bioactive materials for dental implants using powder metallurgy

Ana Mafalda Meneses Costa

Development of bioactive materials for  
dental implants using powder metallurgy

UMinho | 2016

setembro de 2016





Universidade do Minho  
Escola de Engenharia

Ana Mafalda Meneses Costa

Development of bioactive materials for  
dental implants using powder metallurgy

Dissertação de Mestrado  
Ciclo de Estudos Integrados Conducentes ao  
Grau de Mestre em Engenharia Biomédica

Trabalho efetuado sob a orientação de  
Professora Doutora Maria Georgina Macedo Miranda  
Professor Doutor Filipe Samuel Correia Pereira da Silva

## DECLARAÇÃO

Nome: Ana Mafalda Meneses Costa

Endereço eletrónico: mafcosta@live.com.pt      Telefone: 967594337

Bilhete de Identidade/Cartão do Cidadão: 14292970

Título da dissertação: Development of bioactive materials for dental implants using powder metallurgy

Orientadores:

Professora Doutora Maria Georgina Macedo Miranda

Professor Doutor Filipe Samuel Correia Pereira da Silva

Ano de conclusão: 2016

Mestrado em Engenharia de Biomédica

DE ACORDO COM A LEGISLAÇÃO EM VIGOR, NÃO É PERMITIDA A REPRODUÇÃO DE QUALQUER PARTE DESTA TESE/TRABALHO.

Universidade do Minho, \_\_\_\_/\_\_\_\_/\_\_\_\_\_

Assinatura:



*"It always seems impossible until its done"*

Nelson Mandela



## ACKNOWLEDGMENTS

Firstly, I would like to acknowledge to my supervisor Doctor Georgina Miranda for all the support, words of encouragement, dedication and help. Thank you for being so tireless with me, for sharing your knowledge and for being always available to answer my questions

To my co-supervisor Professor Filipe Samuel Silva, whose expertise, knowledge and support was an asset in achieving this dissertation. Thank you for your devotion and for providing me the opportunity to do this work.

To Doctor Oscar Carvalho for all the patience and availability. I would like to thank you for sharing your knowledge and experience as well as for all the help provided on the experimental tests throughout this project.

To Paulo Silva for all the technical assistance and help and to all the technicians who have helped with the development and characterization of samples.

To MSc student Telma Dantas and the researchers Cristiano Abreu, Mihaela Buciumeanu and Gabriela Peñarrieta for the opportunity given to cooperate in their investigations, for all the help and the sharing of knowledge made throughout this project.

To all members of the laboratory who contributed, in one way or another, to the development of this work. I am thankful for all the assistance provided, the encouragement and friendship.

To all of my friends for always being present and for all the words of encouragement given along this journey. A special thanks to Francisco for all the patience, support, for his unconditional trust in me and for encouraging me in the worst moments.

I would like to express my deeply gratitude to my parents for their unconditional love and support. I am grateful to you for always providing me the best education and for your persistence in always keeping me positive and motivated during this project.

Finally, I would also like to acknowledge my sister for always giving me the bests advices, for being present at all times and for always motivating me to pursue my goals.

This work was supported by FTC through the project PTDC/EMS-TEC/5422/2014 and also by project NORTE 01-0145\_FEDER-000018. Additionally, this work was supported by FCT with the reference project UID/EEA/04436/2013, by FEDER funds through the COMPETE 2020 – Programa Operacional Competitividade e Internacionalização (POCI) with the reference project POCI-01-0145-FEDER-006941.

Cofinanciado por:



## ABSTRACT

The long-term success of a dental implant is dictated by a crucial group of conditions. Beyond being able to withstand masticatory loads, the implant must also be able to promote a good integration of its surface with the surrounding bone (osseointegration). In this context, various studies have been made with the aim of improving the osseointegration process in these implants.

Usually, dental implants are made from titanium, normally titanium alloy Ti6Al4V, due to its good mechanical properties. Currently, several studies have also introduced zirconia ( $ZrO_2$ ) and polyether-ether-ketone (PEEK) due to their inherent mechanical properties. However, due to the inert nature of these materials, coating their surface with bioactive materials is an effective solution to improve the osseointegration process. Among the bioactive materials, the most commonly used in these applications are Hydroxyapatite (HAp) and tricalcium phosphate (generally  $\beta$ -TCP) since they are very similar to the inorganic phase of bone. However, during the implantation process, the detachment of the coating may occur.

In the present work, in order to overcome this problem, various bioactive composites were produced by hot pressing (hot pressing) or by cold pressing followed by sintering (Press and sintering) where the matrix is constituted by the material owing suitable mechanical properties and the reinforcement is a bioactive material. In this sense, the composites produced were: Ti6Al4V reinforced with 10 vol% HAp (Ti6Al4V-10%HAp), Ti6Al4V-10% $\beta$ TCP,  $ZrO_2$ -10%HAp,  $ZrO_2$ -10% $\beta$ TCP, PEEK-10%HAp, PEEK- $\beta$ TCP10% (vol.%) which were subsequently characterized through a microstructural and mechanical analysis (hardness and shear tests).

This work allowed to conclude that all samples have reached an effective densification and that the addition of bioactive materials increased the hardness of the samples, when compared to the unreinforced metal, polymer or ceramic matrix. When comparing both processing methods, hot pressing was found more capable to promote full densification and consequently higher mechanical properties. Although, in all samples, the presence of bioactive materials caused a shear strength decrease, the benefits of having a bioactive material and also an implant design solution based in functionally graded materials (FGM) would largely compensate these results.

**Keywords:** dental implants, osseointegration, hot pressing, press and sintering, bioactive composites.



## RESUMO

O sucesso a longo prazo de um implante dentário é ditado por um grupo de condições cruciais. Além de ser capaz de suportar cargas mastigatórias, o implante deve ser capaz de promover uma boa integração da sua superfície com o osso adjacente (osseointegração). Desta forma, vários estudos têm vindo a ser feitos com o intuito de melhorar o processo de osseointegração.

Habitualmente, os implantes dentários são feitos em titânio, geralmente liga Ti6Al4V, devido às suas boas propriedades mecânicas. Atualmente, vários estudos têm introduzido a zirconia ( $ZrO_2$ ) e o poli-éter-éter-cetona (PEEK) devido às suas propriedades mecânicas inerentes. No entanto, devido à natureza inerte destes materiais, o revestimento superficial com materiais bioativos é uma solução efetiva para melhorar o processo de osseointegração. De entre os materiais bioativos, os mais utilizados nestas aplicações são a hidroxiapatite (HAp) e os fosfatos de tricalcio (geralmente,  $\beta$ -TCP) uma vez que são materiais muito semelhantes à fase inorgânica do osso. No entanto, durante o processo de implantação, o destacamento do revestimento pode ocorrer.

No presente trabalho, de forma a superar este problema, produziram-se vários compósitos bioativos por prensagem a quente (*Hot pressing*) ou por prensagem a frio seguido de sinterização (*Press and sintering*) onde a matriz é constituída pelo material que apresenta propriedades mecânicas adequadas e o reforço é um material bioativo. Desta forma, os compósitos produzidos foram: Ti6Al4V reforçado com 10 vol.% HAp (Ti6Al4V-10%HAp), Ti6Al4V-10% $\beta$ TCP,  $ZrO_2$ -10%HAp,  $ZrO_2$ -10% $\beta$ TCP, PEEK-10%HAp, PEEK-10% $\beta$ TCP (vol.%) que foram posteriormente caracterizados através de uma análise microestrutural e mecânica (ensaios de dureza e testes de corte).

Este trabalho permitiu concluir que todas as amostras atingiram uma densificação eficaz e que a adição de materiais bioativos aumenta a dureza das amostras, quando comparadas com a matriz metálica, polimérica ou cerâmica não reforçada. Comparando ambos métodos de processamento, o *hot pressing* mostrou-se mais apto a promover uma densificação total e consequentemente, melhores propriedades mecânicas. Apesar de, em todas as amostras, a presença dos materiais bioativos ter causado a diminuição da resistência ao corte, os benefícios da presença do material bioativo e também a solução de um design do implante baseado em materiais com gradientes funcionais (FGM), compensa largamente estes resultados.

**Palavras-chave:** implantes dentários, osseointegração, prensagem a quente, prensagem a frio e sinterização, compósitos bioativos.





## TABLE OF CONTENTS

Acknowledgments.....	v
Abstract .....	vii
Resumo .....	ix
Table of Contents.....	xi
List of Abbreviations.....	xiii
List of Figures.....	xv
List of Tables.....	xix
Chapter 1 Introduction.....	1
1.1. Motivation .....	2
1.2. Objectives .....	4
Chapter 2 State of The Art.....	5
2.1. Dental Implants.....	6
2.2. Biocompatible Materials .....	11
2.2.1. Metallic Materials .....	12
2.2.2. Ceramic Materials.....	15
2.2.3. Polymeric Materials.....	17
2.3. Bioactive Materials .....	18
2.4. Biocompatible composites .....	23
2.5. Powder Metallurgy .....	24
2.5.1. Press and Sintering.....	28
2.5.2. Hot pressing.....	30
2.6. Final remarks regarding the design of a dental implant.....	31
Chapter 3 Materials and Methods.....	35
3.1. Raw Materials and composites design .....	36
3.2. Methods.....	38
3.2.1. Dispersion Methods.....	38
3.2.2. Hot Pressing.....	40
3.2.3. Press and Sintering.....	44
3.2.4. Materials Characterization .....	45
3.2.4.1. Specimens preparation.....	45
3.2.4.2. SEM/EDS.....	46

3.2.4.3.	Vickers hardness test .....	47
3.2.4.4.	Shear tests.....	48
Chapter 4 Results and Discussion.....		51
4.1.	Dispersion Methods Analysis .....	52
4.1.1.	Ti6Al4V-10HAp powders mixture.....	52
4.1.2.	Ti6Al4V-10 $\beta$ TCP powders mixture.....	56
4.2.	Assessment of the bioactive materials condition after hot pressing.....	59
4.3.	Ti6Al4V and Ti6Al4V-based composites characterization .....	60
4.4.	ZrO <sub>2</sub> and ZrO <sub>2</sub> -based composites characterization.....	65
4.5.	PEEK and PEEK-based composites characterization .....	72
4.6.	Ongoing Research .....	77
Chapter 5 Conclusions .....		83
6.	References.....	87

## LIST OF ABBREVIATIONS

- BOF – Ball-on-flat  
BSE – Backscattered electron image  
cpTi – commercially pure titanium  
EDS – Energy-dispersive x-ray spectroscopy analysis  
FDA – Food and Drug Administration  
FGM – Functionally graded materials  
HAp – Hydroxyapatite  
HP – Hot pressing  
ISO – International Organization of Standards  
LTD – Low Temperature Degradation  
PAEK – Poly-aryl-ether-ketone  
PBS – Phosphate saline  
PEEK - Polyether-ether-ketone  
PFM – Porcelain fused to metal  
PM – Powder Metallurgy  
PS – Press and Sintering  
SE – Secondary electron image  
SEM – Scanning electron microscopy  
SS – Stainless Steel  
TCP - Tricalcium phosphate  
XRD – X-ray diffraction  
YM – Young's Modulus  
Y-TZP – Yttria-stabilized tetragonal zirconia



## LIST OF FIGURES

Figure 1- Bone resorption and teeth drifting. ....	6
Figure 2-(a) dental implant [18] (b) Radiograph of a dental implant relative to the adjacent teeth [19]. ....	7
Figure 3 – Diagram of implant components. A- implant, B-abutment, C-Prosthesis [21]. ....	8
Figure 4 – (a) primary and secondary stability [15] and (b) general schematic of bone structure [28].....	9
Figure 5 – Schematic of the possible interactions with (a) hydrophilic and (b) hydrophobic surfaces [35]......	11
Figure 6-Density of selected metals [52]. ....	12
Figure 7 – Distribution of stresses within (a) the bone (b) main model [57] .....	14
Figure 8 – Gingival recession [19]. ....	14
Figure 9 – Schematic of transformation toughening mechanism in partially stabilized zirconia [71]......	16
Figure 10 – Scheme of the ageing process (a) transformation on a particular grain followed by microcracking and stress transmission to neighboring grains (b) growth of the transformation grains (grey) and water penetration (red) derived by microcracking [73]. ....	17
Figure 11 – Composition of bone [91]. ....	19
Figure 12 – Crystalline structure of hydroxyapatite [91]. ....	22
Figure 13 – X-ray diffraction patterns of HAp sintered for 2h at (a)1250°C, (b) 1400°C and (c) 1450°C [107]. .....	23
Figure 14 - Some of the many powder metallurgy applications (a) pulley-timing automotive component, (b) porous devices for gas distribution, filtration, and flow control applications (c) orthodontic system bracket, slide, and hook, (d) watch fabricated with PM parts [125]. ....	25
Figure 15 – Energy use in MJ/kg of product and material waste as a percent of the starting material for powder technologies and alternative technologies [128]. ....	26
Figure 16 – Tolerance and surface finish capabilities for various technologies, comparing PM with some of the alternative routes [128]. ....	26
Figure 17 – Strength ranges possible via various forming technologies, including several of the common PM approaches[128]. ....	27
Figure 18 – A schematic of increasing homogeneity [125]. ....	27
Figure 19 – A plot of fractional packing density versus composition for bimodal mixtures of large and small spherical particles [125]. ....	28
Figure 20 - A conventional punch and die set for powder compaction [125]. ....	29
Figure 21 – A view of the stages of powder compaction. At low pressures the particles rearrange to eliminate large pores. Depending on the particle hardness, eventually the particles deform at high pressures and particle deformation dominates densification [125]. ....	29
Figure 22 - A cross-sectional view of uniaxial hot pressing [125]. ....	30
Figure 23 – Schematic representation of a hot pressing cycle. ....	31
Figure 24 – Mean $\pm$ standard deviation (SD) of shear bond strength results for conventional porcelain fused to metal specimens (PFM) and for functionally graded specimens (FGMR), after thermal and mechanical cycling [132]. ....	33
Figure 25 – Mechanical properties measured at the metal-ceramic interface for a sharp (PFM) and a graded transition (FGMR): Young's Modulus and Hardness [132]. ....	33
Figure 26-SEM images of (a) Ti6Al4V, (b) ZrO <sub>2</sub> , (c) PEEK, (d) HAp and (e) $\beta$ TCP powders. ....	37

Figure 27-Particle size distribution of (a) Ti6Al4V, (b) HAp, (c) $\beta$ TCP, (d) $ZrO_2$ and (e) PEEK powders (according to the manufacturer). .....	38
Figure 28- Schematic illustration of the dispersion methods used, where powder A corresponds to the bioactive material (HAp or $\beta$ TCP) and powder B to the biocompatible material (Ti6Al4V). .....	39
Figure 29- Molds and punches used to process the materials (a) Ti6Al4V graphite mold and punches (b) PEEK steel mold and punches.....	41
Figure 30 - System used to process $ZrO_2$ and $ZrO_2$ -based composite materials.....	41
Figure 31-Hot Pressing picture and schematic representation. ....	42
Figure 32 – Hot Pressing overall system (1) vacuum machine, (2) hydraulic machine, (3) induction coil.....	43
Figure 33 – Steel mold and punches used to process the materials.....	44
Figure 34-(a) hydraulic press (Bb) Zirkonofen 700 ultra-vacuum sintering furnace.....	45
Figure 35 – MECAPOL P 251 polisher .....	46
Figure 36 – SEM/EDS equipment.....	47
Figure 37 – Vickers micro-hardness tester DuraScan, emcotest.....	48
Figure 38 – Servohydraulic machine Instron 8874. ....	49
Figure 39- System apparatus to measure shear stress.....	50
Figure 40 – SEM image of $\beta$ TCP powder.....	52
Figure 41 – SEM images of Ti6Al4V-10HAp powders mixture after blending (method A) at magnifications of 1000x (left) and 4000x (right). (a) secondary electron image (SE) and (b) backscattered electron image (BSE).54	
Figure 42 - SEM images of Ti6Al4V-10HAp powders mixture after ball-milling (method B) at magnifications of 1000x (left) and 4000x (right). (a) secondary electron image (SE) and (b) backscattered electron image (BSE).54	
Figure 43 - SEM images of Ti6Al4V-10HAp powders mixture after ultrasonification (method C) at magnifications of 1000x (left) and 4000x (right). (a) secondary electron image (SE) and (b) backscattered electron image (BSE). .....	55
Figure 44- SEM images of Ti6Al4V-10HAp powders mixture after ultrasonification followed by ball-milling (method D) at magnifications of 1000x (left) and 4000x (right). (a) secondary electron image (SE) and (b) backscattered electron image (BSE).....	55
Figure 45 – SEM images of Ti6Al4V-10 $\beta$ TCP powders mixture after blending at magnifications of 1000x (left) and 4000x (right). (a) secondary electron image (SE) and (b) backscattered electron image (BSE). .....	57
Figure 46 - SEM images of Ti6Al4V-10 $\beta$ TCP powders mixture after ball-milling at magnifications of 1000x (left) and 4000x (right). (a) secondary electron image (SE) and (b) backscattered electron image (BSE). .....	57
Figure 47 - SEM images of Ti6Al4V-10 $\beta$ TCP powders mixture after ultrasonification at magnifications of 1000x (left) and 4000x (right). (a) secondary electron image (SE) and (b) backscattered electron image (BSE). .....	58
Figure 48 - SEM images of Ti6Al4V-10 $\beta$ TCP powders mixture after ultrasonification follow by ball-milling at magnifications of 1000x (left) and 4000x (right). (a) secondary electron image (SE) and (b) backscattered electron image (BSE).....	58
Figure 49 – XRD plot of (a) HAp powder and (b) HAp sample after Hot Pressing at 1175° during 30 minutes..	60
Figure 50 - SEM images of (a) Ti6Al4V, (b) Ti6Al4V-10HAp and (c) Ti6Al4V-10 $\beta$ TCP samples at magnifications of 500x (left) and 1000x (right). .....	61
Figure 51 – SEM images of Ti6Al4V with marked zone for EDS analysis. ....	63
Figure 52 - SEM images of Ti6Al4V-10HAp with marked zone for EDS analysis.....	63
Figure 53 - SEM images of Ti6Al4V-10 $\beta$ TCP with marked zone for EDS analysis. ....	63
Figure 54 – Average hardness (HV) for Ti6Al4V, Ti6Al4V-10HAp and Ti6Al4V-10 $\beta$ TCP composites.....	64

Figure 55 - Average shear strength for Ti6Al4V, Ti6Al4V-10HAp and Ti6Al4V-10βTCP composites..... 64

Figure 56 - SEM images of ZrO<sub>2</sub> samples (a) hot-pressed and (b) press and sintered, at magnifications of 500x (left) and 1000x (right). ..... 65

Figure 57 - Example of porosity measuring of ZrO<sub>2</sub> (a) hot-pressed and (b) press-and-sintered samples. SEM image in backscattered view (left) and the same SEM image with a threshold filter enhancing the porosity (right). Porosity percentage in the tables. .... 66

Figure 58 - SEM images of ZrO<sub>2</sub>-10HAp samples (a)hot-pressed and (b) press-and-sintered, at magnifications of 500x (left) and 1000x (right). ..... 67

Figure 59 - SEM images of ZrO<sub>2</sub>-10βTCP samples (a)hot-pressed and (b) press-and-sintered, at magnifications of 500x (left) and 1000x (right). ..... 68

Figure 60 - SEM images of ZrO<sub>2</sub> with marked zone for EDS analysis in (a) hot pressed and (b) press-and-sintered samples. ....

Figure 61 - SEM images of ZrO<sub>2</sub>-10HAp with marked zone for EDS analysis in (a) hot pressed and (b) press-and-sintered samples.....

Figure 62 - SEM images of ZrO<sub>2</sub>-10βTCP with marked zone for EDS analysis in (a) hot pressed and (b) press-and-sintered samples.....

Figure 63 - Average hardness (HV) for ZrO<sub>2</sub>, ZrO<sub>2</sub>10HAp and ZrO<sub>2</sub>-10βTCP composites processed by press-and-sinter. .... 71

Figure 64 - Average shear strength for hot pressed and press and sintered ZrO<sub>2</sub>, ZrO<sub>2</sub>-10HAp and ZrO<sub>2</sub>-10βTCP composites. .... 72

Figure 65 - SEM images of (a) PEEK, (b) PEEK-10HAp, (c) PEEK-10βTCP samples at magnifications of 500x (left) and 1000x (right). ..... 73

Figure 66 – SEM images of PEEK with marked zone for EDS analysis. .... 74

Figure 67 – SEM images of PEEK-10HAp with marked zones for EDS analysis. .... 74

Figure 68 – SEM images of PEEK-10βTCP with marked zones for EDS analysis. .... 75

Figure 69 – Average hardness (HV) for PEEK, PEEK-10HAp and PEEK-10βTCP composites..... 76

Figure 70 - Average shear strength for PEEK, PEEK-10HAp and PEEK-10βTCP composites..... 76

Figure 71 - Specific wear rate for the tested Ti based materials against Al<sub>2</sub>O<sub>3</sub> in presence of PBS at 37 °C..... 77

Figure 72 – Specific wear rate for tested ZrO<sub>2</sub> based materials processed by press-and-sintering against Al<sub>2</sub>O<sub>3</sub> in presence of PBS at 37°C. .... 79

Figure 73 - Specific wear rate for tested PEEK based materials processed by press-and-sintering against Al<sub>2</sub>O<sub>3</sub> in presence of PBS at 37°C. .... 80

Figure 74 – Cellular viability of osteoblast cells acquired over 14 days. .... 80





## LIST OF TABLES

Table 1 - Mechanical properties of Ti6Al4V [55]. .....	13
Table 2 – Mechanical and physical properties of aluminum oxide and zirconium oxide [21].....	15
Table 3 – Mechanical properties of PEEK [86, 87]. .....	18
Table 4-Biologically relevant calcium phosphates compounds [96].....	20
Table 5 – Comparative composition and crystallographic of Human Enamel, Bone, and HAp ceramic [93] .....	21
Table 6 - Powders dimension and supplier. ....	36
Table 7 - Composition of the produced materials. ....	36
Table 8 – Chemical composition (in at. %) of marked zone of figure 51. ....	63
Table 9 – Chemical composition (in at. %) of marked zones of figure 52. ....	63
Table 10 – Chemical composition (in at. %) of marked zones of figure 53.....	63
Table 11 – Chemical composition (in at. %) of marked zones in hot-pressed (top) and press-and-sintered (bottom) samples of figure 60.....	69
Table 12 - Chemical composition (in at. %) of marked zones in hot-pressed (top) and press-and-sintered (bottom) samples of figure 61.....	70
Table 13 - Chemical composition (in at. %) of marked zones in hot-pressed (top) and press-and-sintered (bottom) samples of figure 62.....	70
Table 14 – Chemical composition (in at. %) of marked zone of figure 66.....	74
Table 15 – Chemical composition (in at. %) of marked zones of figure 67.....	74
Table 16 – Chemical composition (in at. %) of marked zones of figure 68.....	75



# CHAPTER 1

## INTRODUCTION

---

This chapter gives a framework to the topic presenting a motivation subchapter that elucidates the most important aspects that led to the preparation of this thesis contextualizing the aspects that will be further discussed in the following chapters, as well as a list of the objectives involved in this dissertation.

## 1.1. MOTIVATION

In dentistry, the rehabilitation of completely and partially edentulous patients with dental implants is become increasingly important. In fact, dental implants could be an option for people who lost a tooth due to periodontal disease, an injury, or some other reason. Therefore, it is extremely vital to promote long term success of oral implants, which is significantly associated with a rapid and early osseointegration. Once osseointegration is related with the direct contact of bone to implant surface without interposing soft tissue between them, the surface properties play a major role in the adhesion behaviour of the bone cells to the substrate. In fact, chemistry, energy, topography and wettability play an important role in osseointegration process. For instance, a roughened titanium surface has a shorter healing period and vice-versa [1, 2].

Frequently, dental implants are originally made of commercially pure titanium or Ti6Al4V, due to their excellent biocompatibility, favourable mechanical properties, very high corrosion resistance and other well-documented beneficial results. However, zirconia (zirconium dioxide,  $ZrO_2$ ) became a candidate for substituting titanium, not only because of its excellent biomechanical characteristics and biocompatibility but also due to its bright tooth-like colour [3, 4]. Additionally, poly-ether-ether-ketone (PEEK) is also considered a good substitute for dental implants once it presents good mechanical properties, possess the Young's modulus closest to the bone in comparison with the other two abovementioned materials and also owns a good biocompatibility [5]. However, Ti6Al4V,  $ZrO_2$  and PEEK are defined as bioinert materials, meaning that their interaction with the surrounding tissue when implanted in human body is very weak [6–10]. Therefore, to promote osteogenesis, and consequently, osseointegration, the acceleration of this process could be achieved by incorporating bioactive materials which form a strong chemical bond with the adjacent tissue. This bioactivity could be achieved using bioactive materials such as hydroxyapatite and tricalcium phosphate, due to their crystalline structure similar to the mineral phase of bone and their active surface which provide biological bonding to bone [11, 12].

Since adequate surface properties are important to promote osseointegration, much effort has been made to improve the implant bond to the bone tissue through surface modification. Therefore, coating implants surface with the bioactive materials mentioned above is already a used approach to modify the surface in order to increase the adhesion of the cells to the implant. However, creating a film

Development of bioactive materials for dental implants using powder metallurgy

of bioactive material by plasma spray, sol-gel or many other process, have some limitations upon implantation, because when screwing the implant the film can be detached and loss of material can occur, compromising its role [13].

Therefore, functionally graded materials (FGM) is an interesting approach to overcome the coating detachment once these materials have a gradient composition wherein the content of bioactive material is gradually added towards the surface of these materials, improving the adhesive properties between the reinforcement (bioactive material) and the matrix (metallic, ceramic or polymeric material). This approach also improves the mechanical properties of the FGM once the interior owns the mechanical properties of the matrix and the surface the bioactive properties of the reinforcement, with a gradient between.

## 1.2. OBJECTIVES

The main goal of this dissertation focuses on improving osseointegration of dental implants using powder metallurgy techniques such as Hot Pressing and Press and Sintering, to produce composites materials that have both good mechanical and bioactive properties.

In this sense, several composite materials were produced and characterized, such as Ti6Al4V reinforced with 10 vol.% HAp (Ti6Al4V-10%HAp), Ti6Al4V-10% $\beta$ TCP, ZrO<sub>2</sub>-10%HAp, ZrO<sub>2</sub>-10% $\beta$ TCP, PEEK-10%HAp, PEEK-10% $\beta$ TCP (vol.%). Additionally, these were compared with the matrix materials without reinforcement (Ti6Al4V, ZrO<sub>2</sub> and PEEK), produced using the same route. In these composites, the reinforcement particles are embedded in the matrix, which not only prevents the delamination of the bioactive material but also combine the good mechanical properties of the matrix with the bioactivity of the reinforcement.

The detailed objectives of this dissertation are:

- 1) Optimization of powder dispersion method;
- 2) Sample processing by Hot Pressing of Ti6Al4V, Ti6Al4V-based composites, ZrO<sub>2</sub>, ZrO<sub>2</sub>-based composites, PEEK and PEEK-based composites and by Press and Sintering of ZrO<sub>2</sub> and ZrO<sub>2</sub>-based composites;
- 3) Microstructural characterization of all samples by SEM/EDS analysis;
- 4) Mechanical characterization of all samples through assessment of hardness and shear tests.

# CHAPTER 2

## STATE OF THE ART

---

This section aims to introduce a theoretical framework on dental implants. It begins with a brief review of the dental field, introducing concepts such as osseointegration, biocompatibility and bioactivity. Materials that are commonly used in implantology and new substitutes as biocompatible and bioactive materials are also presented, showing their advantages and disadvantages and outlining a possible solution to overcome these drawbacks. This section also gathers information about biocomposites, addressing the potential of these materials in the implants industry. A detailed description of functionally graded materials and powder metallurgy is afterwards presented, ending this section with some final remarks regarding the design of a dental implant.

## 2.1. DENTAL IMPLANTS

In dentistry, the rehabilitation of completely and partially edentulous patients with dental implants has become increasingly important. In fact, dental implants could be the only restoration option for people who lost a tooth. The tooth absence from the dental arch could have many causes such as congenitally when a permanent tooth does not grow or as result of a disease, of which dental caries, periodontal problems and accidental trauma are the most common. Thus, replacing a missing tooth is extremely important not only to improve the patient's appearance, but more vital to prevent other tooth lost, masticatory function problems or changes in the dental arches such as resorption (the bone tends to shrink over time) and drifting (the neighboring teeth moves to fill the free space), as shown in Figure 1 [14–16]. Therefore, in comparison with other methods such as removable partial dentures or even full dentures, dental implants are currently the best solution, once they preserve not only the neighboring teeth, from drifting and further loosening, but also the bone tissue [17].



**Figure 1-** Bone resorption and teeth drifting.

A dental implant can be defined as an artificial substitute for natural roots of teeth, that are placed under the gums into (endosseous) or onto (sub-periosteal) the jawbone to support a fixed prosthesis (e.g. crowns and bridges) or to stabilize a removable prosthesis Figure 2 shows a schematic representation of a full dental implant, and a radiograph of the position of a dental implant in relation to the adjacent teeth.



## Development of bioactive materials for dental implants using powder metallurgy

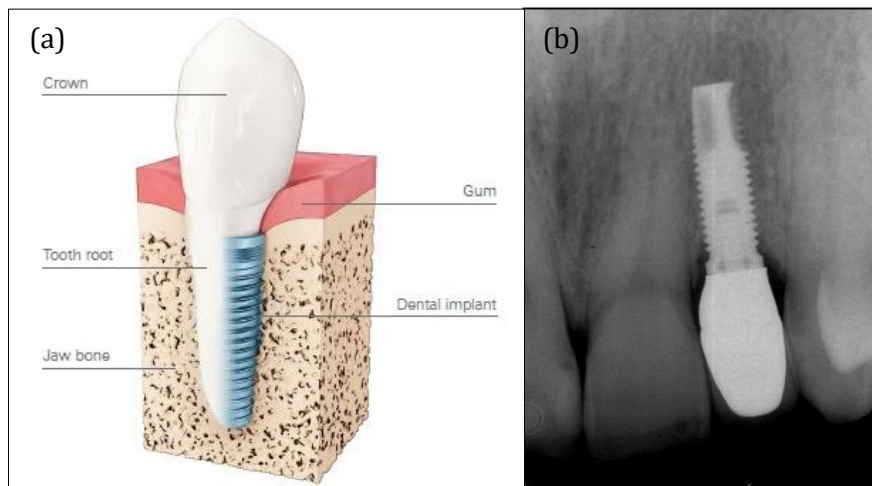


**Figure 2-**(a) dental implant [18] (b) Radiograph of a dental implant relative to the adjacent teeth [19].

Going back in history, several materials like seashell, stones, bones and gold alloys were used in dental interventions, being placed into human jawbone to replace missing teeth [20]. Later on, in the middle ages, allografts and xenografts were used as implants, however many problems have arisen related to this procedure such as infectious diseases and even deaths [20]. In 1948, Dr. Aaron Gershkoff in association with Dr. Norman Goldberg produced the first sub-periosteal implant [20]. The so called modern implants appeared due to a Swedish professor of orthopedics, named Per-Ingvar Branemark, that discovered in his research that bone grows near a titanium implant and attached to the metal without being rejected. This attachment between the bone and the implant was called by Branemark as “osseointegration”. This phenomenon has become a crucial factor in implant stability and consequently, on implants long term clinical success [15, 20].

The placement of a dental implant must be performed according to a series of steps. Firstly, a surgery is performed to promote the fixation of the metallic implant to the bone. When the implant is considered osseointegrated, which occurs after a sequence of biological events that will be mentioned in this section, a second surgery is performed to uncover the implant and expose it to the oral environment to attach an abutment. Lastly, the final prosthesis (fixed or removable) is placed [21]. The abutment will help the attachment between the implant and the prosthesis, as seen in Figure 3.

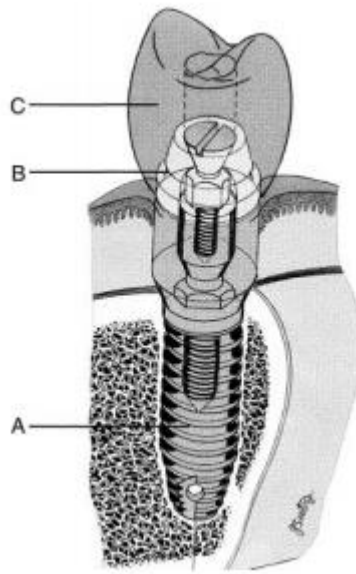


**Figure 3** – Diagram of implant components. A- implant, B-abutment, C-Prosthesis [21].

Immediately after the implantation, the implant is held only by mechanical friction, the so called primary stability. After that, many biological events interact with the implant on the bone-implant interface to promote the formation of new bone, taking place the secondary stability [22, 23]. These biological events comprise four main phases: hemostasis, inflammatory, proliferative and remodeling phase [24–26].

During the surgical intervention, the rupture of the blood vessels will cause the interaction between the dental implant surface and the blood components. In a first phase (hemostasis), seconds after implantation, ions and plasma proteins (such as fibrinogen and fibronectin) begin to adhere and get adsorbed to the surface of the implant. The blood vessel rupture is then stopped by the action of blood platelets, which will start to aggregate by binding with collagen from the traumatized tissue. After that, clotting factors create a clot that was formed due to the conversion of fibrinogen to fibrin and its addition to the platelet aggregate. This blood clot will act as a provisional matrix and adhere to the implant surface. The platelets then start to release a number of substances that will play an important role in cell to cell communication and, consequently, in the wound healing by acting as signaling molecules for recruitment and cell differentiation. [24, 25]

On a second phase (inflammatory phase), hours after the surgery, immune cells clean the wound, tissue debris and bacteria that remains in the site through phagocytic cells (neutrophils first and then macrophages).

## Development of bioactive materials for dental implants using powder metallurgy

The third phase (proliferative phase), occurs with the fibroblasts migrating into the wound and starting to synthesize components of the extracellular matrix. Then, mesenchymal stem cells migrate through the preliminary matrix of the fibrin clot toward the implant surface and platelets cause the differentiation of these cells into the osteoblastic lineage. Thus, osteoclast cells start to resorb the residual bone which will allow bone healing. This will cause the reduction of primary stability, as can be seen in Figure 4(a). Additionally, mesenchymal stem cells migrate also toward existing trabeculae (primary anatomical unit of trabecular bone) and to the implant surface and differentiate into osteoclasts. On the other hand, osteoblastic cells are also differentiated and will form an organic matrix that is mineralized by deposition of calcium phosphate. This will result in an immature woven bone formation around the implant, which will increase the secondary stability (Figure 4(a)).

During the last phase (remodeling phase), the osteoclasts resorb the woven bone and the osteoblasts replace the woven bone by mature bone (lamellar bone). The woven bone forms very quickly and is mechanically weak unlike lamellar bone which has a regular parallel alignment of collagen fibers into the lamella and, thanks to that, is mechanically strong. Lamellar bone is then classified in trabecular bone or spongy bone, and cortical bone or compact bone (Figure 4(b)) [15, 23–26].

According to Branemark, the healing period to allow osseointegration ranges from three to six months. Several studies have been made over the years aiming to reduce this healing time and improving the aesthetics [22, 27].

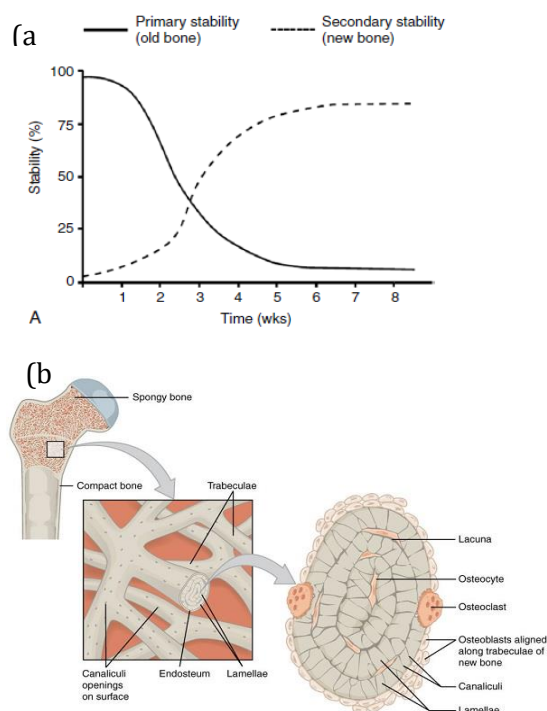


**Figure 4** – (a) primary and secondary stability [15] and (b) general schematic of bone structure [28]

Development of bioactive materials for dental implants using powder metallurgy

In dental implants, biocompatibility, osseointegration and appropriate mechanical properties are the main factors required to reduce the healing time and promote implant long-term success [29–31]. These requirements will be guaranteed by many factors such as the material used for the implant, its design, surface characteristics, health and bone quality, among others. The material of which the implant is made influences directly the biocompatibility, the osseointegration and the mechanical properties of the implant. On the other hand, the design of the implant affects the implant stability because it influences the stress distribution at the bone-implant interface, the surface area and the distribution of forces [20]. However, many studies already identified implant surface properties as the major factor to obtain an effective implant-tissue interaction and osseointegration, once the interaction between the bone and the implant is through its surface [32, 33]. Accordingly, much research has been made in order to control surface characteristics of implants, such as roughness, chemical composition, surface energy, topography, the presence of oxides, etc. Researches have already shown that the surface roughness affects the biological response in terms of osteoblast differentiation, proliferation and adhesion [20, 34–36]. On the other hand, the chemical composition improves the interaction between bone and implant. Surface chemical modification/control can be achieved with coatings through techniques such as plasma spraying, dip coating, electrophoretic deposition, etc [20, 34, 36, 37]. Additionally, surface energy is also an important factor to improve the biological response, once it is related with the wettability of the surface and thus its hydrophilicity. Hydrophilic surfaces will allow protein absorption to the implant surface and subsequent interaction with cells in contrast to hydrophobic surfaces that are subjected to air bubbles entrapment forbidding protein absorption and thus cell adhesion and activation (Figure 5). In this context, many studies have concluded that a moderate hydrophilicity improves the biological response [35, 36].

## Development of bioactive materials for dental implants using powder metallurgy

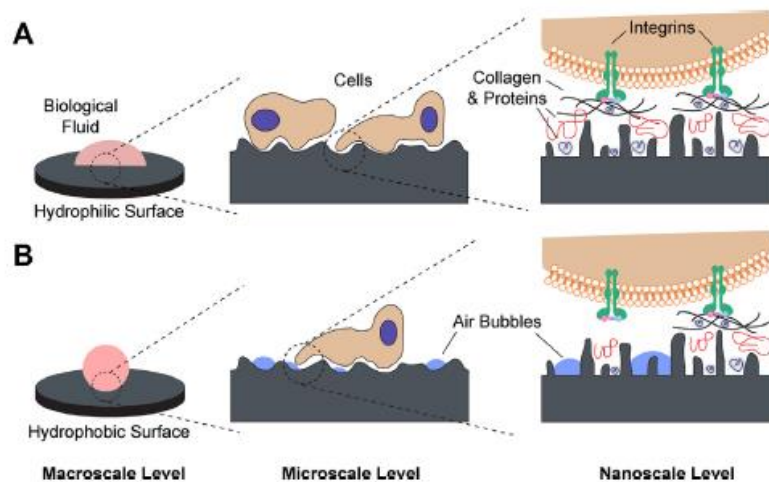


**Figure 5** – Schematic of the possible interactions with (a) hydrophilic and (b) hydrophobic surfaces [35].

## 2.2. BIOCOMPATIBLE MATERIALS

For many years, several materials were used to replace a missing tooth. With time, scientists realized that some materials were more successful than others when in contact with the human body, since the tissue response to certain materials was better than others [38].

In 1987 the term biocompatibility is defined as the “ability of a material to perform with an appropriate host response in a specific situation” [39]. By analyzing this definition, it is possible to conclude that biocompatibility is not an invariant property of a biomaterial, once the tissue response to a material may not be the same for all applications. Thus, the biological response of a material depends on the material itself, the host and the application. For example, in dentistry, when choosing a material for dental implants it is expected that the bone creates a direct connection with the implant surface and thus, a range of biological responses have to occur for osseointegration such as inflammation, unlike to what is expected when choosing a material for a crown where this phenomenon is not desired [40].

The biocompatibility of a material can be assessed by many available methods. These biocompatibility assessment methods are provided by guidance documents developed by International Organization of Standards (ISO) and Food and Drug Administration (FDA) and include cytotoxicity, sensitization, hemocompatibility, pyrogenicity, implantation, genotoxicity, carcinogenicity, reproductive and developmental toxicity and biodegradation testing [41].

Biocompatible materials are nowadays used in several biomedical fields, as for metallic, ceramic and polymeric materials.

## 2.2.1. METALLIC MATERIALS

Metallic alloys are widely used as biomedical materials for medical implants due to their excellent mechanical properties such as mechanical strength and resistance to fracture. These requirements are very important for implants because they are in load-bearing conditions. Among the metallic materials, those that are most commonly used as implants are stainless steel (especially 316L), CoCr alloys and titanium and its alloys, once besides their excellent mechanical properties, they also exhibit good biocompatibility [42–44].

Stainless steel (SS) was in earlier times one of the metallic materials most commonly used in orthopedic applications due to their good mechanical properties, however it is not a good biomaterial for long-term implants once it has poor fatigue strength and poor corrosion resistance [45, 46].

CoCr alloys appeared as a substitute for stainless steel due to having a higher corrosion resistance. However, ions release is a problem in this biomaterial because Co and Cr are toxic to human body and studies have already reported Co as carcinogenic [45, 46].

Titanium and its alloys are extensively used in many fields of engineering, such as aerospace applications, but also in biomedical applications. In fact, titanium and its alloys are the most frequently used materials in dental implantology, as a result of Branemark's findings. They are classified as light metals owning a density of approximately  $4.50 \text{ g/cm}^3$  for pure Ti (Figure 6) and  $4.43 \text{ g/cm}^3$  for Ti6Al4V. Additionally these alloys present excellent mechanical properties, Young's modulus (YM) that are closer to bone (when comparing with the metallic biomaterials previously mentioned), a highest biocompatibility when compared to stainless steels and CoCr alloys and also a good corrosion resistance [44, 45, 47–52].

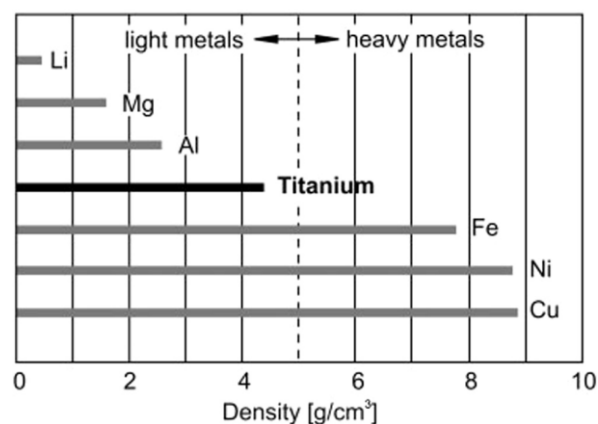


**Figure 6**-Density of selected metals [52].

## Development of bioactive materials for dental implants using powder metallurgy

Between titanium and its alloys, although commercially pure titanium (cpTi) is a very good candidate to dental implants due to their good mechanical properties, the most frequently used material is a titanium alloy - Ti6Al4V [12, 13]. Table 1 lists some mechanical properties of Ti6Al4V.

**Table 1** - Mechanical properties of Ti6Al4V [55].

<b>Property</b>	<b>Range of values</b>
Tensile Strength (MPa)	895-930
Young's Modulus (GPa)	110-114
Yield Strength (MPa)	825-869
Elongation (%)	6-10

While stainless steels have a YM around 190-210 GPa, CoCr alloys YM are between 210-253 GPa, substantially higher than that of bone tissue (10-30 GPa for cortical bone). When the stiffness (Young's modulus) between the implant and the host tissue is different, a process known as "stress shielding" occurs which can lead to bone resorption and non-occurrence of osseointegration process due to the movements between implant and bone. In contrast to SS and CoCr alloys, Ti6Al4V possess a Young's modulus around 110-114MPa which is still a higher value when compared to bone, however is the closest value to the bone in comparison with the other metallic materials, which turns the stress distribution at the interface between bone and implant more acceptable [44, 51–54, 56].

On the other hand, the yield strength of Ti6Al4V ranges between 825 and 869 MPa [55]. This property provides the stress value at which plastic deformation begins to occur. Thus, it is vital to evaluate the mechanical loading on either bone and implant materials to understand the effect of occlusal loading around dental implants at the bone-implant interface. In this sense, Benaïssa et al. studied the effect of mastication loads on the mechanical stresses generated in titanium dental implants. Benaïssa concluded that the mechanical stress is higher in the bone areas closer to the implant (Figure 7(a)), with the maximum Von Mises stress occurring in the dental implant itself. This study also concludes that for the loading conditions tested, the abutment was the most fragile component, since high concentration of stress occurs in the first threads, and that the implant supports this typical loading without plastic deformation [57]. Thus, titanium alloys are suitable metallic biomaterials for dental implants, having the necessary strength to resist fracture under occlusal forces and a Young's modulus more close to bone than other metallic alloys, thus providing a more uniform stress distribution on the bone-implant interface [21].

## Development of bioactive materials for dental implants using powder metallurgy

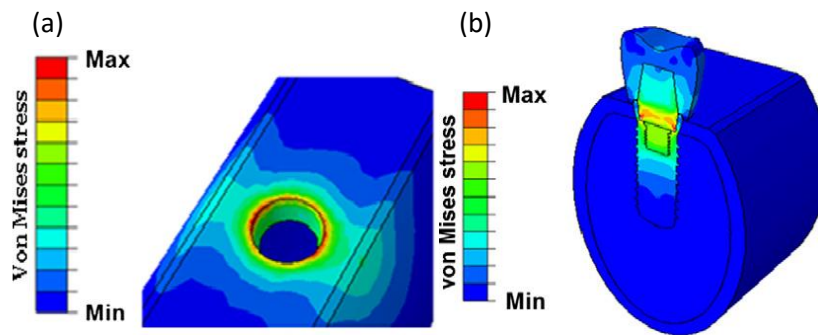


**Figure 7** – Distribution of stresses within (a) the bone (b) main model [57]

Ti6Al4V corrosion resistance and biocompatibility are a consequence of an oxide layer formed in the surface of the titanium alloy. When exposed to atmosphere or to environments that contain oxygen, titanium will absorb the oxygen and form an oxide layer (mainly based on  $\text{TiO}_2$ ) on the surface of the material, acting as a protective barrier. The biocompatibility is also improved by the oxide layer once the attachment and growth of the human bone cells to this layer is very effective [48, 50, 58, 59].

Nevertheless, in oral environment, Ti6Al4V can corrode, which will cause the release of metallic ions to the surrounding tissues, such as vanadium ions, provoking cytotoxicity as well as aluminum ions which have been proven to cause Alzheimer in long-term. Also, in masticatory movements, the loads that are applied through the material to bone causes micromovements that can detach the oxide layer, leading to material loss and release of metallic ions from the material [60].

In the oral environment, wear sliding can occur in presence of saliva and abrasion particles from food intake or tooth brushing. These wear debris can increase corrosion and therefore the degradation of this material [61]. These aspects will cause adverse events on the human tissues promoting peri-implant inflammations and consequently, bone and implant loss [51, 60]. Additionally, bone resorption and consequent recession of the gingiva can expose the implant, causing esthetic complications due to the dark grayish color of titanium, as seen in Figure 8 [62].



**Figure 8** – Gingival recession [19].



## 2.2.2. CERAMIC MATERIALS

Ceramics have become increasingly attractive as new materials for dentistry, once they can surpass the several disadvantages that metals brings when implanted in the human body. Ceramics are nonmetallic inorganic materials that contain compounds of oxygen with metallic or semi metallic elements. These materials are very attractive to dental applications due to their biocompatibility, color stability, good mechanical properties (they exhibit good flexure strength and fracture toughness) [21] , besides good chemical, physical and thermal properties when compared with other materials [21, 62]. Glasses, porcelains, glass-ceramics or highly crystalline structures are some examples of ceramics. As previously mentioned, titanium biostability is due to the oxide layer formed on its surface, that will prevent corrosion. In fact, this oxide layer is a ceramic coating formed spontaneously on the surface of the metal when exposed to oxygen [63].

In recent years, ceramic materials have been increasingly used in dental implants, with high-strength ceramics being the most used in implantology, once they have to withstand the occlusal loads in the masticatory movements[21, 64]. High-strength ceramics, classified as inert in the body, have an important advantage over metallic materials, by exhibiting minimal ion release. Additionally, as mentioned before, bone resorption and consequently peri-implant recession, may turn the implant visible, which turns the dark grayish color of the titanium a drawback in terms of esthetics. Therefore, research on tooth-colored ceramic materials become extremely important not only to overcome this issue but also to reduce the use of metallic materials in the human body [64].

Aluminum oxide or alumina ( $Al_2O_3$ ) and zirconium oxide or zirconia ( $ZrO_2$ ) are the most used ceramic materials in implantology. Table 2 lists some mechanical and physical properties of these two ceramic materials.

**Table 2** – Mechanical and physical properties of aluminum oxide and zirconium oxide [21]

<b>Material</b>	<b>Grade or Condition</b>	<b>Flexure Strength (MPa)</b>	<b>Elongation (%)</b>	<b>Young's Modulus (GPa)</b>	<b>Tensile Strength (MPa)</b>	<b>Density (g/cm<sup>3</sup>)</b>
<b>Aluminum Oxide</b>	Polycrystalline	400-550	0.1	380	220	3.96
<b>Zirconium Oxide</b>	$Y_2O_3$ (stabilized)	1200	0.1	200	350	6.00

Aluminum oxide is very used in implants due to its inertness, high toughness and strength, excellent wear resistance and high wettability in comparison with metallic surface materials. On the other

hand, zirconium oxide has become a good substitute to alumina because although having some similar properties to alumina it possesses a higher fracture toughness, flexure strength and a lower Young's modulus [63, 65].

Zirconia's high strength and toughness derived from its crystallographic forms (monoclinic, tetragonal and cubic) [63]. In fact, the high mechanical toughness and strength are consequence of the stabilization of the tetragonal phase of zirconia (by adding metal oxides like yttria ( $Y_2O_3$ )) at room temperature. Thereby, yttria-stabilized tetragonal zirconia polycrystal (Y-TZP) is often used in implantology [62, 63, 66, 67].

Monoclinic phase is stable from room temperature till  $1170^\circ C$ , the tetragonal phase is stable above  $1170^\circ C$  till temperatures of  $2370^\circ C$ , while up to the melting point the phase is cubic [53]. These phase transitions happen only with pure zirconia, however, when alloying zirconia with metal oxides such as yttria, the tetragonal form is retained metastable at room temperature [53, 63, 68, 69]. This metastable tetragonal phase can transform into a stable monoclinic phase under applied stresses (stress-induced) which will be complemented with a volume increase (3-4%) [53, 63]. This volume increase will lead to compressive stresses that contribute to crack closing and consequently increasing the crack resistance (transformation toughening). This mechanism, presented in Figure 9, increases the reliability and lifetime of Y-TZP implants [40, 53, 63, 70, 71].

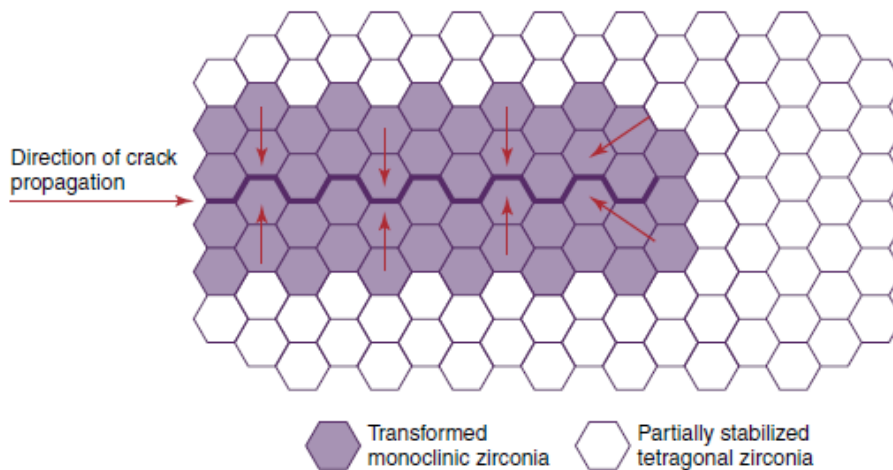


**Figure 9** – Schematic of transformation toughening mechanism in partially stabilized zirconia [71].

However, although this phenomenon imparts a higher mechanical toughness and strength it can increase the susceptibility of the material to low-temperature degradation (LTD). LTD or ageing occurs when the transformation of metastable tetragonal to stable monoclinic happens in the presence of water or water vapor. As said before, when the metastable tetragonal phase changes to stable monoclinic

phase, this transformation leads to volume increase of the grains, creating microcracks. These turn the material susceptible to water penetration, generating a phase destabilization starting in the surface and progressing into the material (figure 10). This phenomenon is enhanced at temperatures in the range of 200°C to 300°C, and will cause the reduction of the mechanical toughness, strength and density [53, 69, 70, 72].

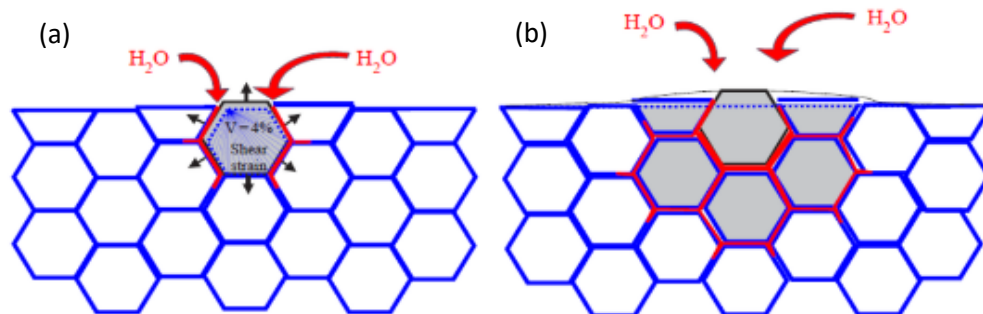


**Figure 10** – Scheme of the ageing process (a) transformation on a particular grain followed by microcracking and stress transmission to neighboring grains (b) growth of the transformation grains (grey) and water penetration (red) derived by microcracking [73].

Nonetheless, several studies on zirconia concluded that, allied to a high mechanical toughness and strength, this material has a good resistance to corrosion, great biocompatibility due to the minimal ion release, increased esthetics and exhibit lower bacteria accumulation when compared with metallic materials, making it extremely appealing for dental implants [8, 62, 66, 69].

### 2.2.3. POLYMERIC MATERIALS

Both titanium and zirconia still have some drawbacks when used as dental materials for implants. A phenomenon that brings some concerns in implantology, once it can lead to bone resorption and consequent implant failure [74–77] is the Young's modulus mismatch between zirconia or titanium implants and bone, with stress shielding occurring on the implantation area. Another aspect concerns the metal ions and debris release, which usually occurs on metallic implants.

In this context, to overcome these limitations and others, much research has been made to find alternatives to these materials. Another broad category of materials that are commonly used in biomedical applications to substitute the materials aforesaid are polymeric materials [75–77], that are known to avoid ions release and being considered inert materials.

Poly-ether-ether-ketone, also known as PEEK, is a polymeric material member of the PAEK family (poly-aryl-ether-ketone) increasingly employed in orthopedic, cranial and spinal implants [75, 78–81].

This material is well known as a high-performance semi crystalline thermoplastic polymer and is a biocompatible material owning several advantages such as good mechanical properties (Young's modulus, strength, and toughness), wear and fatigue resistance, excellent thermal and chemical stability, bioinert properties [61, 76, 79, 80, 82–85]. Table 3 lists the mechanical properties of PEEK [86, 87].

**Table 3** – Mechanical properties of PEEK [86, 87].

Properties	Property range of values
<b>Tensile Strength (MPa)</b>	90-100
<b>Young's Modulus (GPa)</b>	3-4
<b>Yield Strength (MPa)</b>	107
<b>Elongation (min.)</b>	4.9

As previously referred, the Young's modulus of bone is between 10 to 30 GPa, while titanium and zirconia Young's modulus are 110-114 GPa and 200 GPa [21, 55], correspondingly. These differences can cause stress shielding in the local area and therefore bone resorption and implant failure [21, 55, 74]. On the other hand, PEEK presents a Young's modulus ranging between 3 and 4 GPa which is lower than bone's young's modulus. However, this value can be increased up to 18-25 GPa by reinforcing it with carbon fiber, attaining a similar value to bone [5, 74, 77, 78, 82, 88]. Additionally, the carbon fibers reinforcement doubles the tensile strength of PEEK from 90-110 MPa to 214 MPa which will provide mechanical properties close to metal alloys [48, 85]. Nonetheless, with or without reinforcements, PEEK will become a very good substitute for metals or ceramics, by decreasing the stress shielding effect [74, 77, 82].

However, PEEK is a material chemically inert material and due to its low surface energy (hydrophobic surface), protein absorption and consequently cellular adhesion on its surface is limited [84, 85]. Therefore, many researches have been made in order to modify PEEK surface to promote cell adhesion and proliferation [84]. Among these treatments, surface coatings or modifications are known to enhance bioactivity and osseointegration of PEEK implants [78, 75, 88].

### 2.3. BIOACTIVE MATERIALS

Ti6Al4V, ZrO<sub>2</sub> and PEEK are broadly used in dental and orthopedic implants due to their several advantages, already addressed. Still, although these materials own very good mechanical properties, they are generally defined as bioinert materials [8, 89, 90]. Therefore, their ability to interact with the

surrounding tissue is very weak, which can lead to a poor implant to bone fixation. Thus, it is important to enhance the chemical or biological bonding between the implant and bone, with one of the strategies being through the use of bioactive materials [6–10].

The term bioactive was defined by Hench and Ethridge as the: “one that elicits a specific biological response at the interface of the material which results in the formation of a bond between the tissues and the material” [63, 91–93]. Thus, bioactive materials are the ones that react with the surrounding tissue causing a positive reaction on bone tissue formation. Accordingly, bioactivity is related to the interaction between the material surface and the nearby tissue forming a layer on the surface of the material that would allow bone bonding [63, 92, 94]. Hence, these materials have expanded industrially in areas such as medicine and dentistry.

In bone implants, bioactivity and the choice of the bioactive materials are directly related with the natural bone tissue. The bone tissue is mainly composed of bone cells and a calcified matrix commonly called bone matrix. As previously mentioned the bone cells are mainly important to synthesize the organic part of the matrix, to promote the resorption of the bone and to secrete substances to keep the maintenance of the bone (osteoblasts, osteoblasts and osteocytes, respectively). On the other hand, 20% of the bone matrix is mainly composed with an organic phase, 70% an inorganic phase and 10% water, approximately. In turn, the organic phase is mostly constituted by type I collagen (around 95%) and the inorganic phase, also called mineral phase, is composed with higher quantities of calcium phosphates especially hydroxyapatite crystals located along the collagen fibers and some other components in minor amounts such as bicarbonate, magnesium, potassium, etc (Figure 11) [91, 95].

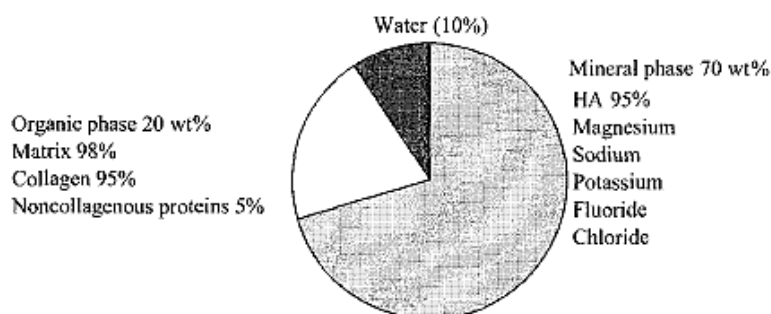


**Figure 11** – Composition of bone [91].

Given the bone composition, the selection of bioactive materials focuses on the use of calcium phosphates, since these components exist in large amounts on the inorganic phase of bone matrix. It is

the combination of collagen fibers with hydroxyapatite crystals which are responsible for bone strength and hardness [23].

Calcium phosphates are bioactive materials that own biocompatible properties due to their high similarity to the naturally apatites of bone, their ability to promote bone formation (osteoconductivity) and their osseointegration. Among all the calcium phosphates listed in Table 4, the most used in dental and orthopedic applications is hydroxyapatite (HA or HAp), although recently tricalcium phosphates also gained attention in these applications due to their favorable properties, like its ability to be resorbed by human body allowing the integration between implant and bone which will subsequently accelerate the process of osseointegration [12, 37, 96–99].

**Table 4**-Biologically relevant calcium phosphates compounds [96]

Name	Chemical formula	Calcium: phosphate ratio
Hydroxyapatite (HA)	$\text{Ca}_{10}(\text{PO}_4)_6(\text{OH})_2$	1.67
Fluorapatite (FA)	$\text{Ca}_{10}(\text{PO}_4)_6\text{F}_2$	1.67
Calcium-deficient hydroxyapatite (CDHA)	$\text{Ca}_{10-x}(\text{HPO}_4)_x(\text{PO}_4)_{6-x}(\text{OH})_{2-x}$ ( $0 < x < 2$ )	1.33– 1.67
Biological apatite (BA)	$\text{Ca}_{8.3}(\text{PO}_4)_{4.3}(\text{CO}_3-\text{HPO}_4)_{1.7}$ (OH) <sub>0.3</sub> BA = carbonated CDHA ( $x = 1.7$ )	1.38– 1.93
Oxyhydroxyapatite (OHA)	$\text{Ca}_{10}(\text{PO}_4)_6(\text{OH})_{2-2x}\text{O}_x\Box_x$ ( $0 < x < 1$ )	1.67
Oxyapatite (OA)	$\text{Ca}_{10}\text{O}(\text{PO}_4)_6$	1.67
Monocalcium phosphate monohydrate (MCPM)	$\text{Ca}(\text{H}_2\text{PO}_4)_2 \cdot \text{H}_2\text{O}$	0.5
Monocalcium phosphate anhydrate (MCPA)	$\text{Ca}(\text{H}_2\text{PO}_4)_2$	0.5
Dicalcium phosphate dihydrate (brushite) (DCPD)	$\text{CaHPO}_4 \cdot 2\text{H}_2\text{O}$	1
Dicalcium phosphate anhydrate (monetite) (DCPA)	$\text{CaHPO}_4$	1
Octacalcium phosphate (OCP)	$\text{Ca}_8(\text{HPO}_4)_2(\text{PO}_4)_4 \cdot 5\text{H}_2\text{O}$	1.33
Tricalcium phosphate (phase $\alpha$ ) ( $\alpha$ -TCP)	$\text{Ca}_3(\text{PO}_4)_2$ (monoclinic)	1.5
Tricalcium phosphate (phase $\beta$ , whitlockite) ( $\beta$ -TCP)	$\text{Ca}_3(\text{PO}_4)_2$ (rhombohedral)	1.5
Tetracalcium phosphate (TTCP)	$\text{Ca}_4\text{O}(\text{PO}_4)_2$	2
Dicalcium phosphate (phase $\alpha$ ) ( $\alpha$ -DCP)	$\text{Ca}_2\text{P}_2\text{O}_7$ (orthorhombic)	1
Dicalcium phosphate (phase $\beta$ ) (calcium pyrophosphate) ( $\beta$ -DCP)	$\text{Ca}_2\text{P}_2\text{O}_7$ (tetragonal)	1
Amorphous calcium phosphate (ACP)	$\text{Ca}_x(\text{PO}_4)_y \cdot n\text{H}_2\text{O}$	1.2–2.2

The symbol  $\Box$  represents a vacancy in the crystallographic lattice.

## Development of bioactive materials for dental implants using powder metallurgy

As previously mentioned, hydroxyapatite is the most widely used bioactive compound in implantology, due to a chemical composition and structure similar with the mineral phase of bone, as seen in Table 5 [37].

This bioactive material has a stoichiometric formula  $\text{Ca}_{10}(\text{PO}_4)_6(\text{OH})_2$  which in turn corresponds to a Ca/P ratio of 10:6, also commonly expressed as 1.67 [95]. This ratio is similar to the natural bone which turns this material a good candidate for dental and orthopedic applications. Additionally, Ca/P ratio is related with the degradation rate and solubility, i.e., these parameters increase with a decrease of the Ca/P ratio [100]. HAp crystallizes in a hexagonal structure with a space group  $\text{P6}_3/\text{m}$  and the following lattice parameters:  $a = b = 9.423\text{\AA}$ ,  $c = 6.875\text{\AA}$ ,  $\alpha = \beta = 90^\circ$   $\gamma = 120^\circ$  [95, 101, 102]. Figure 12 shows the crystal structure of hydroxyapatite.

**Table 5** – Comparative composition and crystallographic of Human Enamel, Bone, and HAp ceramic [93] .

	<i>Enamel</i>	<i>Cortical bone</i>	<i>HA</i>
<b>Constituents (wt%)</b>			
Calcium, $\text{Ca}^{2+}$	36.0	24.5	39.6
Phosphorus, P	17.7	11.5	18.5
(Ca/P) molar	1.62	1.65	1.67
Sodium, $\text{Na}^+$	0.5	0.7	Trace
Potassium, $\text{K}^+$	0.08	0.03	Trace
Magnesium, $\text{Mg}^{2+}$	0.44	0.55	Trace
Carbonate, $\text{CO}_3^{2-}$	3.2	5.8	—
Fluoride, $\text{F}^-$	0.01	0.02	—
Chloride, $\text{Cl}^-$	0.30	0.10	—
Total inorganic	97.0	65.0	100
Total organic	1.0	25.0	—
Absorbed $\text{H}_2\text{O}$	1.5	9.7	—
<b>Crystallographic properties</b>			
Lattice parameters ( $\pm 0.03\text{ nm}$ )			
<i>a</i>	0.9441	0.9419	0.422
<i>c</i>	0.6882	0.6880	0.6880
Crystallinity index	70–75	33–37	100
Crystallite size, nm	$130 \times 30$	$25 \times 2.5\text{--}5.0$	
<b>Products after sintering &gt;800°C</b>			
	HA + TCP	HA + CaO	HA
<b>Mechanical properties</b>			
$E$ (GPa)	14	20	10
Tensile strength (MPa)	70	150	100

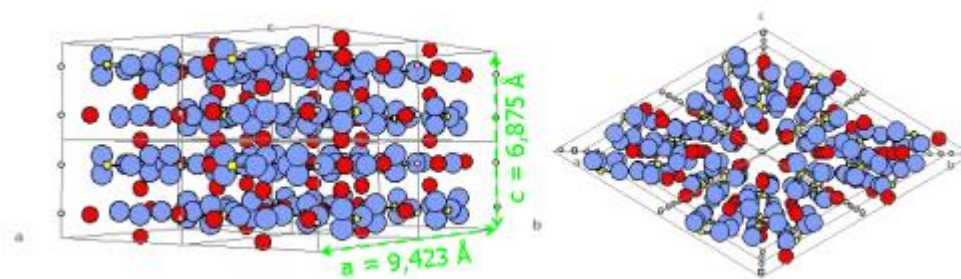


**Figure 12** – Crystalline structure of hydroxyapatite [91].

On the other hand, tricalcium phosphates (TCP) are another calcium phosphates that could be used in orthopedic and dental implants once they are also biocompatible materials and have osteoconductive properties [94]. These phosphates have a Ca/P ratio of 1.5 [92, 94] and exist in two crystal forms:  $\beta$  and  $\alpha$ . Both have similar chemical composition ( $\beta$ - $\text{Ca}_3(\text{PO}_4)_2$  and  $\alpha$ - $\text{Ca}_3(\text{PO}_4)_2$ ) with differences in their crystalline structure. In one hand,  $\alpha$ -TCP has a crystalline structure with a monoclinic space group  $\text{P}2_1/a$  with  $a = 12.887\text{\AA}$ ,  $b = 27.280\text{\AA}$  and  $c = 15.219\text{\AA}$ . On the other  $\beta$ -TCP has a crystalline structure rhombohedral with a space group  $\text{R}3c$  and the following lattice parameters:  $a = b = 10.439\text{\AA}$ ,  $c = 37.375\text{\AA}$  [103, 104].

The differences in the crystalline structures of  $\alpha$ -TCP and  $\beta$ -TCP confer different solubilities to these compounds. Comparing also with hydroxyapatite, the order of the solubility is as follows:  $\alpha$ -TCP >  $\beta$ -TCP  $\gg$  HAp, being  $\alpha$ -TCP the more soluble in physiological medium [99, 105]. In this sense, the ones that have longer permanence in the body are HAp and  $\beta$ -TCP. Thus, between  $\alpha$ -TCP and  $\beta$ -TCP, the  $\beta$ -phase was considered more stable than the  $\alpha$ -phase [92, 105].

In this sense, one of the main differences between HAp and TCP is their degradation rate.

Another aspect to consider is the thermal decomposition of these materials. In fact, many researchers have determined the effect of temperature on the decomposition of these bioactive materials. At high temperatures, HAp can release the OH<sup>-</sup> ions causing dehydration which, according to C.F. Koch et. al, could occur at temperatures above 900°C, followed by the decomposition of HAp in  $\beta$ -TCP,  $\alpha$ -TCP or other compounds [96]. On the other hand, Chunyan Wang et al. reported that HAp releases its OH<sup>-</sup> ions at temperatures around 1000°C and then proceeds to its decomposition into  $\beta$ -TCP and other compounds at temperatures greater than 1350°C, which in turn decompose to  $\alpha$ -TCP at temperatures around 1450°C [106]. Muralithran et al. evaluated the effects of sintering temperatures on hydroxyapatite when the HAp powder was cold isostatically pressed at 200 MPa and sintered in air at temperatures around 1000 to 1450°C. The results from X-ray diffraction analysis, XRD, (Figure 13)



## Development of bioactive materials for dental implants using powder metallurgy

showed that when the material is sintered at 1250°C the peaks corresponding to hydroxyapatite are detected, which does not happen when the material is sintered at 1400°C once the XRD revealed the presence of  $\alpha$ -TCP. When using a sintering temperature of 1450°C,  $\beta$ -TCP, and other compounds are identified [107].

A final remark on these bioactive materials concerns their brittle nature, which make these materials not suitable for load-bearing applications [31, 37, 108–111].

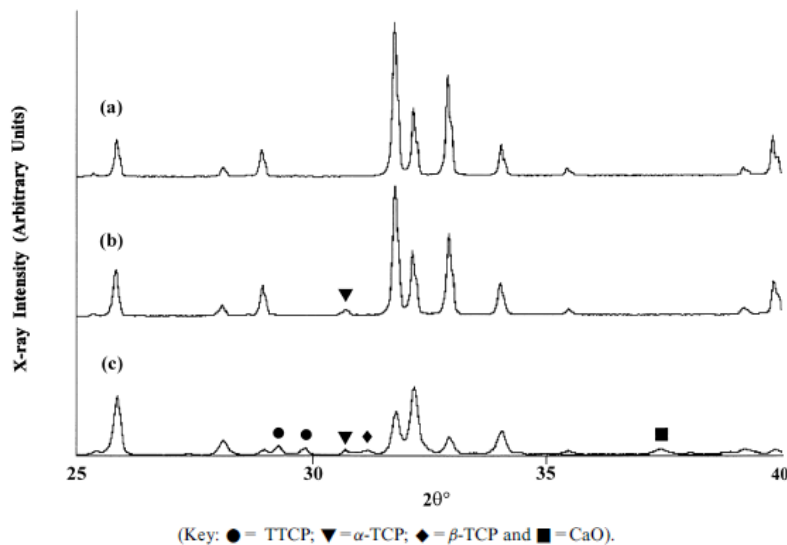


**Figure 13** – X-ray diffraction patterns of HAp sintered for 2h at (a) 1250°C, (b) 1400°C and (c) 1450°C [107].

## 2.4. BIOCOMPATIBLE COMPOSITES

When a material has two or more distinct constituents, it can be defined as a composite material, with these constituents being named matrix and reinforcement(s). Composites have the advantage of combining the properties of each constituent material, desirably creating better properties than each material possess individually. Hence, it is the possibility to combine different properties that make these materials widely used in dental and orthopedic applications [78, 87, 91, 112].

In load-bearing dental and orthopedic applications, these materials became very useful once it becomes beneficial to combine suitable mechanical properties with biocompatible ones, promoting osseointegration in order to create a good bond between the bone and the implant (bioactivity) [91].

As already mentioned throughout this literature review, although Ti6Al4V, ZrO<sub>2</sub> and PEEK own very good mechanical properties they do not integrate very well with the surrounding tissue. On the other

hand, bioactive materials such as calcium phosphates (HAp and  $\beta$ -TCP) develop a good bond with the neighboring tissue due to their similarity with the mineral bone. However, calcium phosphates are brittle materials, which is a drawback in such applications (implantology). To overcome these problems, calcium phosphates are traditionally used as coating materials, once this combination promotes bioactivity of the calcium phosphates (HAp and  $\beta$ -TCP) in the outer regions, while assuring favorable mechanical properties of Ti6Al4V, ZrO<sub>2</sub> or PEEK [31, 98, 110, 113, 114]. Several techniques such as plasma spraying, sputtering, electrophoresis, ion beam-assisted deposition, among other, are now used to create coatings in several base materials [37, 96, 108, 109, 115–118]. These coatings promote osseointegration which leads to a long-term success of implants [119]. In fact, Sergio Allegrini Jr. et al reported that the presence of hydroxyapatite promotes the maturation of collagen fibers on titanium implants leading to a faster osseointegration [120].

However, when concerning implants, the existence of a coating can be a detrimental aspect, once during implantation, the adhesive strength of the coating could be compromised and the coating can be delaminated/destroyed, thus releasing debris along the implantation site. This phenomenon can lead to the implant rejection and extraction. In this sense, the use of composites that combine the biocompatibility and bioactivity of HA or  $\beta$ -TCP with the favourable mechanical properties of Ti6Al4V, ZrO<sub>2</sub> or PEEK would allow to overcome this problem [109, 115, 121–124]. With these solution, Ti6Al4V, ZrO<sub>2</sub> or PEEK would act as matrix and HA or  $\beta$ -TCP as reinforcement material. These composites, having bioactive reinforcement particles embedded in the matrix, can avoid the occurrence of delamination, as occurs in coating solutions.

## 2.5. POWDER METALLURGY

Powder metallurgy (PM) gathers several manufacturing processes, where a powder material is converted into shaped objects that can be used in several applications. The ancient Incas used powders to made jewelry from metal powder. The use of powder metallurgy for the production of filaments arises with the invention of the electric lamp by Thomas Edison in 1879. Later on, in 1909 W.D. Coolidge starred one of the greatest landmarks of PM when he developed a ductile tungsten filament using tungsten powder for Edison's lamp. Thereafter, porous bearings, cemented carbides and electrical and magnetic materials were developed using PM [125–127].

This technology can be used in numerous applications such as automotive components, structures with controlled porosity, electrical and electronics applications, aesthetic materials and devices,

## Development of bioactive materials for dental implants using powder metallurgy

biomedical components (like implants), among others [125]. Some examples of PM applications can be seen in figure 14.

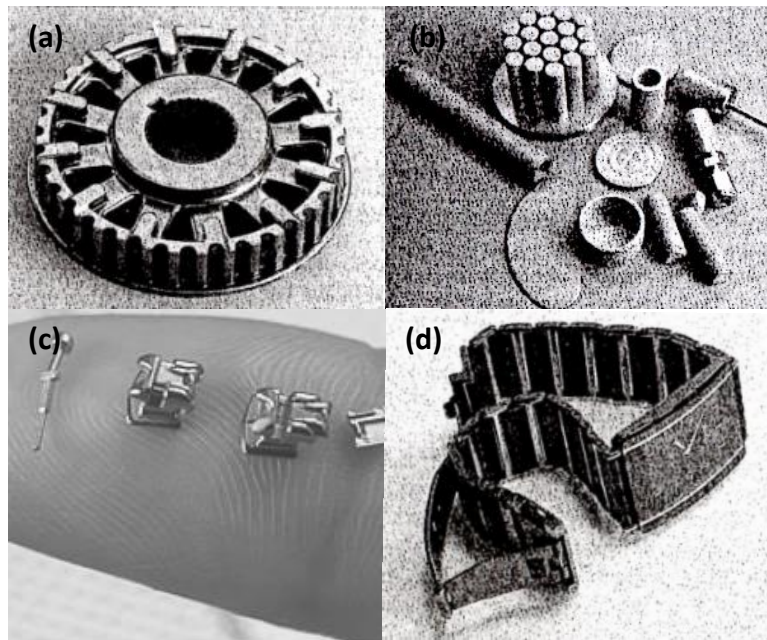


**Figure 14** - Some of the many powder metallurgy applications (a) pulley-timing automotive component, (b) porous devices for gas distribution, filtration, and flow control applications (c) orthodontic system bracket, slide, and hook, (d) watch fabricated with PM parts [125].

Powder metallurgy techniques have become competitive in comparison with conventional methods like casting, machining, hot forging, etc [125, 126]. This competitiveness is related to the various advantages of these powder metallurgy techniques. In one hand, unlike many opponents, these techniques can be applied to almost all materials such as metals, ceramics, polymers, alloys, composites, etc. On the other hand, as in any technique, the economic factor becomes essential when producing components. These PM techniques, own a high productivity which is related to a large-volume production with a residual material waste and low energy consumption, as can be seen in Figure 15, which demonstrates the comparison of energy consumption and materials waste between powder metallurgy and alternative techniques [125, 128].

Development of bioactive materials for dental implants using powder metallurgy

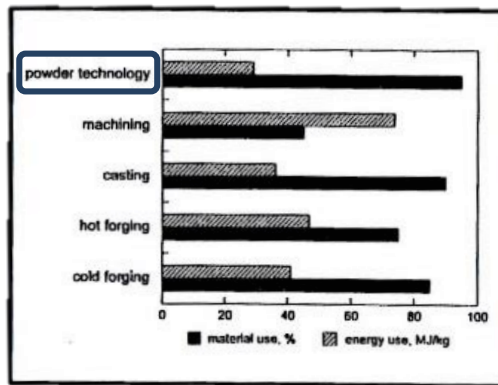


**Figure 15** – Energy use in MJ/kg of product and material waste as a percent of the starting material for powder technologies and alternative technologies [128].

Additionally, PM techniques also provide a good precision, in which compared with other techniques (Figure 16), offering a good tolerance and surface finishing [125]. However, once the tooling costs in PM technologies are quite elevated, they only are considered economical in terms of cost if the production rates are high [125, 126, 128]

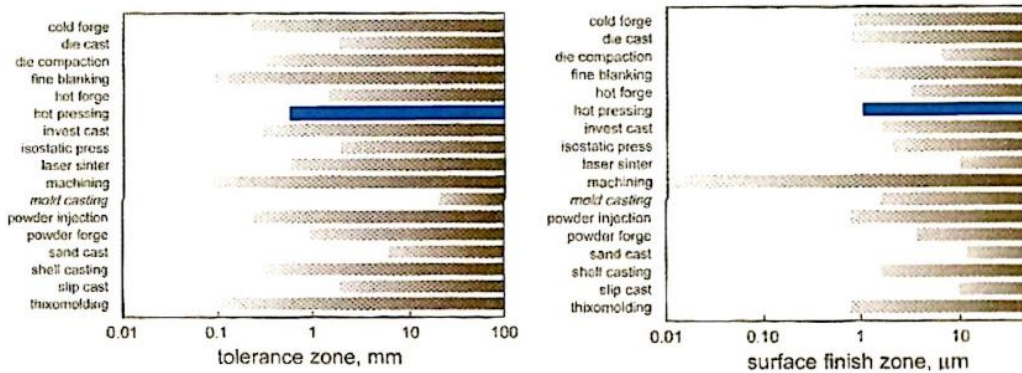


**Figure 16** – Tolerance and surface finish capabilities for various technologies, comparing PM with some of the alternative routes [128].

Another advantage of powder metallurgy technologies is the ability to produce materials with high strength, depending on the technique. Figure 17 shows the comparison of strength ranges when using several technologies including PM's ones [125, 128].

## Development of bioactive materials for dental implants using powder metallurgy

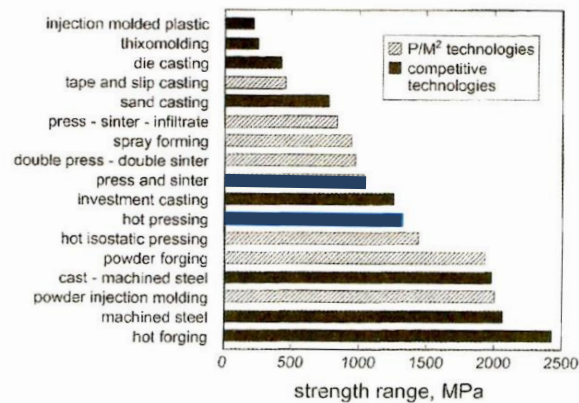


**Figure 17** – Strength ranges possible via various forming technologies, including several of the common PM approaches[128].

Over time, the use of PM techniques has evolved and is constantly growing once operating with powders makes possible the manufacture of certain materials that are not possible to produce with other techniques. Thus, once powders are the inputs of this technology, its properties and characteristics are essential to understand how they affect the process of consolidation. One of these characteristics is agglomeration since very small particles are naturally cohesive and form clusters, due to van der Waals forces. The solution to overcome this problem is to deagglomerate the particles constituting the agglomerate without fracturing them. The same effect of agglomeration can be seen when using powders to fabricate composites. The powders mixing step will have a huge influence on the homogeneity of the mixture, which will influence the powder consolidation process and dictate the material final properties. Figure 18 shows the various homogeneity levels, indicating on the right-hand side the optimal level of a homogeneously dispersed mixture [125].

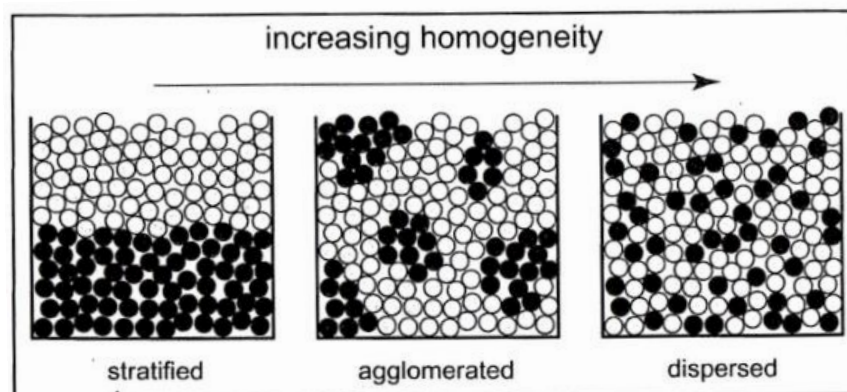


**Figure 18** – A schematic of increasing homogeneity [125].

When increasing the homogeneity of the mixture, the packing density also increases. This characteristic is also important in the consolidation phase and is related to other essential characteristics of powder, such as powder shape and size. In one hand, concerning powder shape, the more irregular is the form of the particle, the lower the packing density. On the other hand, as can be seen in Figure 19, when particles have different sizes, the smaller ones fill the spaces between the larger ones, increasing the packing density. This phenomenon can be counteracted if there were high concentrations of smaller particles that will cause a decrease in the packing density by separating the larger particles [125].

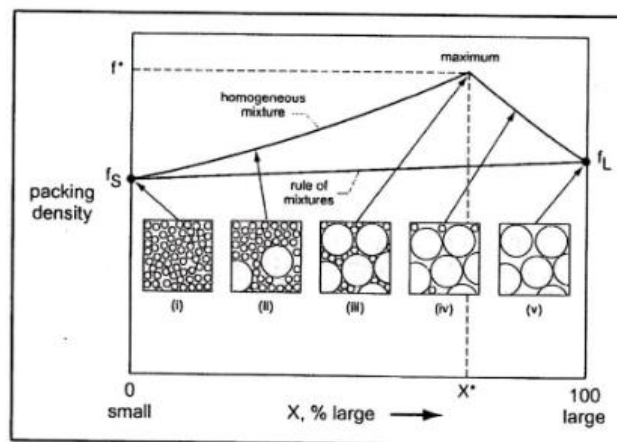


**Figure 19** – A plot of fractional packing density versus composition for bimodal mixtures of large and small spherical particles [125].

Among the powder metallurgy techniques, press and sintering and hot pressing will be addressed throughout this dissertation.

### 2.5.1. PRESS AND SINTERING

Press and Sintering (PS) is a PM technique that densifies powders by applying pressure and afterwards sintering them without pressure applied. The compaction process goes through several stages. Initially, the powder is placed in a mold (die) (Figure 20), being pressure applied (usually at room temperature) by an upper and lower punch, that by moving apply pressure along an axis, in order to press the powder.



## Development of bioactive materials for dental implants using powder metallurgy

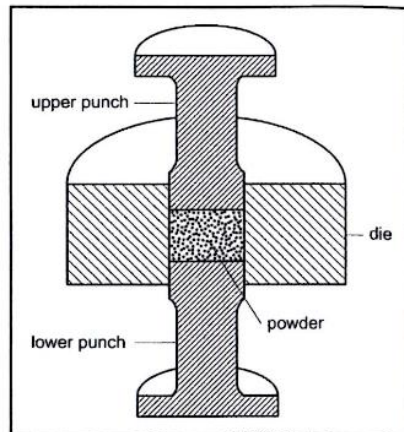


**Figure 20** - A conventional punch and die set for powder compaction [125].

As pressure is applied, the powder particles accommodate (repacking), deform and finally bond, as shown in Figure 21.

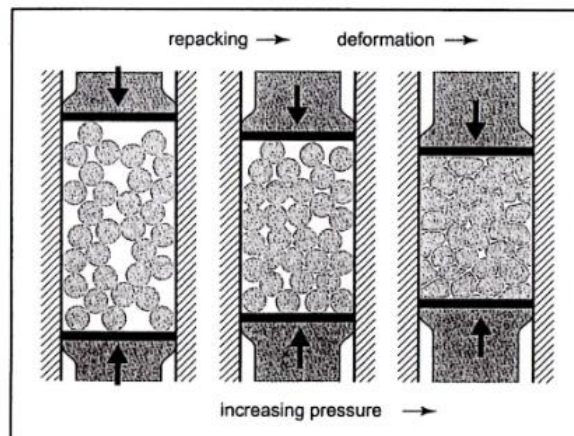


**Figure 21** – A view of the stages of powder compaction. At low pressures the particles rearrange to eliminate large pores. Depending on the particle hardness, eventually the particles deform at high pressures and particle deformation dominates densification [125].

This process typically requires the presence of a binder that will allow maintaining the integrity of the compact formed (also referred to as green compact), until the sintering process, that will ensure the consolidation of the green compact [1,4]. The binder will be burned off the compact during sintering.

This technology enables the production of materials with low manufacturing cost, however, the densification process does not preclude the presence of porosity. It is known that by decreasing porosity, higher mechanical properties are obtained. Thus, for materials that require high performance, full densification is essential to prevent its failure. Therefore, applying stress, simultaneously with temperature, will help to eliminate the porosity by collapsing the pores. The temperature will turn the materials ductile and allow their deformation without hardening. This complete densification is then

achieved by using processes with pressure and temperature simultaneously such as Hot Pressing process [1,4].

### 2.5.2. HOT PRESSING

Hot Pressing (HP) is a full density process that applies pressure and temperature simultaneously. HP process begins with the proper mixture of powders which will be subsequently placed in a mold (die), heated and compacted by double-action punches in a hot-pressing equipment [129, 130]. The mold material most commonly used is graphite, that enables temperature increases up to 2500°C when under vacuum [130]. The increase on the powder temperature is commonly achieved by heating the mold via radiation from an external heat source (Figure 22) [126, 130], typically through an induction system, with a coil which is located around the mold.

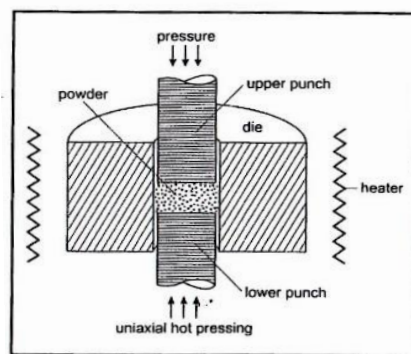


**Figure 22** - A cross-sectional view of uniaxial hot pressing [125].

Graphite molds allow the induction of temperature, however can contaminate the material, whereby measures to prevent direct contact of the powder with the graphite should be taken [125].

When the powder is placed inside the mold, with a correct positioning of the punches, the system is placed in the hot pressing equipment, more precisely in a chamber that applies a desired atmosphere (usually vacuum but argon or nitrogen can also be used). A schematic representation of a HP cycle can be seen in Figure 23. An initial pressure is applied to promote the rearrangement of the powders. Subsequently, the powder is heated to the desired temperature. The desired pressure is then applied and both parameters are maintained for a time period until the powder reaches its full densification (called sintering stage). Finally, the pressure and temperature are removed, allowing the material to cool [125, 126, 129, 130].



## Development of bioactive materials for dental implants using powder metallurgy

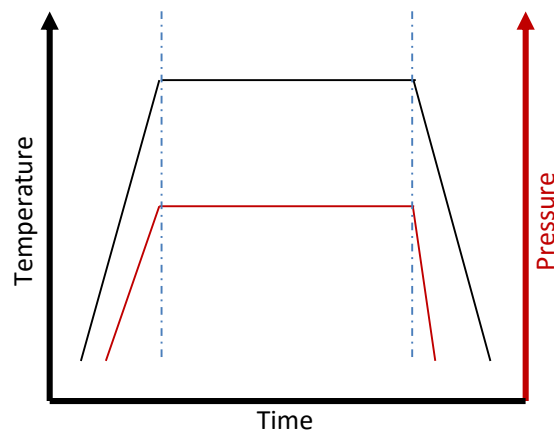


**Figure 23** – Schematic representation of a hot pressing cycle.

Overall, full density processes will increase the materials properties, such as strength, hardness, ductility, wear resistance, etc. Moreover, using temperature and pressure simultaneously will enable to densify the materials at much lower temperatures than in conventional sintering process [107]. Similarly, densification is achieved at lower pressures with the assistance of high temperature, which does not occur in PS process [126]. And although HP processes are somehow expensive, the properties achieved make them suitable for numerous applications [125]. And as seen in Figure 16, HP offers a good tolerance and surface finishing in comparison with several technologies including other PM techniques. Likewise, Figure 17 demonstrates that in general, HP produces materials with high strength when compared to PS.

Despite these advantages, HP also has some weaknesses, such as a lower production rate in comparison with press and sintering, and the presence of contaminants on the surface of the powders which prevents an effective sintering as in PS process. [125, 128].

## 2.6. FINAL REMARKS REGARDING THE DESIGN OF A DENTAL IMPLANT

In implantology, the selection of biomaterials is an essential aspect to promote a long-term success of the implant, to enhance osseointegration and also to maintain the necessary mechanical properties of the implant in load-bearing applications.

As mentioned before, Ti6Al4V, ZrO<sub>2</sub> and PEEK are biocompatible materials that own good mechanical properties, although having a poor integration with the surrounding tissue. Therefore, the addition of a bioactive material increases the bioactivity of these base materials. Many researches have

Development of bioactive materials for dental implants using powder metallurgy

focused their work in surface modifications to improve the bioactivity of these materials, like the application of a bioactive coating on their surface, however, delamination of the coating may lead to the loss of the desired properties. Thus, biocomposites become a good solution to overcome this problem, once these bioactive materials are reinforcing a matrix that exhibits good mechanical properties, making the final composite a material with both mechanical and bioactive performance, preventing delamination to occur. It is expected though that by adding these bioactive materials, the mechanical properties are decreased.

Functionally graded materials (FGMs) are composites that present a gradual transition in composition and structure, resulting in a transition of the properties of a material [123, 131]. The idea to create a dental implant having an FGM transition would be extremely advantageous. This approach would allow that the content of the bioactive materials gradually increases from the inside (0%) to its outside (10%), in which this gradual transition reduces the properties mismatch of the final material. As an example, the implant inner part would be made of Ti6Al4V and HAp content would gradually increase from there, finishing with an outer part of Ti6Al4V-HAp composite. Thus, the interior of the implant guarantees the mechanical properties and the outside, that is in contact with the surrounding tissue, the bioactive properties [123].

Some studies regarding dental applications used different materials discussed in this work, however, these studies have been proven that the adhesion strength of two different materials through a gradual transition (FGMs) is superior in comparison to coatings. B. Henriques et al. studied the shear bond strength of conventional porcelain fused to metal (PFM) in comparison with a functionally graded dental restoration after thermal-mechanical cycling. He concluded that the FGM presents a higher shear bond strength than the sharp transition PFM, as seen in Figure 24 [132].

## Development of bioactive materials for dental implants using powder metallurgy

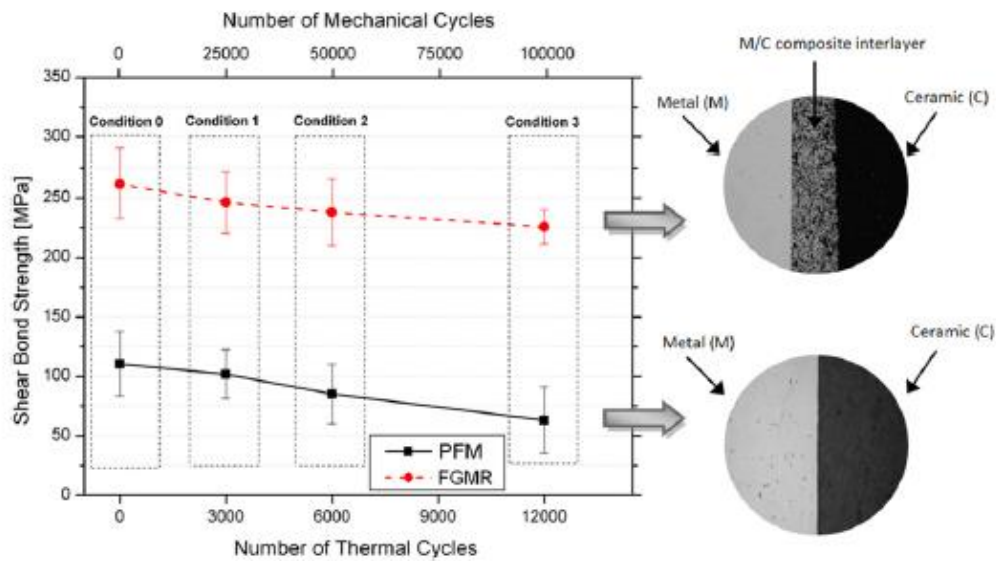


**Figure 24** – Mean  $\pm$  standard deviation (SD) of shear bond strength results for conventional porcelain fused to metal specimens (PFM) and for functionally graded specimens (FGMR), after thermal and mechanical cycling [132].

Additionally, in the same study, the evaluation of the mechanical properties revealed that a sharp transition between materials results in an abrupt transition of mechanical properties, causing a mismatch in mechanical properties which does not happen in the FGM solution, that exhibits a gradual transition in properties along the interlayer (Figure 25) [132].

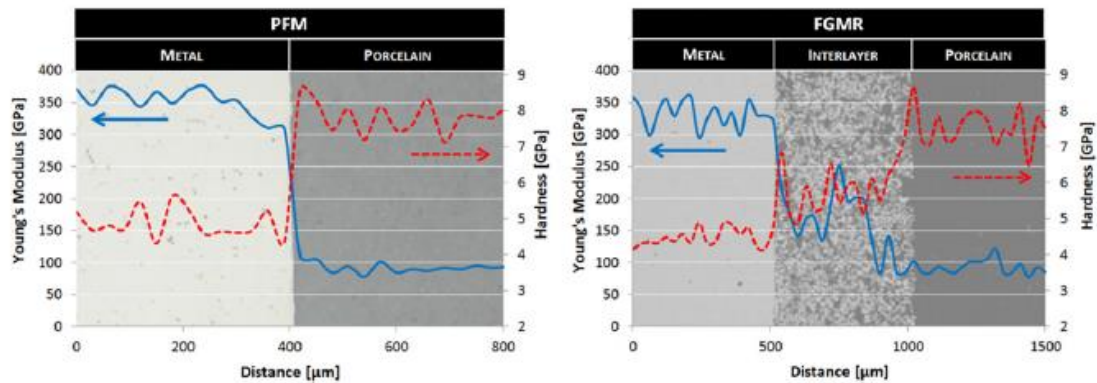


**Figure 25** – Mechanical properties measured at the metal-ceramic interface for a sharp (PFM) and a graded transition (FGMR): Young's Modulus and Hardness [132].

This dissertation focuses on the production and characterization of different types of composites, metal-based, ceramic-based and also polymer-based composites that would be incorporated in the design of a functionally graded transition between the inner and outer region of a dental implant.



# CHAPTER 3

## MATERIALS AND METHODS

---

The following chapter presents the experimental procedure of this dissertation referring the materials used for producing all the samples as well as a description of the methods used as for sample processing but also for its characterization.

## 3.1. RAW MATERIALS AND COMPOSITES DESIGN

The experimental procedure of this dissertation focuses on processing different types of samples by powder metallurgy techniques, namely HP and PS and subsequent characterization of the samples thus produced. In this sense, for the processing of these composites, different materials were required, ranging from Ti6Al4V, ZrO<sub>2</sub>, PEEK, HAp and  $\beta$ TCP. Table 6 shows the particle size of each raw material used as well as its manufacturer. Table 7 lists the composition of each sample, for unreinforced materials and composites.

**Table 6** - Powders dimension and supplier.

Raw Material	Particle size, d50 ( $\mu$ m)	Commercial designation/ Supplier
<b>Ti6Al4V</b>	32.53	Ti6Al4V/TLS Technik
<b>ZrO<sub>2</sub></b>	60	TZ-3YB-E/Tosoh corporation
<b>PEEK</b>	50	VESTAKEEP® 2000FP/Evonik Industries
<b>HAp</b>	10	nanoXim.Hap203® /Fluidinova S.A.
<b><math>\beta</math>TCP</b>	2.26	BETA-TCP/Trans-Tech,Inc

**Table 7** - Composition of the produced materials.

Produced Materials	Composition (vol.%)
<b>Ti6Al4V</b>	100% Ti6Al4V
<b>Ti6Al4V-10HAp</b>	90% Ti6Al4V – 10% HAp
<b>Ti6Al4V-10<math>\beta</math>TCP</b>	90% Ti6Al4V – 10% $\beta$ TCP
<b>ZrO<sub>2</sub></b>	100% ZrO <sub>2</sub>
<b>ZrO<sub>2</sub>-10HAp</b>	90% ZrO <sub>2</sub> – 10% HAp
<b>ZrO<sub>2</sub>-10<math>\beta</math>TCP</b>	90% ZrO <sub>2</sub> – 10% $\beta$ TCP
<b>PEEK</b>	100% PEEK
<b>PEEK-10HAp</b>	90% PEEK – 10% HAp
<b>PEEK-10<math>\beta</math>TCP</b>	90% PEEK – 10% $\beta$ TCP

The morphology of Ti6Al4V, ZrO<sub>2</sub>, PEEK, HAp and  $\beta$ TCP powders were analyzed using scanning electron microscopy (SEM) images and are presented in figure 26, respectively. From SEM images, it is possible to observe that all powders have a spherical shape, excepting the PEEK powder that possess an irregular shape. The corresponding particle size distribution of each raw material can be seen in figure 27.

## Development of bioactive materials for dental implants using powder metallurgy

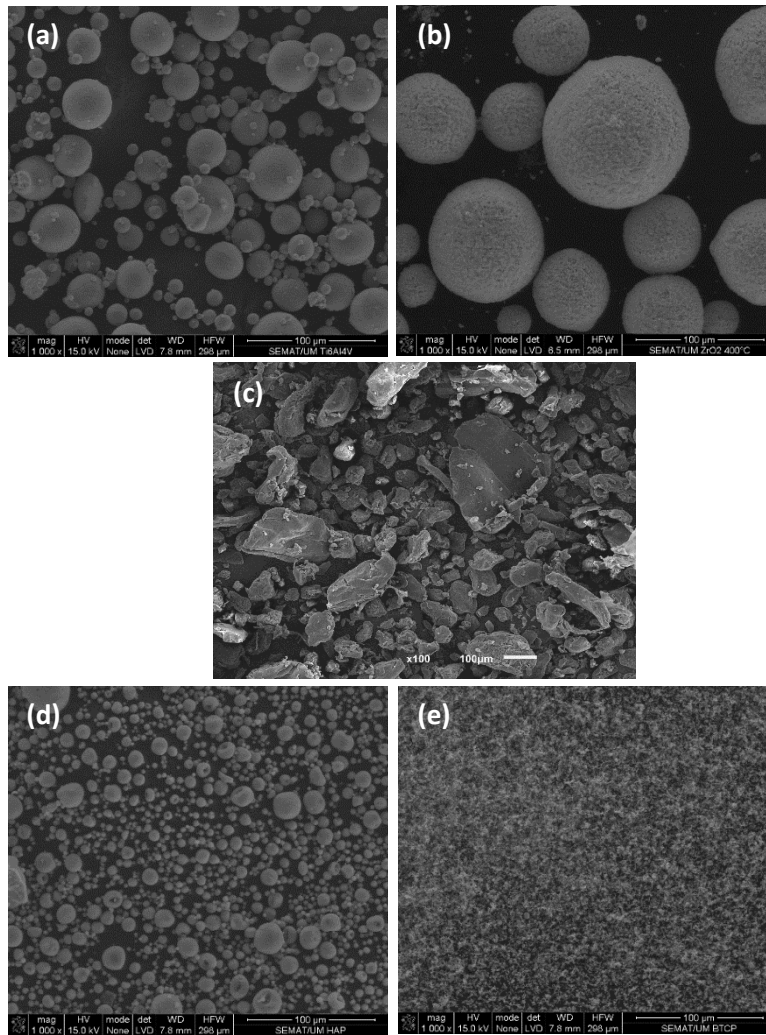


**Figure 26**-SEM images of (a) Ti6Al4V, (b) ZrO<sub>2</sub>, (c) PEEK, (d) HAp and (e) βTCP powders.

## Development of bioactive materials for dental implants using powder metallurgy

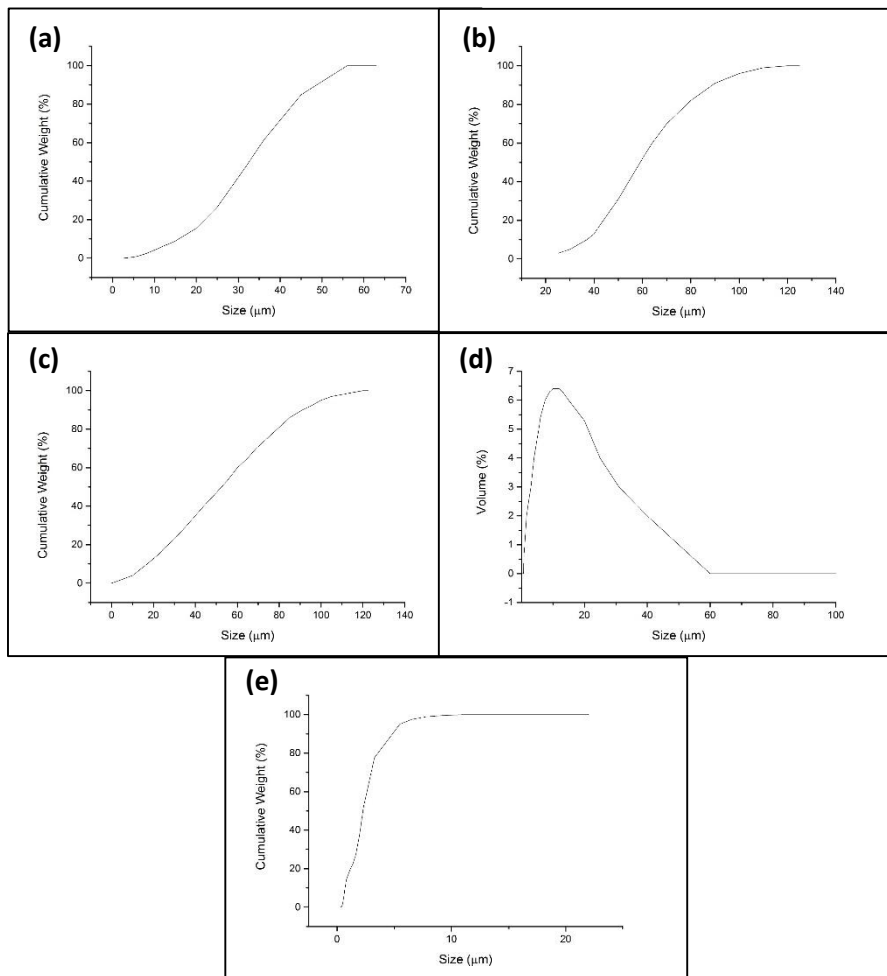


**Figure 27**-Particle size distribution of (a) Ti6Al4V, (b) HAp, (c)  $\beta$ TCP, (d) ZrO<sub>2</sub>, and (e) PEEK powders (according to the manufacturer).

## 3.2. METHODS

### 3.2.1. DISPERSION METHODS

As mentioned, when using powder metallurgy to fabricate composites, a prior efficient mixing of the powders is mandatory in order to obtain final parts with suitable mechanical performance. Some powders are cohesive and naturally they stick together and it is difficult to separate or disperse for further powder processing and characterization. This formation of agglomerates, especially when using small sized reinforcements, occurs due to attractive Van de Waals forces [125, 133, 134], and can also lead to parts with lower density [135]. Thus, dispersion methods are required to deagglomerate the particles, such as mechanical stirring, ultrasonic agitation, etc [125].



## Development of bioactive materials for dental implants using powder metallurgy

In this context, four different dispersion methods were used to prepare composite mixtures and were compared in order to conclude which one would be the most suitable for further processing of implants with the desired properties. This comparison between the different dispersion methods was made using Ti6Al4V-HAp and also Ti6Al4V- $\beta$ TCP and further extrapolated for the other composites. Figure 28 illustrates the four different dispersion methods addressed.

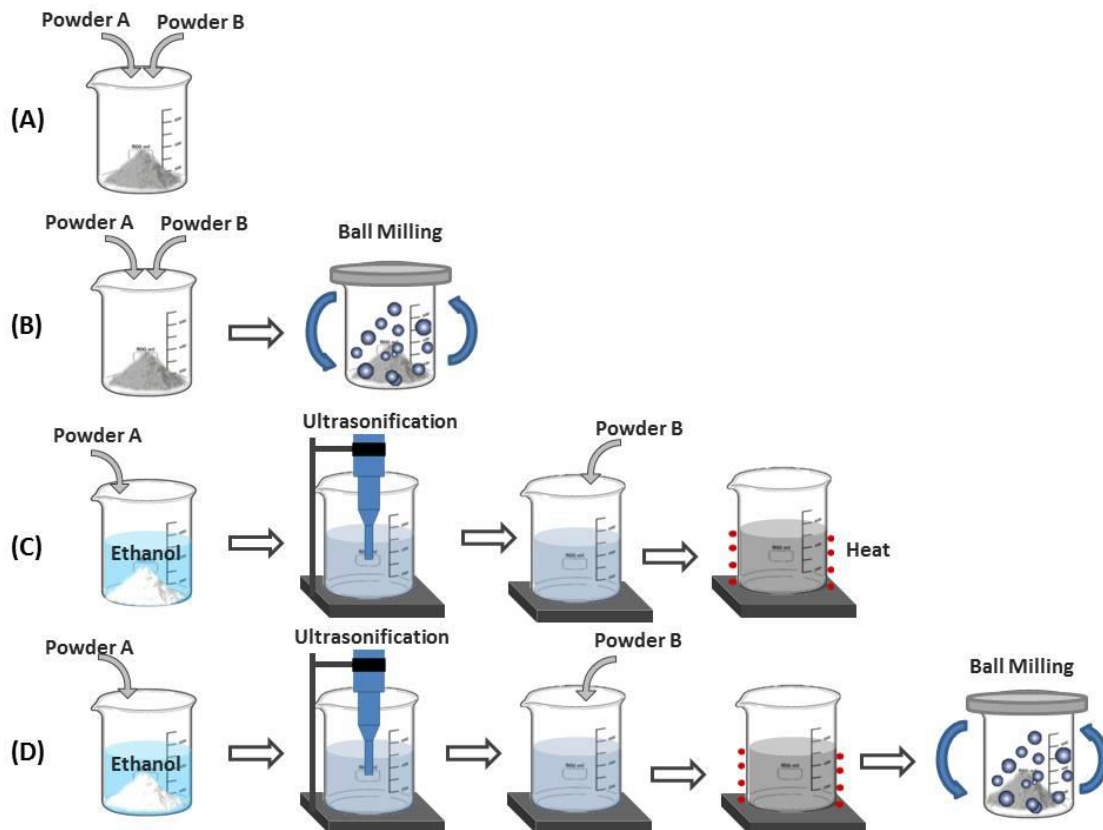


**Figure 28-** Schematic illustration of the dispersion methods used, where powder A corresponds to the bioactive material (HAp or  $\beta$ TCP) and powder B to the biocompatible material (Ti6Al4V).

The first dispersion method (A) comes down to simply blending the matrix and reinforcement powders. Ti6Al4V-10HAp mixture was prepared using a batch of 0.29g of HAp along with 3,65g of Ti6Al4V. Another batch of Ti6Al4V-10 $\beta$ TCP was prepared using 0.28g of  $\beta$ TCP with 3,65g of Ti6Al4V.

The second dispersion method (B) corresponds to ball milling. Ball milling, more specifically high energy ball milling is a grinding method that can be used as a dispersion method once it is able to separate materials due to the interaction between the balls [136]. For this procedure 240 polymeric balls with a diameter of 6mm approximately were placed together with the following amount of powder: 0.29g of HAp with 3,65g of Ti6Al4V (Ti6Al4V-10HAp mixture) and 0.28g of  $\beta$ TCP with 3,65g of Ti6Al4V (Ti6Al4V-10 $\beta$ TCP mixture) and mixed by using a high-energy vertical shaker mill.

The third dispersion method (C) that was used was ultrasonification, in which ultrasound energy is used to agitate particulates in a solution. The principle behind this technique is that when ultrasonic waves propagate in a medium, alternating low and high pressure waves are generated, leading to the formation of vacuum bubbles that subsequently collapse. This phenomenon, known as cavitation, provokes high pressure between the particles and separate them from each other, making ultrasound an effective way for deagglomeration [137–139]. Following this procedure, 0.29g of HAp or 0.28g of  $\beta$ TCP were weighed and placed together with a small quantity of alcohol. The ultrasound was applied on this solution during 30 seconds (40KHz, 200W) and then a weighted amount of Ti6Al4V (3.65g) powder was introduced. The volume of alcohol was strictly controlled to make the solution viscous in order to prevent the occurrence of decantation. After that, the solutions (Ti6Al4V+HAp in alcohol / Ti6Al4V+  $\beta$ TCP in alcohol) were heated on a furnace for about one hour and a half at 60°C to allow alcohol evaporation.

The final dispersion method (D) that was tested comprises a combination of ultrasonification and ball milling. Firstly, the bioactive material was weighed (0.29g of HAp or 0.28g of  $\beta$ TCP) and mixed with a small amount of alcohol. Afterwards, ultrasound was applied and after some seconds, Ti6Al4V (3.65g) was added to this solution. The final solution was then dried in a furnace (similarly to the procedure described above) and finally ball milled with 240 polymeric balls having a diameter of 6 mm.

From the four dispersion methods that were tested, ultrasonification (C) was found to be the best process, once it shows better dispersion of the reinforcing bioactives in the selected matrix, as will be further discussed on chapter 4. This method was applied for producing all the composite materials (Ti6Al4V-based composites, ZrO<sub>2</sub>-based composites and PEEK-based composites).

### 3.2.2. HOT PRESSING

Different materials demanded different molds and in this work, three types of molds were designed and produced. During the hot pressing process, pressure is applied by two cylindrical punches with a diameter of 8 mm, that are inserted inside the mold. Ti6Al4V and Ti6Al4V-based composites were processed using a graphite mold with a cylindrical shape with the following dimensions: 8 mm internal diameter x 36 mm external diameter x 30 mm height. PEEK and PEEK based- composites were processed using a steel mold [8 mm internal diameter x 29 mm external diameter x 45mm height]. Figure 29 illustrates each type of mold and punches. On the other hand, ZrO<sub>2</sub> and ZrO<sub>2</sub>-based composites were processed with a graphite mold with ceramic inserts as can be seen in figure 30.

## Development of bioactive materials for dental implants using powder metallurgy

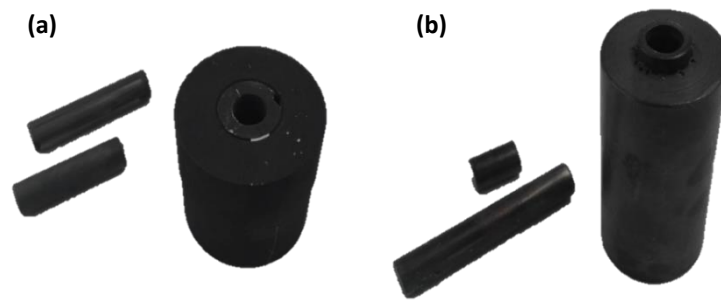


**Figure 29-** Molds and punches used to process the materials (a) Ti6Al4V graphite mold and punches (b) PEEK steel mold and punches.

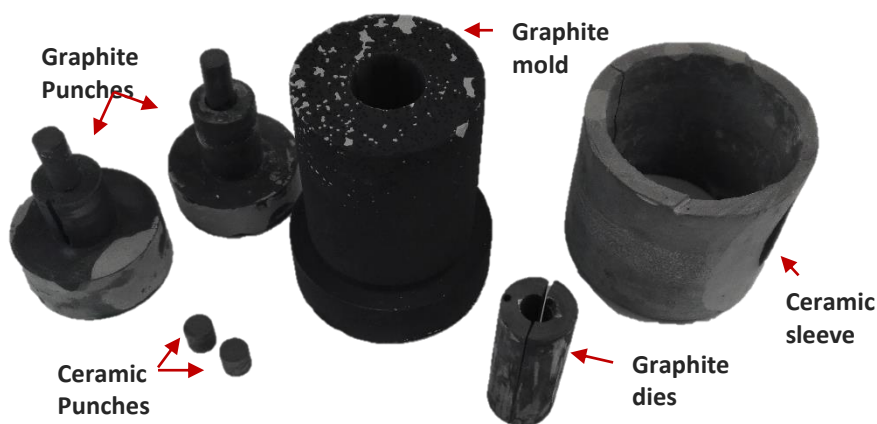


**Figure 30** - System used to process  $ZrO_2$  and  $ZrO_2$ -based composite materials.

Different materials demand different processing conditions, that will be subsequently described in detail.

### **A: Processing of Ti6Al4V and Ti6Al4V-based composites**

In this section Ti6Al4V, Ti6Al4V-10HAp composite and Ti6Al4V-10 $\beta$ TCP samples processing condition will be described.

Initially, the powder mixtures were prepared using the dispersion method mentioned above (C). Subsequently, the powders were weighed and placed into the graphite mold. The mold was previously painted on its inside as well as in the extremities of the punches with zirconia ink in order to prevent the direct contact between the graphite and the sample and consequently prevent the diffusion of carbon into the samples. Posteriorly, when the powder was inside the mold and the punches were properly positioned, it was again painted with zirconia ink to prevent radiative heat transfer to the chamber. The mold was positioned so that the thermocouple was located close to the site where the powders are placed, in order to acquire temperature values closest to the ones that powders are in fact withstanding.

## Development of bioactive materials for dental implants using powder metallurgy

The mold/thermocouple system was placed inside the chamber and centered with the induction coil (the apparatus can be seen in figure 31). Vacuum was performed by a vacuum machine (Alcatel Adixen 2005SD) numbered 1 in figure 32 and an initial pressure was applied to the mold. The powder was heated gradually with a heating rate of  $78^{\circ}/\text{min}$  until it reaches  $1175^{\circ}$  and then, a pressure of 40MPa was stipulated and maintained for 30 minutes. The heat was provided by an induction coil represented by the number 3 in figure 32 (most noticeable in figure 31) and pressure through a hydraulic pump numbered by the number 2 also presented in figure 32. The process parameters for Ti6Al4V and Ti6Al4V-based composites was based on previous studies [140]. During this cycle, the values of pressure and temperatures were kept approximately constant. After this time stage the induction was turned off and the sample was allowed to cool inside the chamber till room temperature. Vacuum was removed and the sample was demolded using a manual press.

The final samples have a diameter of 8 mm and an average height size of 2 mm, as predicted.

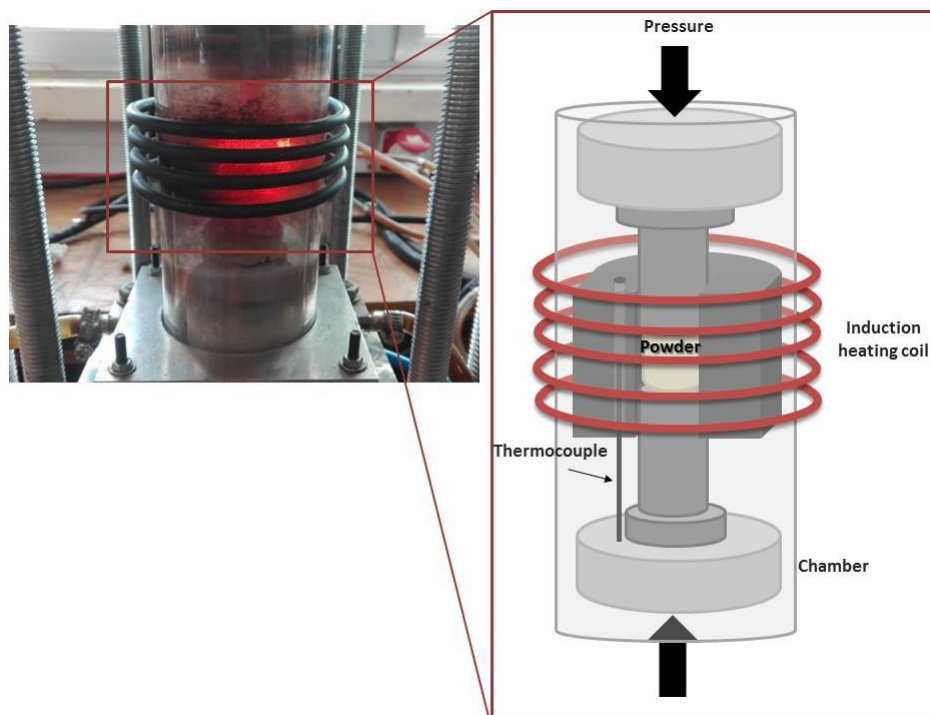


**Figure 31**-Hot Pressing picture and schematic representation.

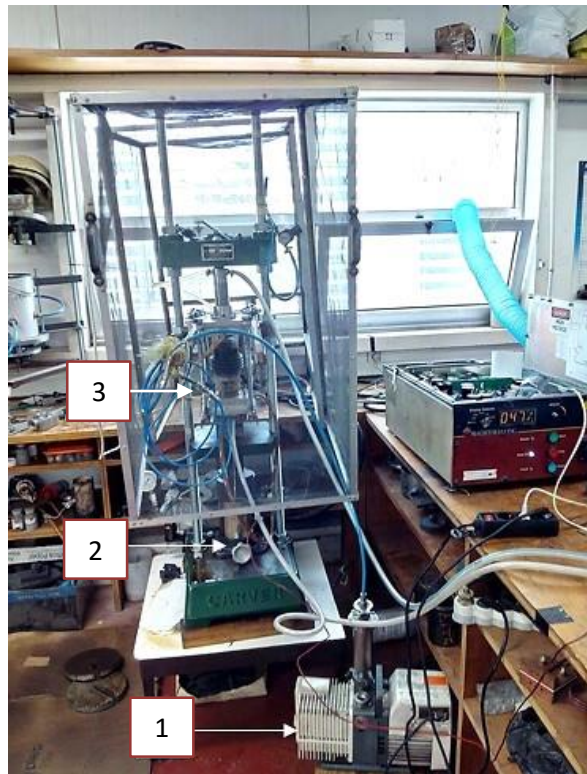


**Figure 32** – Hot Pressing overall system (1) vacuum machine, (2) hydraulic machine, (3) induction coil.

### **B: Processing of $ZrO_2$ and $ZrO_2$ -based composites**

$ZrO_2$ ,  $ZrO_2$ -10HAp and  $ZrO_2$ -10 $\beta$ TCP hot pressing general procedure was somehow similar to Ti6Al4V, however some relevant differences are found. Before the hot pressing process and powder mixtures by ultrasonification, the  $ZrO_2$  powder was heated at 400°C for 30min to remove the binder and prevent discoloration of  $ZrO_2$  after the sintering process. Furthermore, the mold and the extremities of the punches were painted with zirconia ink and the powder was weighed and placed inside the mold. After painting the mold outer surfaces, the mold was placed to assure a correct thermocouple positioning. When correctly positioned inside the chamber, the powder was heated to 1175°C with a heating rate of 117.5°C/min while the pressure was gradually applied until 100 MPa. This temperature and pressure were thus maintained constant over 15 minutes [141]. Samples with 8 mm diameter and an average height size of 2 mm were obtained.

### **C: Processing of PEEK and PEEK-based composites**

PEEK, PEEK-10HAp and PEEK-10 $\beta$ TCP samples were produced using a steel mold and punches. Consequently, it was not necessary to use zirconia ink since steel doesn't react with PEEK, however it

## Development of bioactive materials for dental implants using powder metallurgy

was required to paint the punches with a coupling grease in order to promote the lubrication of the punches to reduce friction during the pressing. In this case, the powder was weighted and placed directly inside the steel mold and the steel punches positioned. After placing and positioning the mold inside the chamber, an initial pressure was applied to compress the powder. The mold was then heated until reaching 380°C (above the melting point of PEEK (345°C)) using a heating rate of 80°/min. Posteriorly, the temperature was decreased until 300°C and a pressure of 25MPa was applied and upheld for 5 seconds. The induction was turned off and the following process was identical to the previous approaches. When room temperature was achieved, the sample was removed and demolded, remaining with the desired dimensions of 8mm (diameter) x 2mm (height). The processing temperature and pressure selection was based on previous studies [51].

### 3.2.3. PRESS AND SINTERING

Beside hot pressing process, press and sintering were also performed to produced  $ZrO_2$  and  $ZrO_2$ -based composite samples. In this process, the samples were produced using a steel mold and punches were the steel mold has 10mm internal diameter x 40mm external diameter x 50mm height and the punches have both 8mm in diameter but one has 56mm in height and the smaller has 13mm (figure 33).



**Figure 33** – Steel mold and punches used to process the materials

In this case, contrary to what happens before the hot pressing process of  $ZrO_2$  and  $ZrO_2$ -based composites, the  $ZrO_2$  powder was not heated at 400°C for 30min to remove the binder once in this technique the binder is essential to the maintenance of the green compact. The  $ZrO_2$ -HAp and  $ZrO_2$ - $\beta$ TCP powder mixtures were prepared based on the dispersion method selected before.

The press and sintering process begins with the placement of a zinc stearate inside the mold and on the extremities of the punches to facilitate the extraction of the sample out of the mold. Subsequently,



## Development of bioactive materials for dental implants using powder metallurgy

the smaller punch is positioned on the mold, the powder weighed and placed into the mold followed by the positioning of the higher punch. Then, the powder inside the mold is pressed slowly by a hydraulic press (figure 34(a)) with a pressure of 200MPa which was maintained for 30 seconds and then gradually removed. Once pressed, the samples were removed from the mold with subsequent sintering in a sintering furnace Zirkonofen 700 ultra-vacuum (figure 34(b)) until the sample reaches 1500°C and kept for 2 hours with a heating and cooling rate approximately of 8°C/min [142]. The final samples have a diameter of 8mm and an average size of 2mm in height, as predicted.



**Figure 34-**(a) hydraulic press (Bb) Zirkonofen 700 ultra-vacuum sintering furnace.

### 3.2.4. MATERIALS CHARACTERIZATION

#### 3.2.4.1. Specimens preparation

Once the samples are processed, they need to be prepared for further characterization, starting with the polishing of the samples and finishing with its cleaning.

The polishing was performed using a MECAPOL P251 polisher (figure 35) and different types of sand papers with different meshes. With this procedure, the purpose is to polish the surface of the samples in order to obtain surfaces with near mirror finishing. The series of sand papers used for polishing all the samples were: P180, P320, P600, P800, P1200, P2000 and P4000. The polishing initiates with the sand paper with the largest grain size (P180) followed by the sand paper with a mesh smaller than the previous one (P320), and so forth. Between the exchanges of the papers, the sample is rotated 90 ° in relation to the previous position, in order to assess if the previous scratches were

eliminated. Lastly, after polishing, the samples were all cleaned for 8 minutes in a digital ultrasonic cleaner.



**Figure 35** – MECAPOL P 251 polisher

#### **3.2.4.2. SEM/EDS**

The different powder mixtures of the different dispersion methods and the final samples (after polishing) were analyzed by Scanning Electron Microscopy (SEM) and Energy-dispersive X-ray spectroscopy analysis (EDS). SEM analysis provides high magnification imaging of the surface of the material which facilitates the image interpretations. SEM generates an electron beam that interacts with the sample creating signals that make possible the acquisition of an image. On the other hand, EDS technique detects x-rays arising from the ionization of the atoms of a sample which suffered from high-energy radiation. This x-rays are converted into signals and consequently into an X-ray energy histogram. With SEM/EDS images it is possible not only to obtain information concerning the topography and composition of the material (SEM) but also provides its chemical characterization (EDS). Thus, this study focuses on the analysis of the surface of the samples produced in order to assess the bonding/interface between matrix and reinforcement, the existence of porosity, chemical composition, the possible degradation of bioactive materials and the potential formation of new compounds during the processing of the samples [143, 144]. Figure 36 shows the SEM/EDS equipment used for the analysis, a NanoSEM - FEI Nova 200 (FEG/SEM); EDAX - Pegasus X4M (EDS/EBSD).





**Figure 36** – SEM/EDS equipment.

Porosity analysis was performed by image processing using the software image J by the application of a threshold filter of the images obtained from SEM.

### 3.2.4.3. Vickers hardness test

Vickers hardness tests were performed in order to obtain the micro-hardness of the samples produced. This method consists of indenting the samples with a diamond indenter and from this indentation two diagonals will be measured, allowing the calculation of the hardness by using the following equation:

$$HV = 1,8544 \times \frac{F}{d^2},$$

where  $d$  is the arithmetic mean of the two diagonals and  $F$  the load in kgf.

The tests were performed along the polished sample using a Vickers micro-hardness tester (DuraScan, emcotest). This process uses a quadrangular pyramid that will create an impression on the surface of the material (indentation) in a lozenge form. For this technique the samples need to be with parallel faces and the face that will be analyzed polished. The calculation of the average hardness values was obtained from 5 indents for each sample. Vickers hardness was measure on Ti6Al4V and Ti6Al4V-based composites under a load of 500g for 15s [145] and PEEK and PEEK-based composites hardness was measure using 100g load and a 15s loading time [146]. ZrO<sub>2</sub> and ZrO<sub>2</sub>-based composites hardness

was measure with a load of 500g for 15s. Figure 37 shows the Vickers micro-hardness tester used for the determination of the hardness of all samples.



**Figure 37** – Vickers micro-hardness tester DuraScan, emcotest.

#### **3.2.4.4. Shear tests**

In order to assess the shear strength of the produced materials (Ti6Al4V, Ti6Al4V-HAp; and Ti6Al4V- $\beta$ TCP; ZrO<sub>2</sub>; ZrO<sub>2</sub>-HAp, ZrO<sub>2</sub>- $\beta$ TCP; PEEK; PEEK- HAp; PEEK- $\beta$ TCP), shear tests were performed. This test assesses the maximum stress that the material can sustain before rupture. Four samples were tested for each material that was processed and the average value was calculated.

The sample was positioned with half of the sample fixed in a metal support, leaving the other half exposed, in which the cutting insert will actuate. The test was conducted in a servohydraulic machine presented in figure 38 (Instron 8874) with a capacity load cell of 25kN, with a crosshead speed of 0.02 mm/s, at room temperature ( $\approx 25^{\circ}\text{C}$ ).



**Figure 38** – Servohydraulic machine Instron 8874.

Figure 39 shows the custom-made stainless steel apparatus along with a sliding part armed with a cutting tool.

With the displacement and load taken from the universal testing machine, the stress-strain graph can be built and the maximum shear stress determined according to the following equation:

$$\tau_{\text{máx}} = \frac{\textit{maximum load}}{\textit{(diameter} \times \textit{thickness)}}$$

where  $\tau$  is expressed MPa, the maximum load in N and the diameter and thickness in mm.

Development of bioactive materials for dental implants using powder metallurgy

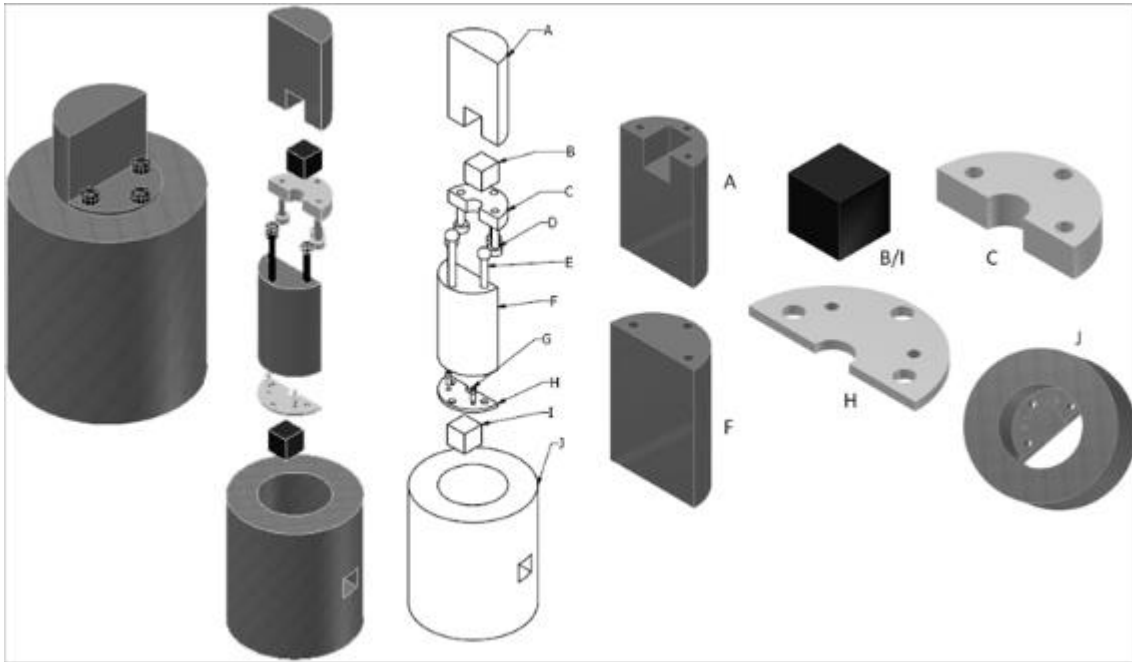


**Figure 39-** System apparatus to measure shear stress

# CHAPTER 4

## RESULTS AND DISCUSSION

---

Chapter 4 reports all the results of the samples characterization as well as a discussion of them. This chapter is divided into subchapters in order to highlight and explain all the results of the different types of samples in an organized and perceptible way. The first subchapter exhibits the results and discussion from the different powder dispersion methods, then a subchapter that evaluate the bioactive materials condition after hot pressing. The follow three subchapters the analysis of the results of all samples already processed by the appropriate processing method. Finally, in a last subchapter it is presented some additional studies made by other researches that are still on going.

#### 4.1. DISPERSION METHODS ANALYSIS

The fabrication of composites with suitable mechanical properties is largely related to the prior mixing of the powders. Powder agglomeration may compromise the mechanical properties of a composite; therefore, it is essential to mix the powders to obtain a dispersed homogeneous mixture. It is visible in figure 40, representing a SEM image of  $\beta$ TCP powder, that the particles constituting the powder are naturally agglomerated. This can be explained, as previously mentioned, by the attractive Van der Waals forces, especially when using powders with small particle sizes [125, 133, 134, 147]. Therefore, in order to enhance the mechanical properties of these composites, different mixing processes were performed on Ti6Al4V-10HAp and Ti6Al4V-10 $\beta$ TCP powders mixtures, as described in detail in Chapter 3 - Materials and methods.

These results are presented divided into two sections: a first section presenting the results of the different mixing processes of Ti6Al4V-10HAp mixtures and a second section showing the results of Ti6Al4V-10 $\beta$ TCP mixtures.

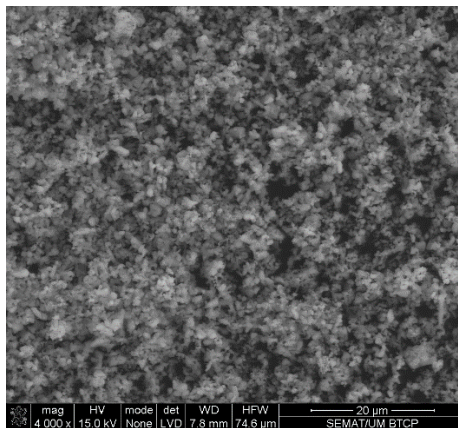


**Figure 40** – SEM image of  $\beta$ TCP powder.

##### 4.1.1. Ti6Al4V-10HAP POWDERS MIXTURE

Figure 41 shows SEM images of Ti6Al4V-10HAp powders mixture using the first dispersion method (A), that is simply blending the powders. Likewise, it is possible to observe in figure 42 the SEM images of Ti6Al4V-10HAp powders mixture when mixed by ball milling (B). Ultrasonic agitation (C) results are visible in figure 43 and finally, the images from the combination of ultrasonification with ball milling, the last dispersion method (D), are presented in figure 44. These SEM images show two types of detection modes: the first one is secondary electron image (SE) and the second one backscattered electron image

(BSE). SE images provides information about the morphology of the powders and BSE images are related to the atomic number of the specimen, which means that this type of detection mode provides information about the different elements, due to the differences in their atomic contrast. With this detection mode, it is then possible to distinguish on the images (presented in b) images of each figure) the presence of Ti6Al4V in a lighter color and HAp in a darker color. Particle size of each powder could allow to distinguish Ti6Al4V from HAp once Ti6Al4V have a higher particle size ( $d_{50}=32.53\mu\text{m}$ ) in comparison with the bioactive material ( $d_{50}=10\mu\text{m}$ ).

By analyzing the images below, it is possible to conclude that among these four dispersion methods, the ones who presented a better distribution of the HAp in the matrix (Ti6Al4V) are the method (A) and (C).

In figure 41 (dispersion method A), it is possible to observe a homogeneous mixture between Ti6Al4V and HAp powders. However, when high energy ball milling was performed (B) on these mixtures, figure 42 shows that hydroxyapatite particles not have the same particle size that had initially ( $d_{50}=10\mu\text{m}$ ). In fact, it can be observed that the HAp particles fracture and start to surround the Ti6Al4V particles, phenomenon that could prevent further compaction and sintering, since it will decrease particle packing and, consequently, the bonding between Ti6Al4V particles [125]. This phenomenon was not verified when Ti6Al4V-10HAp powder mixtures where ultrasonic mixed (C). Figure 43 demonstrates that the process of ultrasonification allows a homogenous dispersion of the powders without the occurrence of the fracture of the particles, as happens in ball milling process. Thus, in the fourth method (D) after ultrasonification a ball milling process were performed (figure 44) and the same phenomenon of HAp particle fracture occurs.

This study allowed concluding that the most suitable powder dispersion method, for guaranteeing a further effective compaction and sintering are methods (A) and (C).



## Development of bioactive materials for dental implants using powder metallurgy

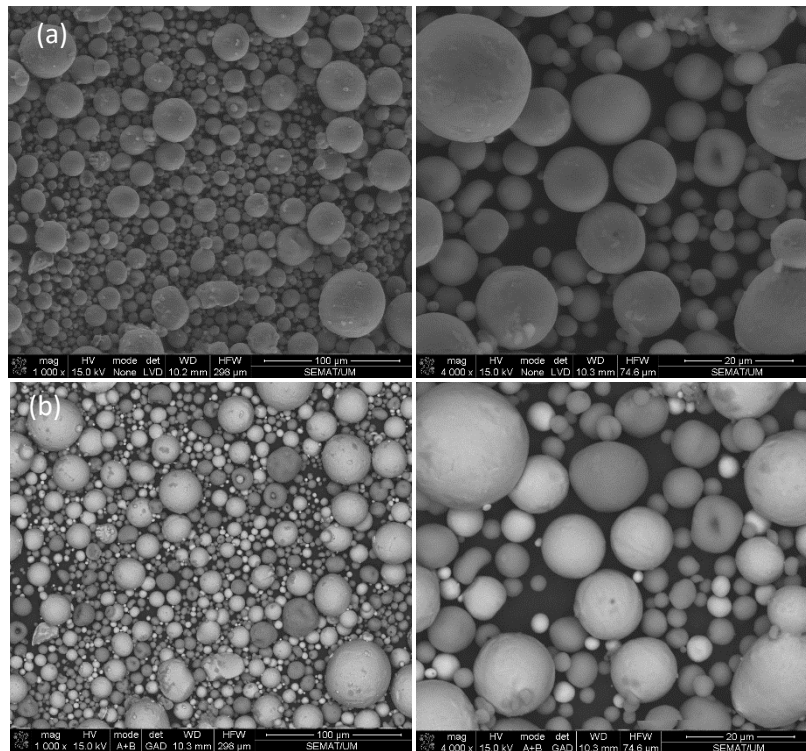


**Figure 41** – SEM images of Ti6Al4V-10HAp powders mixture after blending (method A) at magnifications of 1000x (left) and 4000x (right). (a) secondary electron image (SE) and (b) backscattered electron image (BSE).

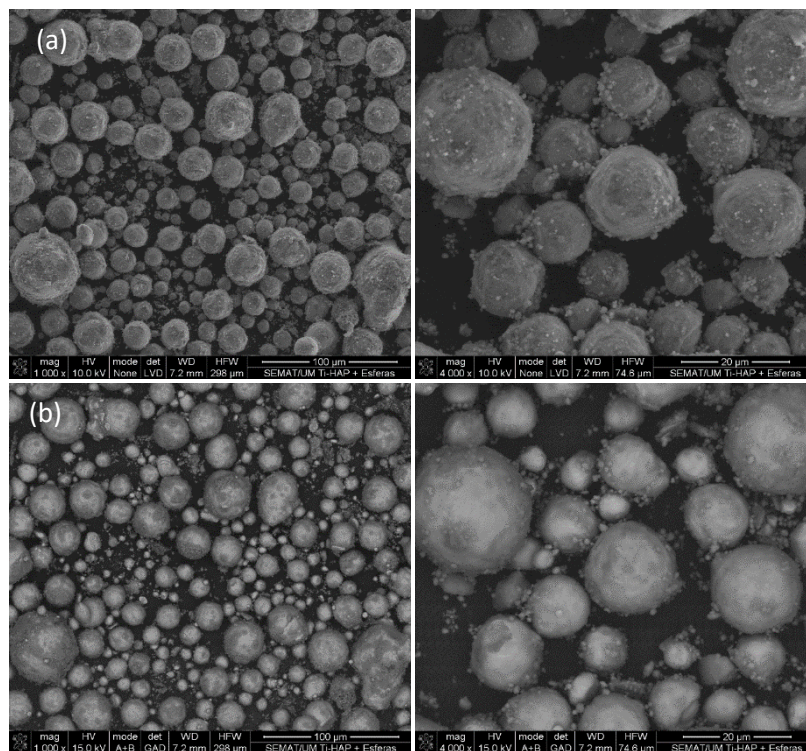


**Figure 42** - SEM images of Ti6Al4V-10HAp powders mixture after ball-milling (method B) at magnifications of 1000x (left) and 4000x (right). (a) secondary electron image (SE) and (b) backscattered electron image (BSE).



## Development of bioactive materials for dental implants using powder metallurgy

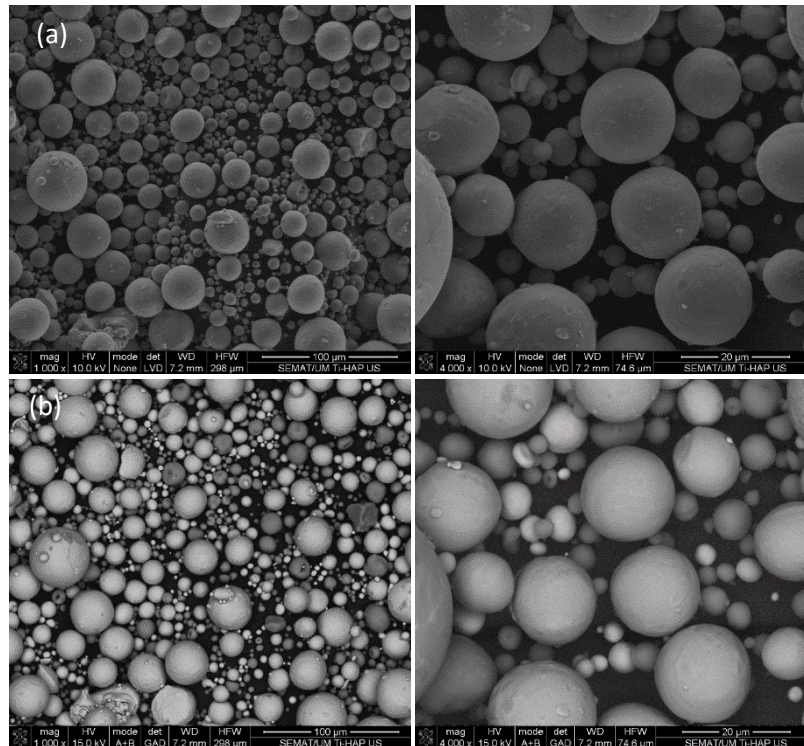


**Figure 43** - SEM images of Ti6Al4V-10HAp powders mixture after ultrasonification (method C) at magnifications of 1000x (left) and 4000x (right). (a) secondary electron image (SE) and (b) backscattered electron image (BSE).

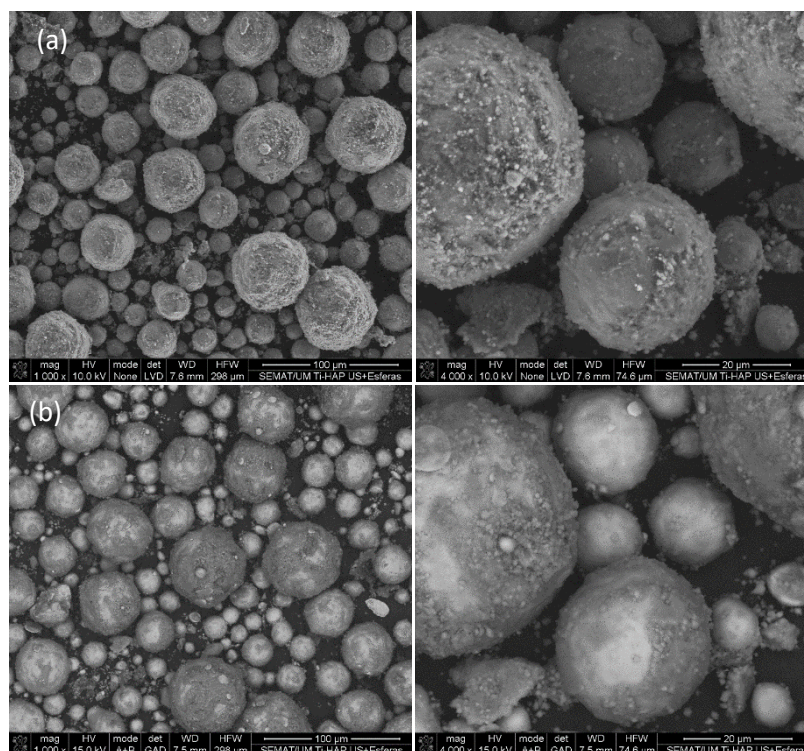


**Figure 44** - SEM images of Ti6Al4V-10HAp powders mixture after ultrasonification followed by ball-milling (method D) at magnifications of 1000x (left) and 4000x (right). (a) secondary electron image (SE) and (b) backscattered electron image (BSE).

4.1.2. Ti6Al4V-10 $\beta$ TCP POWDERS MIXTURE

The following figures report the results obtained from the different dispersion methods for Ti6Al4V-10 $\beta$ TCP powder mixture. SEM images of the first dispersion method of blending the powders (method (A)) are indicated in figure 45. Ball milling powder mixture (method (B)) results can be observed in figure 46 and ultrasonification method (C) in figure 47. Finally, figure 48 corresponds to the results from the powder dispersion method (D).

Unlike what happens in Ti6Al4V-10HAp mixtures, the results from the first dispersion method (A) were not satisfactory. As previously mentioned in this chapter,  $\beta$ TCP particles are naturally agglomerated, due to their lower particle size ( $d_{50}=2.26\mu\text{m}$ ). This fact alone allows concluding that simply blending the powders would not deagglomerate the powder particles, as can be clearly seen in figure 45. Further, when the powder mixture was subjected to the ball milling process (B), a very similar outcome was verified, as can be seen in figure 46, showing that the  $\beta$ TCP particles are covering the Ti6Al4V particles. However, when using simply ultrasonic agitation (C), not only the  $\beta$ TCP particles are not involving the Ti6Al4V particles, but they are homogeneously dispersed between Ti6Al4V particles (figure 47). This does not occur when performing ball milling after ultrasonification (D) once it is observable in figure 48 that results similar to those obtained by the ball milling process were achieved.

Therefore, in this powder mixtures, these SEM images allowed to conclude that the most suitable powder dispersion method for achieving an effective compaction and sintering are method (C), ultrasonification.

Thus, the most suitable method for Ti6Al4V-10HAp and Ti6Al4V-10 $\beta$ TCP powder mixtures is ultrasonification (method (C)), once both results are positive for a homogeneous reinforcement dispersion. The different results founded in both powders mixtures, Ti6Al4V-10HAp and Ti6Al4V-10 $\beta$ TCP, are related to the differences of particle sizes of each bioactive material. As mentioned,  $\beta$ TCP particle size are low ( $d_{50}=2.26\mu\text{m}$ ) once HAp particle size are  $10\mu\text{m}$ , thereby, the probability of particle agglomeration is higher on  $\beta$ TCP than on HAp, once smaller particle have higher tendency to agglomeration [125].

In light of these conclusions, ultrasonification method was selected to be used for preparing all the other composites mixtures, namely PEEK and PEEK-based composites and  $\text{ZrO}_2$  and  $\text{ZrO}_2$ -based composites.



## Development of bioactive materials for dental implants using powder metallurgy

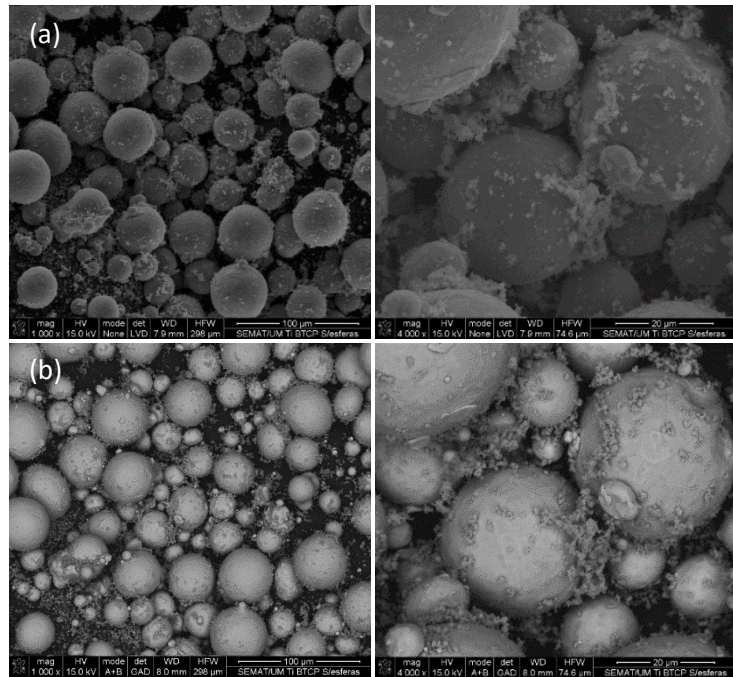


**Figure 45** – SEM images of Ti6Al4V-10βTCP powders mixture after blending at magnifications of 1000x (left) and 4000x (right). (a) secondary electron image (SE) and (b) backscattered electron image (BSE).

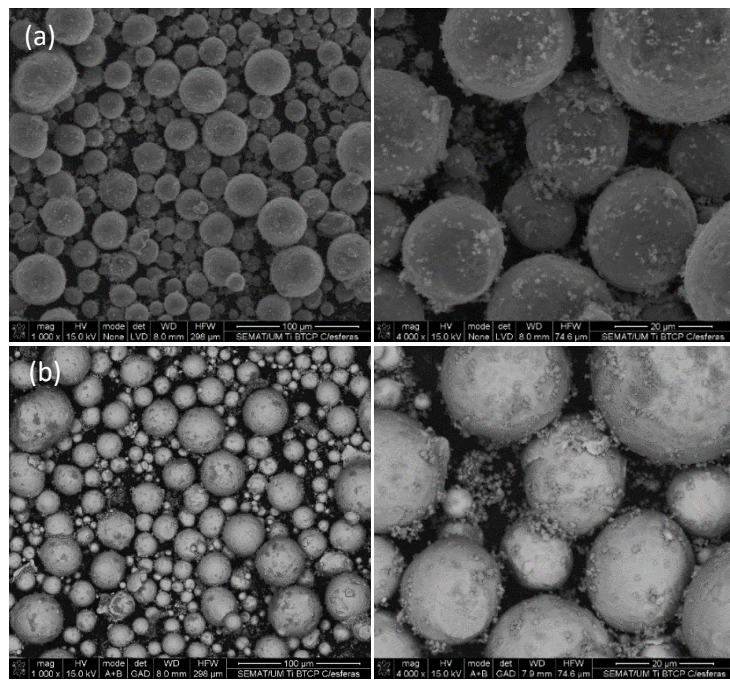


**Figure 46** - SEM images of Ti6Al4V-10βTCP powders mixture after ball-milling at magnifications of 1000x (left) and 4000x (right). (a) secondary electron image (SE) and (b) backscattered electron image (BSE).

## Development of bioactive materials for dental implants using powder metallurgy

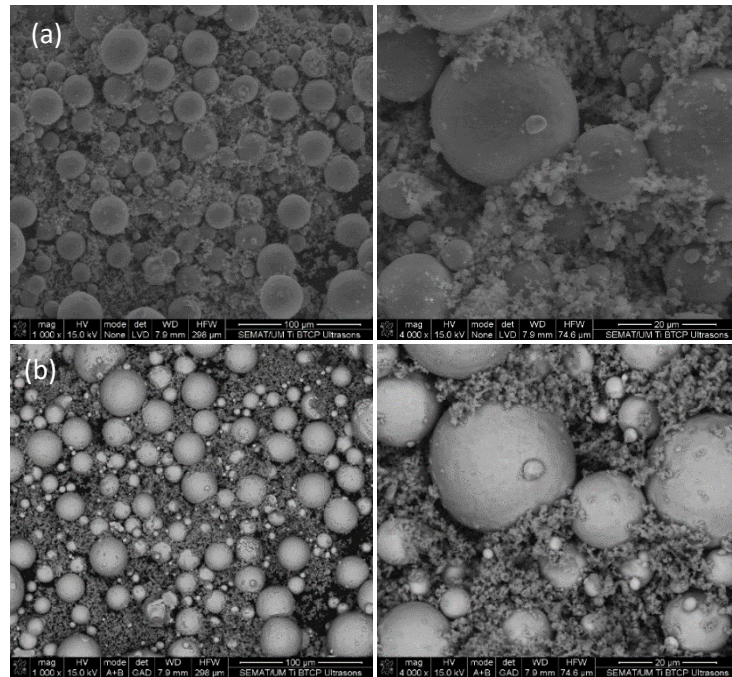


**Figure 47** - SEM images of Ti6Al4V-10 $\beta$ TCP powders mixture after ultrasonification at magnifications of 1000x (left) and 4000x (right). (a) secondary electron image (SE) and (b) backscattered electron image (BSE).

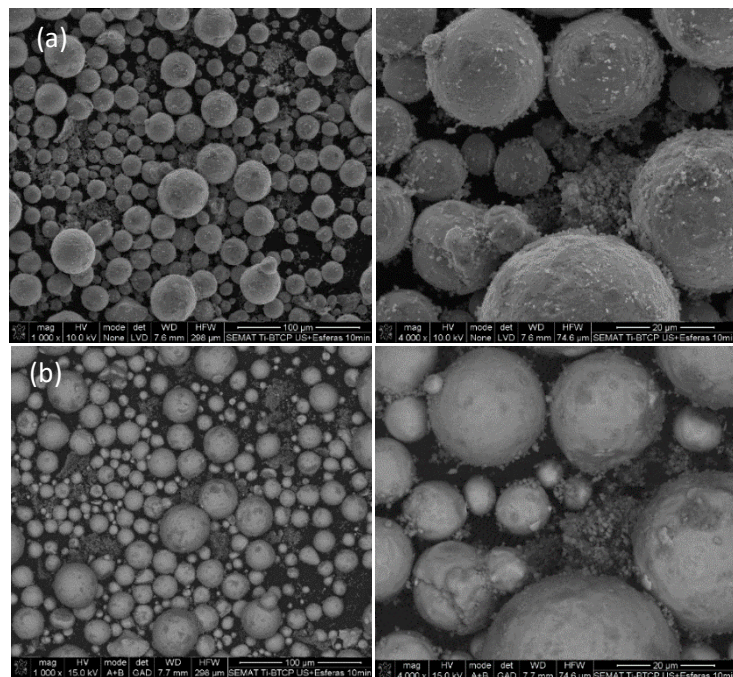


**Figure 48** - SEM images of Ti6Al4V-10 $\beta$ TCP powders mixture after ultrasonification followed by ball-milling at magnifications of 1000x (left) and 4000x (right). (a) secondary electron image (SE) and (b) backscattered electron image (BSE).

#### 4.2. ASSESSMENT OF THE BIOACTIVE MATERIALS CONDITION AFTER HOT PRESSING

Since these materials are going to be processed at high temperatures, another aspect to take in consideration is the thermal behavior of HAp and  $\beta$ TCP. In fact, many studies have been made in order to analyze the effect of temperature on these materials.

As previously mentioned, the decomposition of  $\beta$ TCP occurs at temperatures well above those used in this study for the processing of the samples (around 1450°C) [106], however the same does not occur with HAp. Several studies already report that HAp can suffer decomposition when exposed to certain temperatures and/or environment conditions [96, 106, 107, 14–150]. Therefore, degradation of HAp not only could lead to the loss of its bioactive properties but also could inhibit densification, which would reduce the composite mechanical properties [107].

Therefore, a XRD analysis was performed on hydroxyapatite after sintering at 1175°C during 30 minutes. XRD analysis was also done in hydroxyapatite initial powder in order to compare with the sintered HAp XRD spectrum. The results are evidenced in figure 49. From this analysis it is possible to conclude that, despite the peaks are not extremely well-defined, the peaks of the powder spectrum are in accordance with HAp peaks, thereby demonstrating that there are no other components in the starting powder. The sintered HAp XRD spectrum revealed more defined peaks, with higher intensity (figure 49(b)), which proves the crystallization of the HAp powder. Chunyan Wang et al. reported similar results when investigating the influence of temperature on HAp, concluding that, with the increase of temperature, the HAp powder crystallized better [106]. Y. Yang et al. when investigating the interaction between HAp and titanium at high temperatures also reported XRD spectra with similar results [148].

Comparing these two spectra, it is possible to conclude that the peaks presented in sintered-HAp corresponds to the peaks of the HAp powder. This indicates that no considerable degradation occurred on HAp when sintering at 1175°C during 30 minutes.



## Development of bioactive materials for dental implants using powder metallurgy

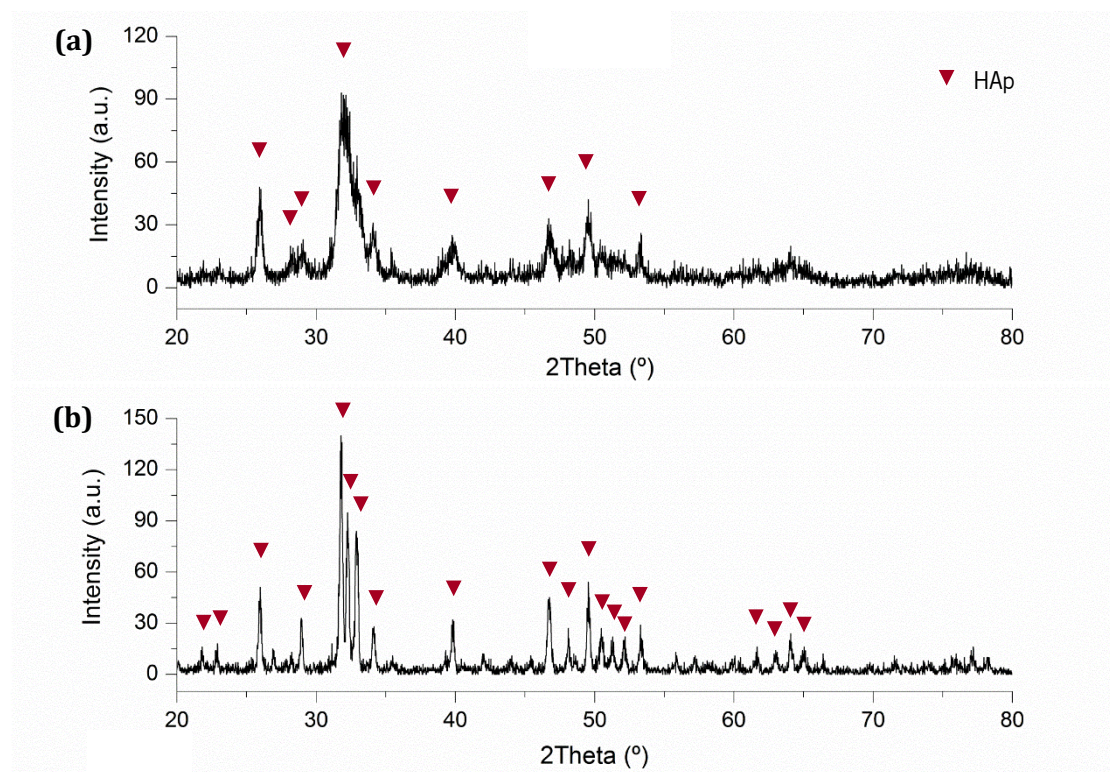


**Figure 49** – XRD plot of (a) HAp powder and (b) HAp sample after Hot Pressing at 1175° during 30 minutes.

#### 4.3. Ti6Al4V AND Ti6Al4V-BASED COMPOSITES CHARACTERIZATION

After selecting the most effective dispersion method and assessing the HAp conditions, a complete characterization of the samples processed by hot pressing was performed. In this subchapter, the results for the Ti6Al4V and Ti6Al4V-based composites are presented and discussed. For a comparative analysis, in addition to the analysis of Ti6Al4V-based composites, the investigation of the samples constituted only by the metal matrix (Ti6Al4V) were also characterized. SEM images of polished surfaces of Ti6Al4V, Ti6Al4V-10HAp and Ti6Al4V-10 $\beta$ TCP, at magnifications of 500x and 1000x are presented in figure 50 (a), (b), (c), respectively. Ti6Al4V images exhibit a good densification due to the absence of considerable porosity on the sample, which means that hot pressing parameters were adequate to achieve full densification. This absence of porosity is known to lead to an improvement of the mechanical properties of the sample [125].

When adding a bioactive reinforcement to Ti6Al4V, it is possible to distinguish the reinforcement from the metallic matrix due to the different coloring, as seen in both Ti6Al4V-10HAp and Ti6Al4V-

## Development of bioactive materials for dental implants using powder metallurgy

10 $\beta$ TCP SEM images (Figure 11). As observed in Ti6Al4V samples, both reinforced samples present a good densification, once no visible porosity was detected for these samples.

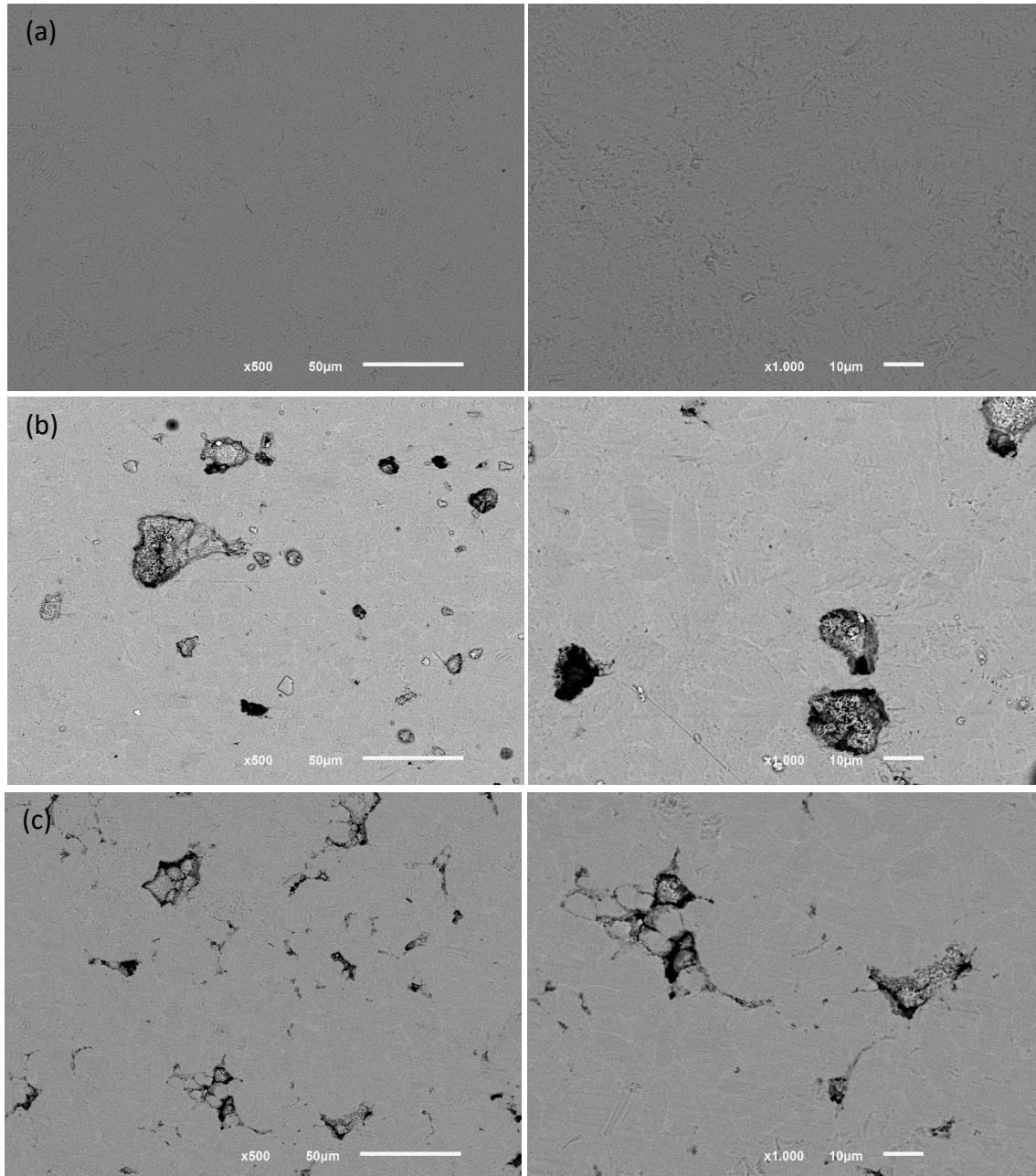


**Figure 50** - SEM images of (a) Ti6Al4V, (b) Ti6Al4V-10HAp and (c) Ti6Al4V-10 $\beta$ TCP samples at magnifications of 500x (left) and 1000x (right).

Additionally, an analysis of the chemical composition of each samples was performed by EDS. EDS analysis on Ti6Al4V sample was done to compared the results with the ones obtained on the composite samples. Ti6Al4V EDS results are shown in Table 8 that exhibits the chemical composition,

in atomic percentage, of the marked zone of figure 51. The chemical compositions of four marked zones of Ti6Al4V-10HAp sample are presented in table 9, and the marked zones can be visible in figure 52.

The first zone, marked as Z1, is a zone where the bioactive material can be found due to the presence of the elements of HAp. However, being HAp formula  $\text{Ca}_{10}(\text{PO}_4)_6(\text{OH})_2$ , its chemical composition in atomic percentage should be 22.72% Ca 13.64% P, 59.09% O and 4.55% H, approximately, which is not observed in the obtained results. This could be explained by the fact that EDS is a semi-quantitative analysis, although not excluding a minor possible formation of other components, thereby indicating decomposition of hydroxyapatite, which may happen either by high temperature processing, atmosphere used, or by reaction with Ti6Al4V. Given the obtained composition, the absence of hydrogen in the chemical composition could be explain by the process of dihydroxylation. Researchers have reported that this phenomenon of loss of the radical OH is gradual but occurs at temperatures below at which is used to process the samples of this study [107, 148]. Additionally, the same quantity of calcium (Ca) and oxygen (O) could represent the presence of calcium oxide that was formed by the decomposition of hydroxyapatite. Moreover, the possible formation of calcium titanate ( $\text{CaTiO}_3$ ) is not ruled out. Some studies revealed that sinterization of HAp/Ti6Al4V under vaccum conditions could lead to the formation of titanium dioxide ( $\text{TiO}_2$ ) due to the interaction of the Ti ions with the O ions derived from HAp, which could further interact with Ca ions from HAp leading, consequently, to the formation of  $\text{CaTiO}_3$  [151]. In a second zone, marked as Z2 in figure 52, a small percentage of phosphorus (P) and aluminium (Al) but with higher quantities of Ti is found. This may indicate that this zone may belong to a bioactive material cluster, formed during hot pressing, that was fractured and removed, possibly as a result of the polishing of the sample. The third zone, marked as Z3, indicate the metallic matrix composition once the chemical composition of this zone is similar to the chemical composition of the Ti6Al4V sample (table 8). However, the absence of vanadium (V) that is subsequently found in the fourth zone (Z4) which could indicate that during processing, the V migrated to the grain boundary forming the delimitation observed in figure 52 in a lightest color.

Finally, the chemical compositions of several marked zones of Ti6Al4V-10 $\beta$ TCP sample (figure 53) are presented in table 10. Similar results were found in the EDS analysis of this sample. The first zone, Z1, indicate a high quantity of titanium (86.9 at. %), 10.7 at. % of P, 2 at. % of Al and a very low amount of Ca (0.4 at.%). These amounts could also indicate that this zone could belong to a bioactive cluster, formed during hot pressing, that was removed when polishing the sample. The second zone, Z2, indicate the metallic matrix composition due to the its chemical composition similar to the composition



Development of bioactive materials for dental implants using powder metallurgy

of Ti6Al4V sample (table 8). However, similar to Ti6Al4V-10HAp, the absence of V in this zone which is found in a third zone (Z3) could be related to the grain boundary migration of V.

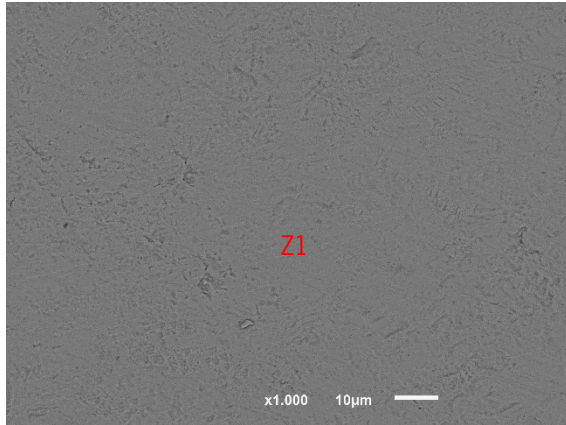


**Table 8** – Chemical composition (in at. %) of marked zone of figure 51.

Elements	<b>Z1</b>
Ti	90.5
Al	5.5
V	4.0

**Figure 51** – SEM images of Ti6Al4V with marked zone for EDS analysis.

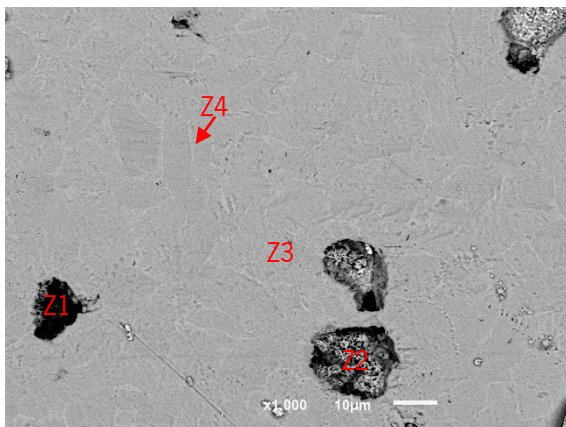


**Table 9** – Chemical composition (in at. %) of marked zones of figure 52.

Elements	<b>Z1</b>	<b>Z2</b>	<b>Z3</b>	<b>Z4</b>
Ti	38.2	90.0	94.4	82.4
O	30.7	-	-	-
Ca	27.9	-	-	-
Al	1.8	1.6	5.6	5.1
P	1.3	8.5	-	0.4
V	-	-	-	12.1

**Figure 52** - SEM images of Ti6Al4V-10HAp with marked zone for EDS analysis.

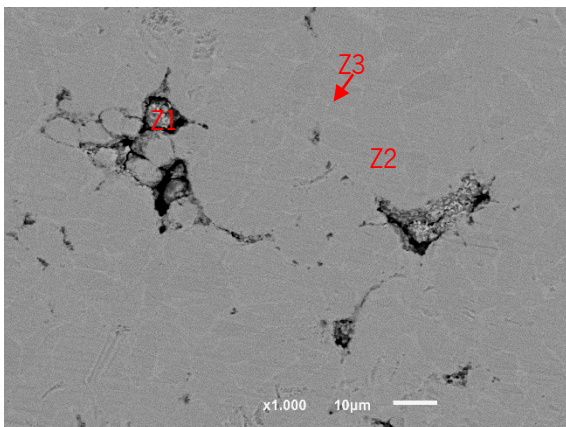


**Table 10** – Chemical composition (in at. %) of marked zones of figure 53.

Elements	<b>Z1</b>	<b>Z2</b>	<b>Z3</b>
Ti	86.9	94.2	83.0
O	-	-	-
Ca	0.4	-	-
Al	2.0	5.4	5.3
P	10.7	0.4	0.4
V	-	-	11.2

**Figure 53** - SEM images of Ti6Al4V-10βTCP with marked zone EDS analysis.

for

## Development of bioactive materials for dental implants using powder metallurgy

Subsequently, the samples were characterized in terms of hardness and shear strength. The hardness values (figure 54) for Ti6Al4V, Ti6Al4V-10HAp, Ti6Al4V-10 $\beta$ TCP were 340.20 HV, 473.33 HV and 520.60 HV, respectively. The hardness value of Ti6Al4V samples are in agreement with the values found in the literature [145]. Moreover, it is also expected that the addition of hard bioactive materials as a reinforcement will increase hardness values [90, 152]. On the other hand, shear test results exhibited shear strength values for Ti6Al4V, Ti6Al4V-10HAp, Ti6Al4V-10 $\beta$ TCP of 547.73 MPa, 209.54 MPa and 188.50 MPa, respectively (figure 55). These results show that the reinforcement significantly decrease the shear strength, which are in accordance with the literature [90, 123], once these fragile areas reduce the effective resistant area of the sample cross-section subjected to shear.

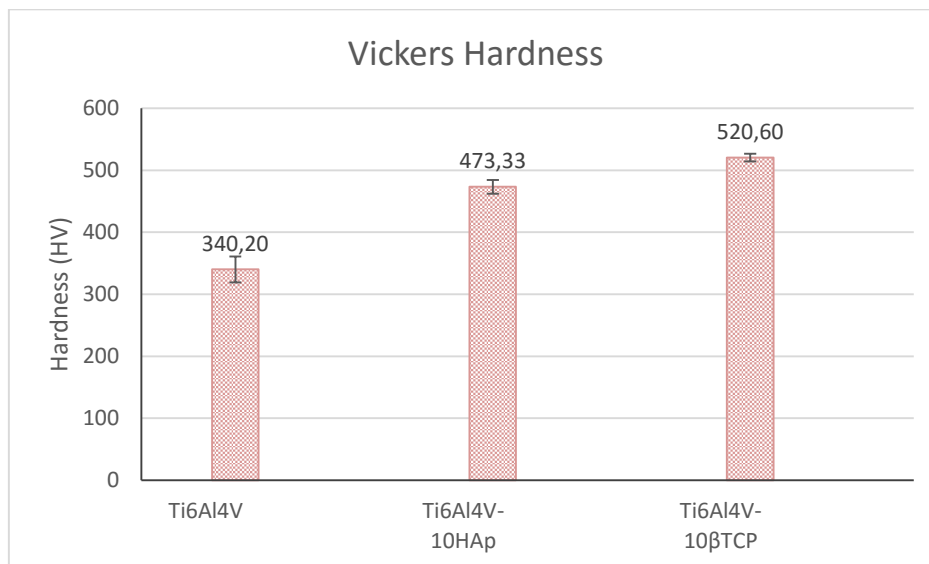


**Figure 54** – Average hardness (HV) for Ti6Al4V, Ti6Al4V-10HAp and Ti6Al4V-10 $\beta$ TCP composites.

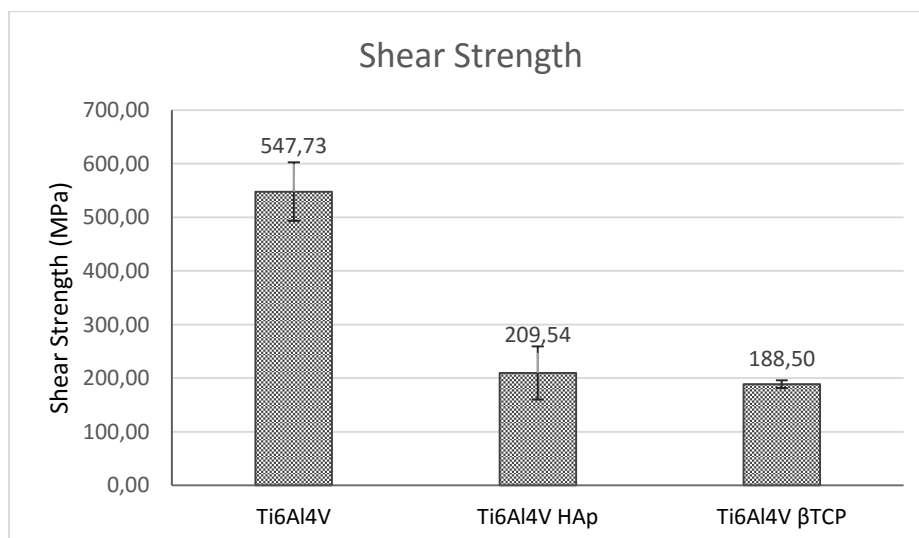


**Figure 55** - Average shear strength for Ti6Al4V, Ti6Al4V-10HAp and Ti6Al4V-10 $\beta$ TCP composites.

4.4. ZrO<sub>2</sub> AND ZrO<sub>2</sub>-BASED COMPOSITES CHARACTERIZATION

The following subchapter presents the results of ZrO<sub>2</sub> and ZrO<sub>2</sub>-based composites samples. Similarly, to Ti6Al4V and Ti6Al4V-based composites, EDS analysis were made in samples constituted by the ceramic matrix (ZrO<sub>2</sub>) for comparison with the results of ZrO<sub>2</sub>-based composites samples.

Besides ZrO<sub>2</sub> and ZrO<sub>2</sub>-based composites processed by hot pressing, also ZrO<sub>2</sub> and ZrO<sub>2</sub>-based composites samples processed by press-and-sintering were characterized.

SEM images of ZrO<sub>2</sub> samples processed by hot pressing and by press-and-sintering are shown in figure 56.

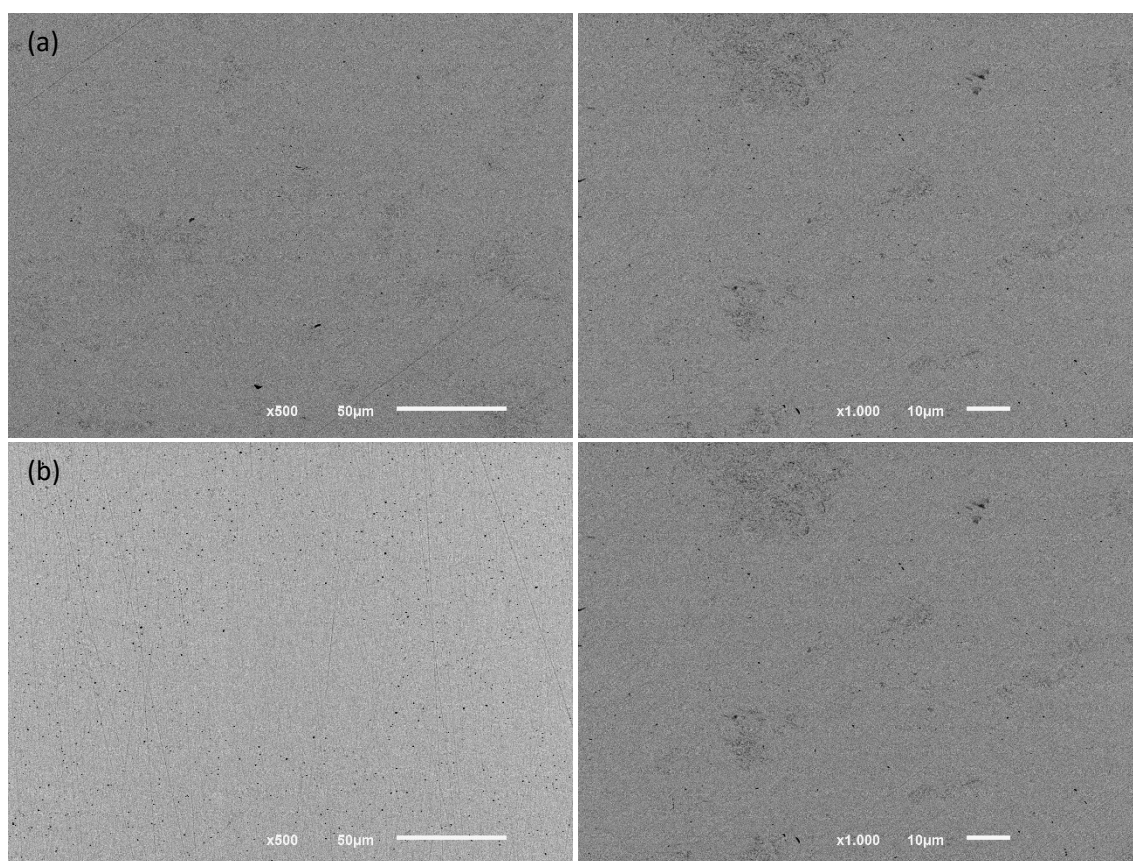


**Figure 56** - SEM images of ZrO<sub>2</sub> samples (a) hot-pressed and (b) press and sintered, at magnifications of 500x (left) and 1000x (right).

By analyzing figure 56, it is possible to identify the presence of some residual porosity in both samples, processed by hot pressing as by press and sintering, so it is possible to conclude that the densification was not total. However, it could also be concluded that the densification was better in the samples processed by hot pressing than in those produced by press and sintering. This conclusion was confirmed by image analysis using ImageJ software. With this software it is possible to apply a threshold filter to the images acquired, to highlight the pores and thus measure the percentage of porosity of the

## Development of bioactive materials for dental implants using powder metallurgy

sample. An example of this procedure application is shown in figure 57, for each sample, being the black dots the porosity found on the samples. This procedure revealed an average porosity value of 0.0855 and 0.3360 % for hot-pressed and press-and-sintered samples, respectively. These values correspond to a densification of 99.9% for HP samples against 99.7% for PS ones. Although the value found for PS was lower than for HP, both procedures allow a good densification.

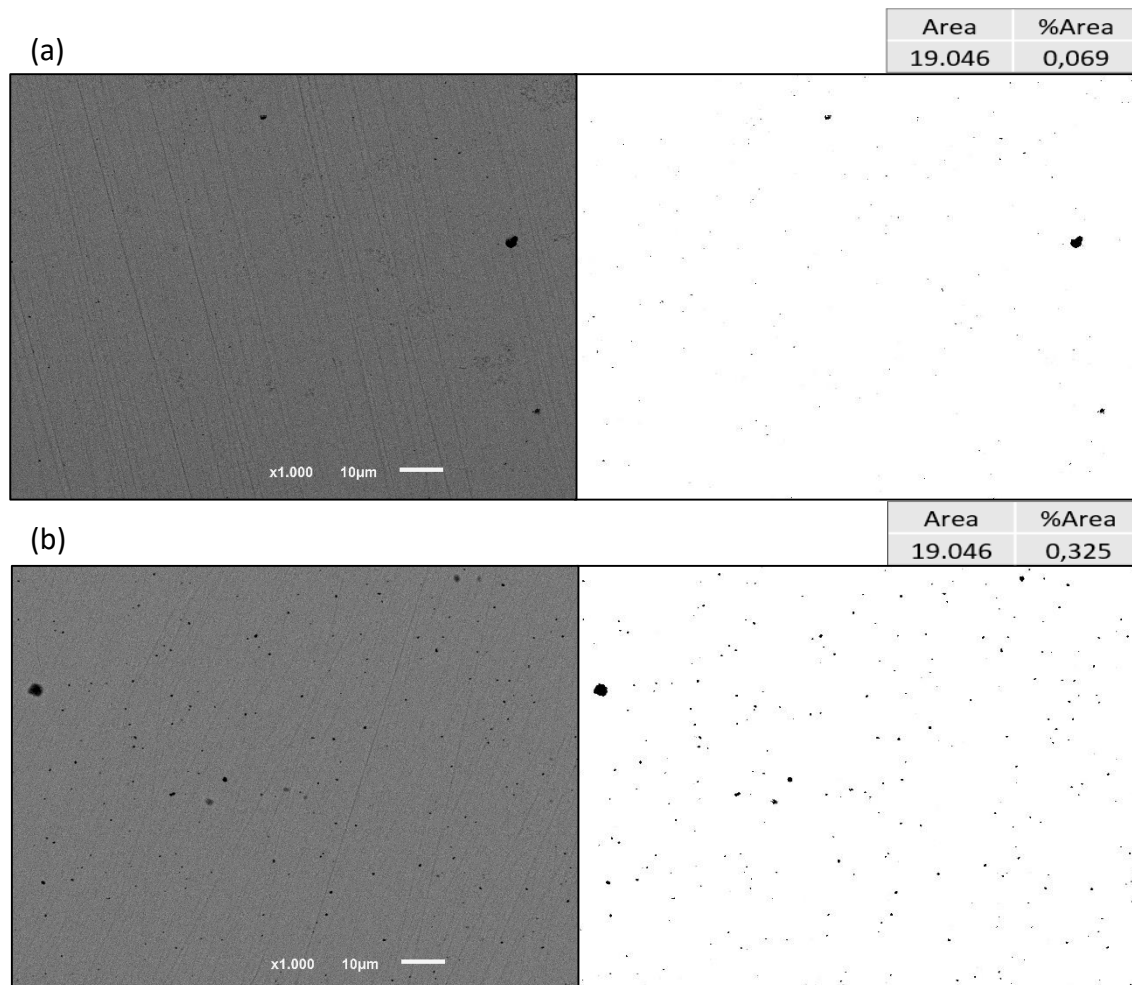


**Figure 57** - Example of porosity measuring of ZrO<sub>2</sub> (a) hot-pressed and (b) press-and-sintered samples. SEM image in backscattered view (left) and the same SEM image with a threshold filter enhancing the porosity (right). Porosity percentage in the tables.

SEM images of ZrO<sub>2</sub>-based composites processed by hot pressing as well as of the composites produced by pressing and sintering are presented below. SEM images of ZrO<sub>2</sub>-10HAp samples produced by both processing methods are shown in figure 58. For both, it is possible to identify the HAp particles dispersed in the ZrO<sub>2</sub> matrix. Image analysis was not possible to performed in this samples to measure porosity once the software cannot distinguish the pores from the reinforcement, what could lead to higher porosity values than they would be in reality. However, it is visible more porosity in press-and-sintered

## Development of bioactive materials for dental implants using powder metallurgy

samples than in hot-pressed ones, even though both samples presented low porosity. Analogous conclusions can be taken from  $ZrO_2$ -10 $\beta$ TCP SEM images, presented in figure 59. These results showing higher porosity in press-and-sintered samples are in accordance with literature [125]. Nevertheless,  $ZrO_2$ -based composite samples seem to present lower porosity than zirconia samples, which may indicate that the reinforcement improves the densification process.

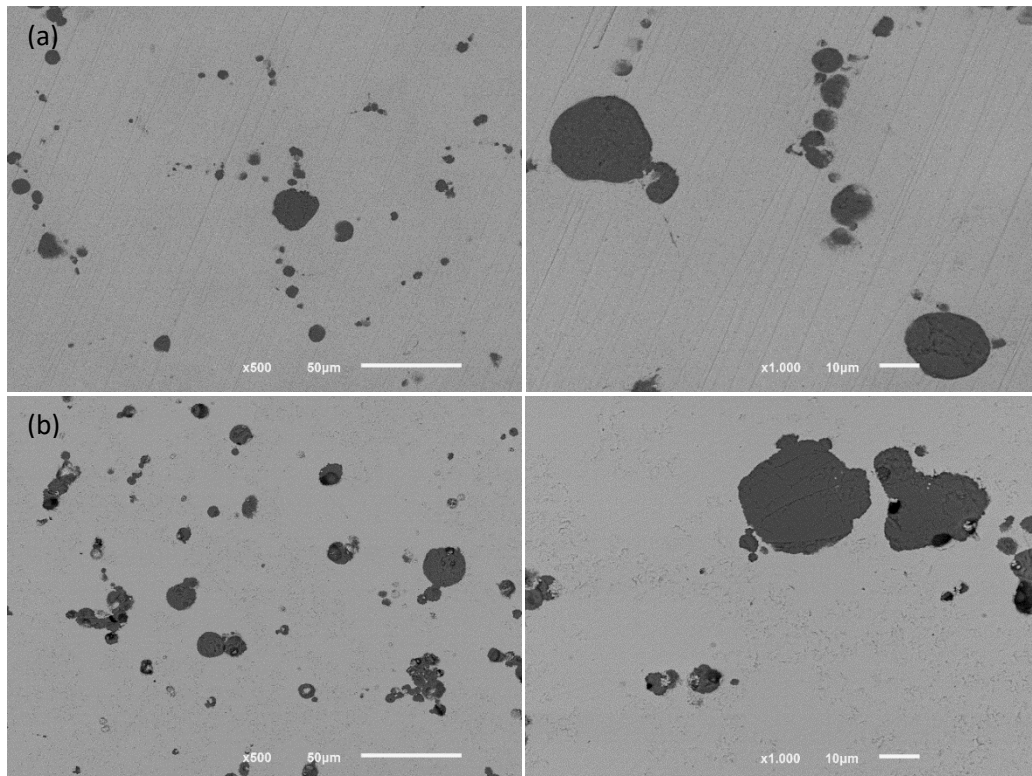


**Figure 58** - SEM images of  $ZrO_2$ -10HAp samples (a) hot-pressed and (b) press-and-sintered, at magnifications of 500x (left) and 1000x (right).

## Development of bioactive materials for dental implants using powder metallurgy

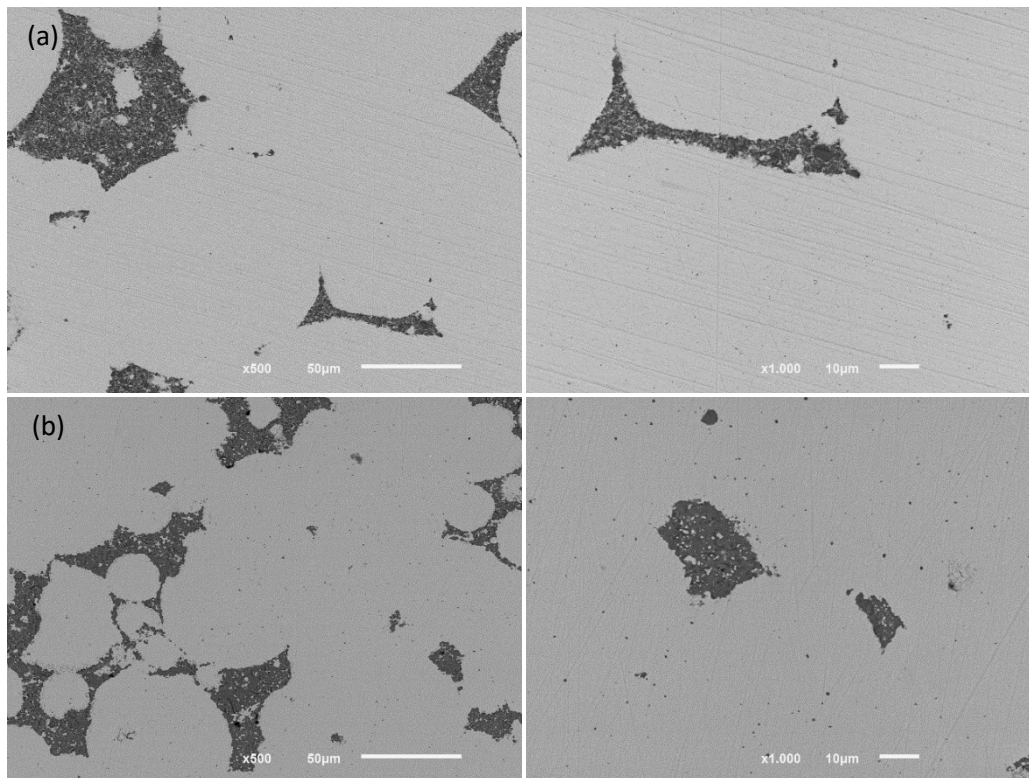


**Figure 59** - SEM images of  $ZrO_2$ -10 $\beta$ TCP samples (a) hot-pressed and (b) press-and-sintered, at magnifications of 500x (left) and 1000x (right).

Furthermore, in order to measure the chemical composition of each sample, EDS analysis were performed. Once again, EDS analysis of  $ZrO_2$  samples (HP and PS) was made in order to compare these results with the ones obtained for  $ZrO_2$ -based composites. Table 11 displays the chemical composition, in atomic percentage, for hot-pressed and press-and-sintering samples, of the marked zones in figure 60(a) and (b) respectively. The values obtained for both samples were similar; allowing concluding that the processing method does not influences the chemical composition of  $ZrO_2$ .

The chemical composition of  $ZrO_2$ -10HAp samples processed by hot pressing and by press and sintering are presented in table 12. The chemical composition was made for different zones in the samples in order to identify the ceramic matrix and the bioactive reinforcement. Those marked zones are identified in figure 61. The first zone (Z1), in both samples, correspond to the bioactive reinforcement, due to the presence of the typical elements of HAp. As mentioned, HAp atomic percentages are 22.72% Ca 13.64% P, 59.09% O and 4.55% H, approximately, which are similar to the results obtained for HP and PS samples, indicating that in these zones minor or no reaction occurred. The increase of Ca in  $ZrO_2$ -10HAp processed by HP may indicate a possible decomposition of HAp, not discarding the hypothesis of calcium oxide formation, although the semi-quantitative EDS analysis by itself could induce some of



these changes. It is also possible to observe from the EDS analysis of these zones the absence of hydrogen in the chemical composition which may indicate the occurrence of dehydroxylation. The second zone (Z2), in both samples, indicate that these regions correspond to the ceramic matrix, once these values are similar to those obtained in the  $ZrO_2$  samples (table 11).

EDS analysis performed in  $ZrO_2$ -10 $\beta$ TCP HP and PS samples revealed analogous results as those obtained in  $ZrO_2$ -10HAp samples. Table 13 shows the chemical composition of the marked zones shown in figure 62, from each sample. The first zone (Z1), for both samples, corresponds to the bioactive reinforcement. Likewise, being  $\beta$ TCP formula  $Ca_3(PO_4)_2$ , the chemical composition (at. %) should be approximately as follow: 23.08% Ca, 15.4% P and 61.5% O. Therefore, these values when compared with the obtained ones are similar, allowing to conclude that minor or no reaction occurred in these zones on both samples. One the other hand, when analyzing the values obtained for the second zone (Z2), in both samples, it is possible to conclude that these zone corresponds to the ceramic matrix due to the similarity with the values obtained in  $ZrO_2$  samples (table 11).

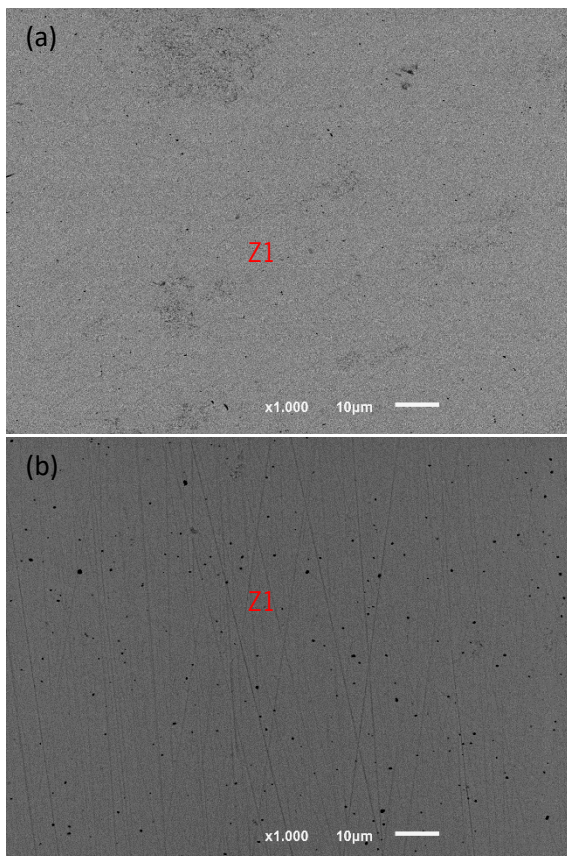


**Figure 60** - SEM images of  $ZrO_2$  with marked zone for EDS analysis in (a) hot pressed and (b) press-and-sintered samples.

**Table 11** – Chemical composition (in at. %) of marked zones in hot-pressed (top) and press-and-sintered (bottom) samples of figure 60.

<b>HP</b>	
Elements	<b>Z1</b>
O	53.8
Zr	46.2
<b>PS</b>	
Elements	<b>Z1</b>
O	52.5
Zr	47.5

## Development of bioactive materials for dental implants using powder metallurgy

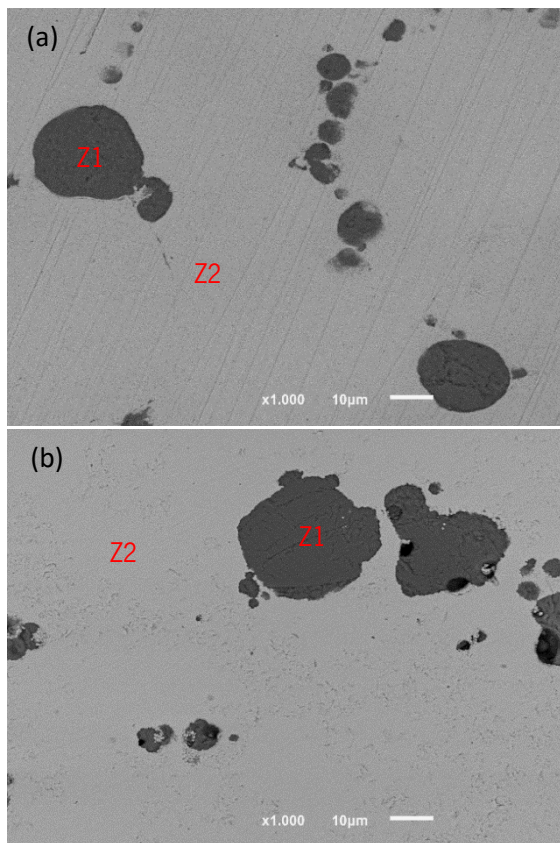


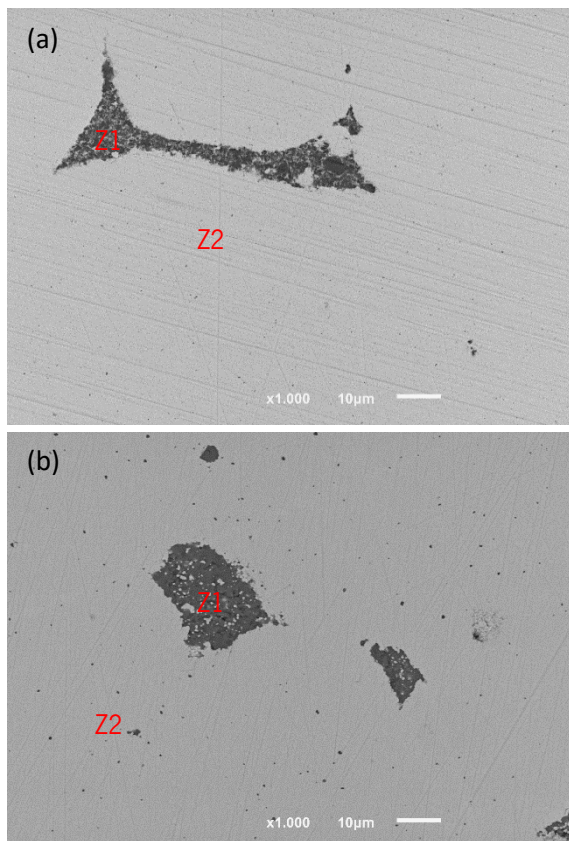
**Table 12** - Chemical composition (in at. %) of marked zones in hot-pressed (top) and press-and-sintered (bottom) samples of figure 61.

<b>HP</b>		
Elements	<b>Z1</b>	<b>Z2</b>
O	45.5	51.5
Zr	6.7	47.1
Ca	30.3	1.2
P	16.2	0.2
Cl	1.3	-

<b>PS</b>		
Elements	<b>Z1</b>	<b>Z2</b>
O	50.2	54.0
Zr	5.8	44.8
Ca	27.9	1.2
P	16.2	-

**Figure 61** - SEM images of  $ZrO_2$ -10HAp with marked zone for EDS analysis in (a) hot pressed and (b) press-and-sintered samples.



**Table 13** - Chemical composition (in at. %) of marked zones in hot-pressed (top) and press-and-sintered (bottom) samples of figure 62.

<b>HP</b>		
Elements	<b>Z1</b>	<b>Z2</b>
O	49.2	54.2
Zr	13.2	44.7
Ca	23.6	1.1
P	1.0	-
Cl	0.7	-

<b>PS</b>		
Elements	<b>Z1</b>	<b>Z2</b>
O	50.4	55.6
Zr	10.0	42.8
Ca	24.9	1.2
P	14.7	0.4

**Figure 62** - SEM images of  $ZrO_2$ -10 $\beta$ TCP with marked zone for EDS analysis in (a) hot pressed and (b) press-and-sintered samples



## Development of bioactive materials for dental implants using powder metallurgy

The measured Vickers hardness for  $ZrO_2$ ,  $ZrO_2$ -10HAp and  $ZrO_2$ -10 $\beta$ TCP for PS samples were 1490.5 HV, 1418.25 HV and 1701.75 HV, respectively, as can be seen in figure 63. The hardness value of  $ZrO_2$  are similar to those found in literature [153]. The addition of a bioactive reinforcement on  $ZrO_2$  samples should increase the hardness of the composite due to the higher stiffness of the bioactive material. This is confirmed on the results obtained on  $ZrO_2$ -10 $\beta$ TCP samples, however this didn't occur on  $ZrO_2$ -10HAp.

Shear tests were performed for  $ZrO_2$  and  $ZrO_2$ -based composites processed by hot pressing and also  $ZrO_2$  and  $ZrO_2$ -based composites samples processed by press-and-sintering. Shear test results indicate shear strength values for  $ZrO_2$ ,  $ZrO_2$ -10HAp and  $ZrO_2$ -10 $\beta$ TCP hot-pressed samples are 172.91 MPa, 123.41 MPa, 168.13 MPa, respectively (average and standard deviation values shown in figure 64). On the other hand, shear strength values for  $ZrO_2$ ,  $ZrO_2$ -10HAp and  $ZrO_2$ -10 $\beta$ TCP press-and-sintered samples are 122.92 MPa, 115.87 MPa and 120.56 MPa, respectively, as can be seen in figure 64. The results obtained for both samples show that the addition of the reinforcement decreased the shear strength, as expected. When comparing with HP samples, PS samples present lower shear strength values, which can be explained by the presence of higher porosity in these samples in comparison with HP samples.

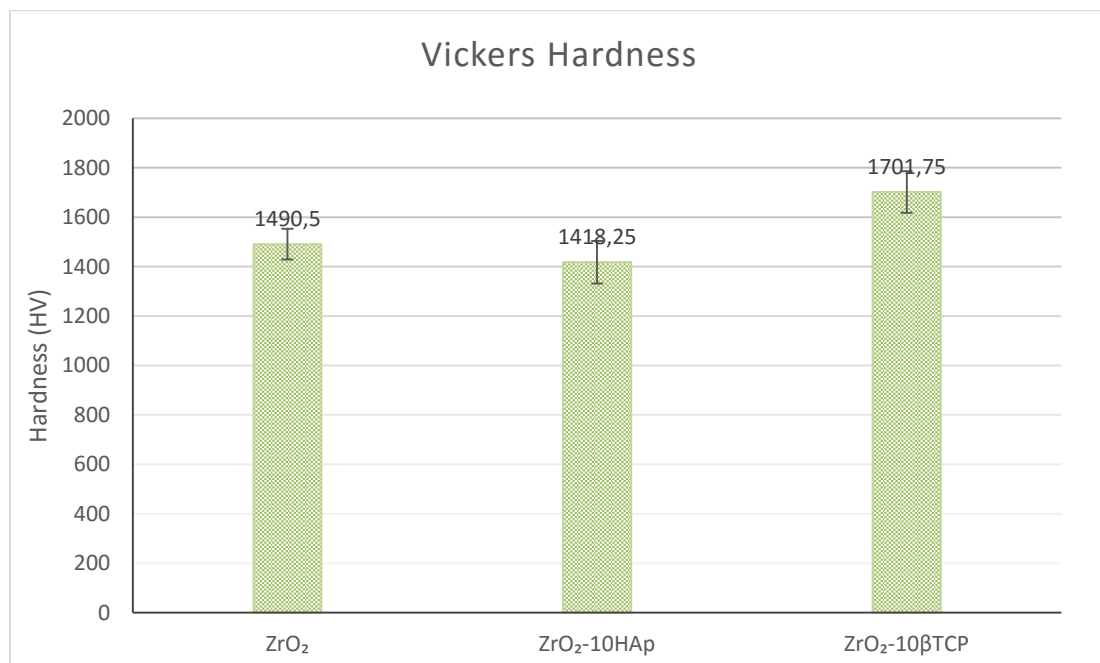


**Figure 63** - Average hardness (HV) for  $ZrO_2$ ,  $ZrO_2$ -10HAp and  $ZrO_2$ -10 $\beta$ TCP composites processed by press-and-sinter.

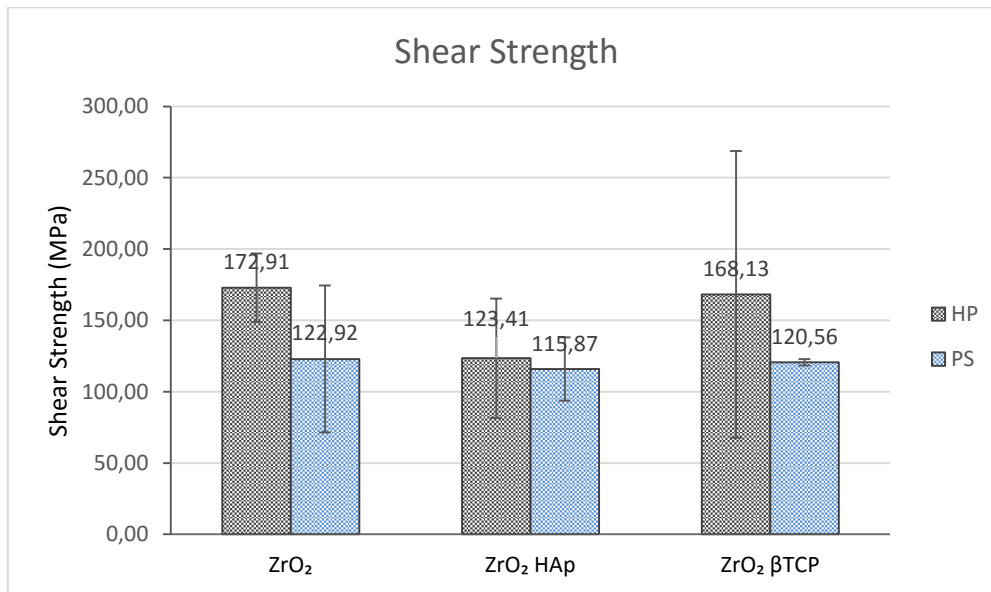


**Figure 64** - Average shear strength for hot pressed and press and sintered ZrO<sub>2</sub>, ZrO<sub>2</sub>-10HAp and ZrO<sub>2</sub>-10βTCP composites.

#### 4.5. PEEK AND PEEK-BASED COMPOSITES CHARACTERIZATION

This subchapter will present and discuss the results from PEEK and PEEK-based composites, presenting a comparative analysis between PEEK and composite samples. SEM images of PEEK and PEEK-based composites samples are presented in figure 65.

From SEM analysis of PEEK samples (figure 65(a)), it is observable a homogeneous surface without no porosity. The same results are observed in PEEK-based composites (figure 65(b) and (c)) where it is also possible to identify the HAp (figure 65(b)) and βTCP (figure 65(c)) particles dispersed in the polymeric matrix, in which the white phase is the bioactive material and the dark one is PEEK. These results allow to conclude that the absence of porosity on PEEK and PEEK-based composites was due to a full densification of the samples and to a good dispersion of the bioactive materials in the matrix.

## Development of bioactive materials for dental implants using powder metallurgy

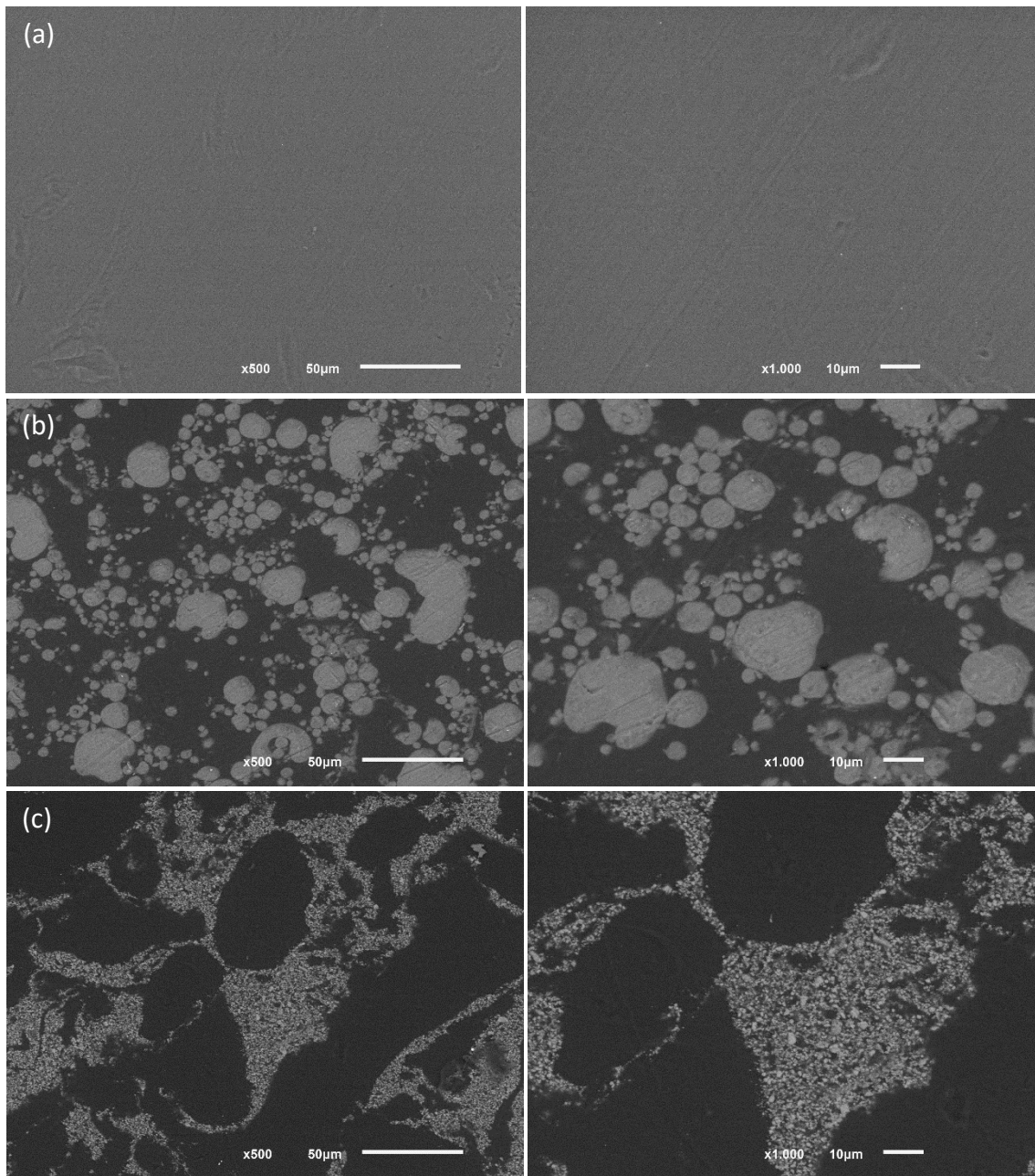


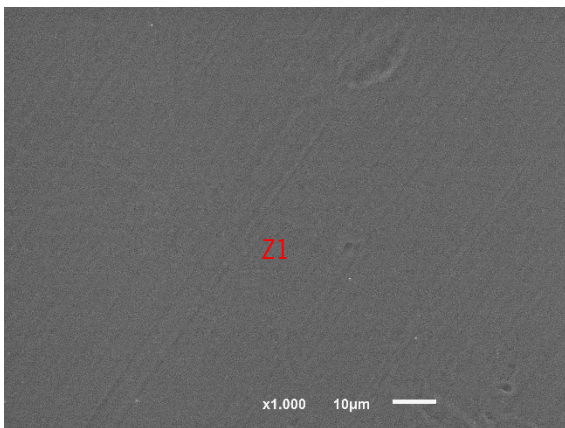
**Figure 65** - SEM images of (a) PEEK, (b) PEEK-10HAP, (c) PEEK-10 $\beta$ TCP samples at magnifications of 500x (left) and 1000x (right).

Furthermore, the EDS results shown in table 14, 15 and 16 correspond to the chemical composition, in atomic percentage, of PEEK, PEEK-10HAP, PEEK-10 $\beta$ TCP marked zones in figures 66,67,68, respectively.

Table 14 indicates the chemical composition (at. %) of the marked zone on PEEK sample shown in figure 66. These values were acquired in order to be compared with the ones of PEEK-based composites.

## Development of bioactive materials for dental implants using powder metallurgy

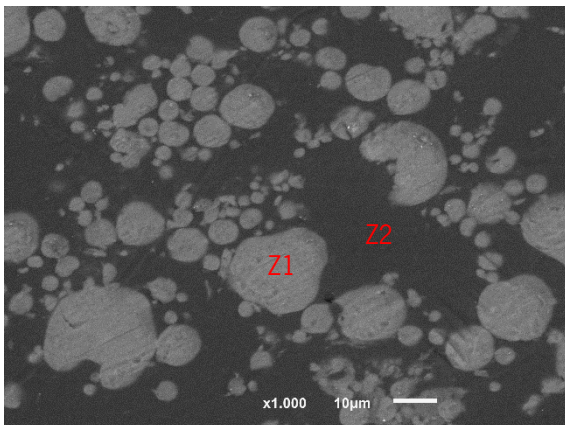
The chemical composition of PEEK-10HAp and PEEK-10 $\beta$ TCP samples are presented in table 15 and 16, respectively. In these samples, EDS analysis were performed in two zones, as can be seen in figure 67 and 68. For both samples, the results obtained from Z1 still own a high percentage of PEEK composition but higher content of Ca and P are found in these zone in comparison with the second zone Z2. This higher content of Ca and P corresponds to a zone of agglomeration of the bioactive material. The second zone, when compared with the results obtained from PEEK samples, allow to conclude that this zone only presents the polymeric matrix once the chemical composition is similar to the composition obtained in table 14.



**Table 14** – Chemical composition (in at. %) of marked zone of figure 66.

Elements	<b>Z1</b>
C	85.3
O	14.7

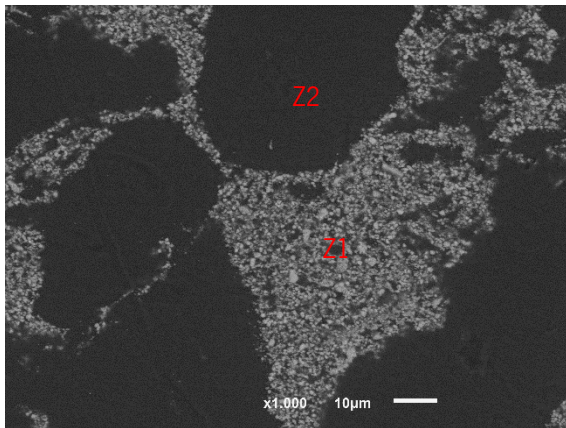
**Figure 66** – SEM images of PEEK with marked zone for EDS analysis.



**Table 15** – Chemical composition (in at. %) of marked zones of figure 67.

Elements	<b>Z1</b>	<b>Z2</b>
C	67.8	84.2
O	23.7	14.4
Ca	5.0	0.9
P	3.5	0.6

**Figure 67** – SEM images of PEEK-10HAp with marked zones for EDS analysis.

**Table 16** – Chemical composition (in at. %) of marked zones of figure 68.

Elements	Z1	Z2
C	73.1	83.2
O	19.8	14.8
Ca	4.0	1.1
P	3.1	0.8

**Figure 68** – SEM images of PEEK-10 $\beta$ TCP with marked zones for EDS analysis.

Vickers hardness and shear strength results for PEEK, PEEK-10HAp and PEEK-10 $\beta$ TCP are given in figure 69 and figure 70, respectively. Vickers hardness results indicate hardness values for PEEK, PEEK-10HAp and PEEK-10 $\beta$ TCP of 25.86 HV, 29.27 HV and 29.05 HV, respectively (average and standard deviation values shown in figure 69). PEEK-based composites revealed higher hardness than PEEK samples, which is expected due to higher stiffness of the bioactive materials. These results are in accordance with literature [10, 89].

On the other hand, shear tests results indicate shear strength values for PEEK, PEEK-10HAp and PEEK-10 $\beta$ TCP of 67.81 MPa, 65.10 MPa and 66.91 MPa, respectively (figure 70). PEEK-based composites present relatively lower shear strength when compared with PEEK samples. This could be explained by the difference in thermal expansion coefficients between the materials, which can lead to internal stresses and thus reduce the overall mechanical properties; and/or could be a result of cracks that may exist around the HAp particles that, when the load is applied, leads to sample fracture [10, 154]. However, this decrease on shear strength of PEEK-based composites is low, which can be explained by the good densification achieved in this samples.

## Development of bioactive materials for dental implants using powder metallurgy

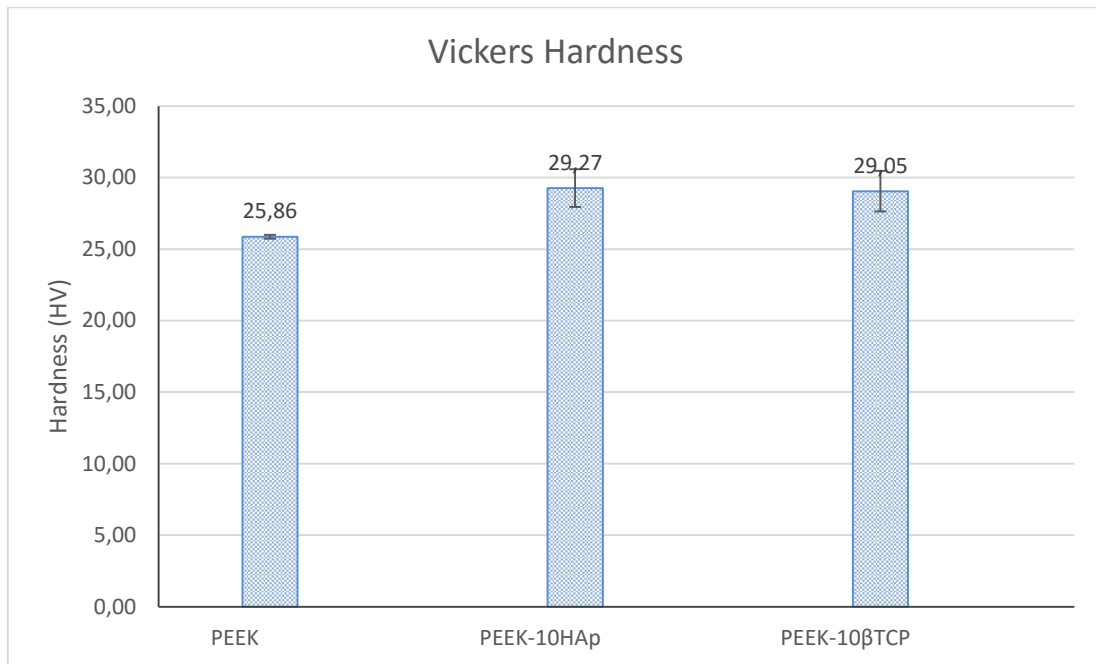


**Figure 69** – Average hardness (HV) for PEEK, PEEK-10HAp and PEEK-10 $\beta$ TCP composites.

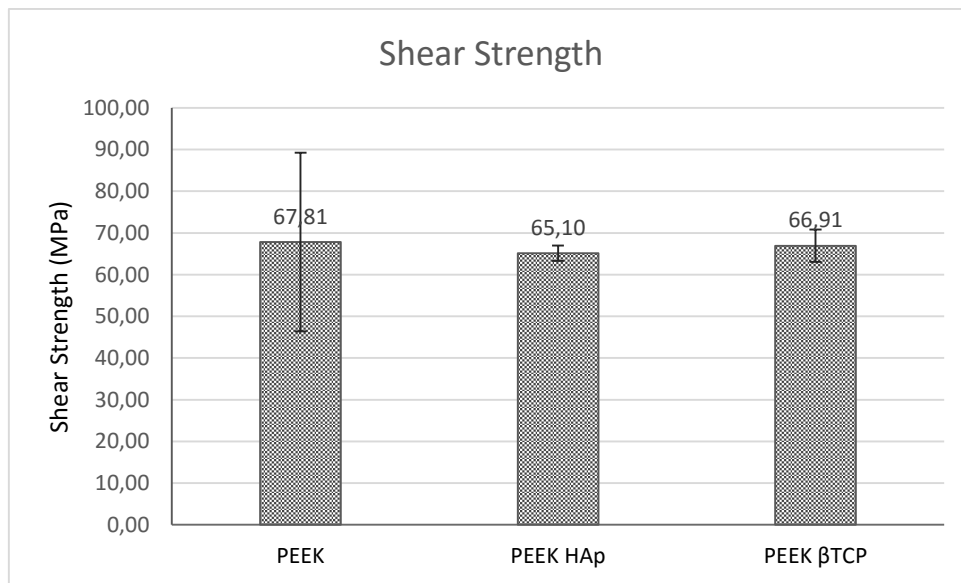


**Figure 70** - Average shear strength for PEEK, PEEK-10HAp and PEEK-10 $\beta$ TCP composites.

## 4.6. ONGOING RESEARCH

Some of the samples processed in this study are being used to perform other tests, conducted by other researchers. For the different materials, they comprise wear and biological tests, with some preliminary results being presented in this section. Additionally, corrosion, tribocorrosion and fatigue tests will be further performed on these samples.

Wear tests were performed on all samples in order to measure the wear rate of the samples, in order to conclude on the potential of these composites for use in implantology, by comparing them with the non-reinforced materials.

Wear tests of Ti6Al4V and Ti6Al4V-based composites samples were performed by MSc student Telma Dantas. To accomplish these tests, samples were processed by hot pressing according to the process previously described in this thesis. Then, ball-on-flat (BOF) sliding wear test were performed. In this test, an alumina ball slides against the samples with the application of a vertically load through the ball. The sliding was accomplished with a constant stroke length of 4mm, an oscillating frequency of 1Hz and in a phosphate buffered saline (PBS) medium at 37°C. Therefore, the alumina ball applied a normal load of 3N, 5N and 30N on the samples during 1-hour sliding time which corresponds to a total sliding distance of 28.8 m.

The specific wear rate measured for Ti6Al4V and Ti6Al4V-based composites are presented in figure 71.

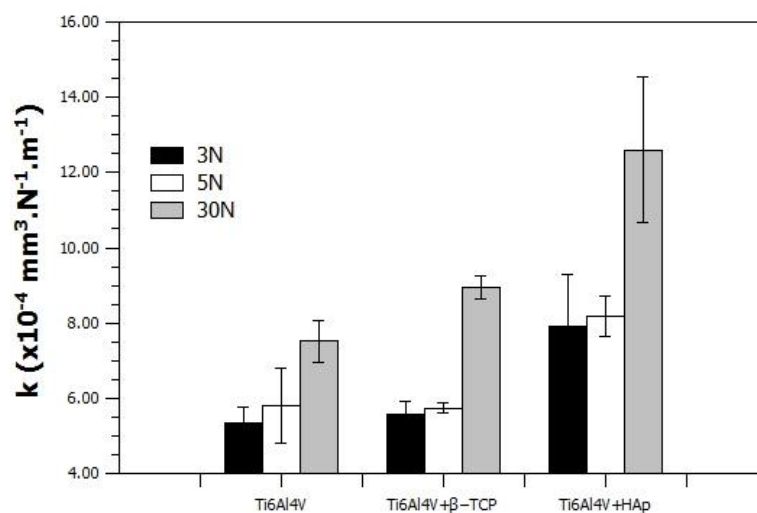


**Figure 71** - Specific wear rate for the tested Ti based materials against  $\text{Al}_2\text{O}_3$  in presence of PBS at 37 °C.

It can be visible that the specific wear rate for Ti6Al4V-based composites increases in comparison with Ti6Al4V samples. This means that the addition of a bioactive material to Ti6Al4V decreases the wear resistance of the composite, which can be explained by the presence of agglomerates of the bioactive particles that, during sliding, fracture and are detached from the samples, leaving cavities that will increase wear rate. Figure 53 and 54 also shows the presence of some of these grooves before wear tests, which also indicates that, for these samples, the wear rate will be higher than those in which these cavities does not exist. Additionally, bioactive particles released at the sample surface will enhance abrasion and consequently increasing of wear rate. The differences between the two Ti6Al4V-based composites could be associated to the particle size of each bioactive material. Once HAp has a particle size of 10  $\mu\text{m}$  (d50), the clusters will be bigger than  $\beta\text{TCP}$  that has a particle size of 2.26  $\mu\text{m}$  (d50) which will indicate a higher wear rate on Ti6Al4V-10HAp samples than on Ti6Al4V-10 $\beta\text{TCP}$  ones. Another aspect to take in consideration is the chemical bonding between these bioactive materials with Ti6Al4V. Previous studies reported the bonding strength on metal/HAp interface as a weakness on the final product. Therefore, during wear tests, being the bonding strength between these materials poor, the detachment of HAp particles could occur which will consequently increase wear rate [155, 156]. On the other hand, it is understandable that a higher load applied to the sample will intensify abrasion and consequently wear rate.

Similarly, wear tests on  $\text{ZrO}_2$  and  $\text{ZrO}_2$ -based composites samples processed by press and sintering were carried out by researcher Cristiano Abreu. The experimental procedure was very similar with the one used in Ti6Al4V and Ti6Al4V-based composites samples. The reciprocating sliding tests were performed at 5N normal load by an alumina ball, at a sliding frequency of 1 Hz, with a stroke length of 4 mm in presence of PBS at 37°C during 1h (total sliding distance=28.8mm). Figure 72, shows the specific wear rate measured for the studied samples at the parameters mentioned above. It can be visible that, contrary to what happens on Ti6Al4V and Ti6Al4V-based composites samples, the wear resistance increases with the addition of the bioactive phase. It is possible to observe in figure 60(b), 61(b) and 62(b) that the porosity in  $\text{ZrO}_2$  samples seems to be a little higher than on  $\text{ZrO}_2$ -based composites, which could be related to a higher wear rate in  $\text{ZrO}_2$  samples. Therefore, being the porosity of  $\text{ZrO}_2$  samples higher, this could mean that the densification of  $\text{ZrO}_2$ -based composites was higher, leading to better mechanical properties. These results could also be related to the adhesion between  $\text{ZrO}_2$  and the bioactive materials, once both materials are ceramics.



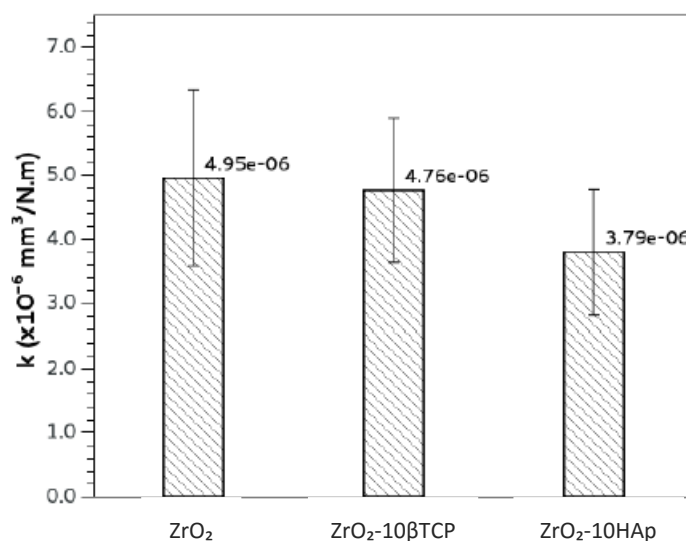


**Figure 72** – Specific wear rate for tested ZrO<sub>2</sub> based materials processed by press-and-sintering against Al<sub>2</sub>O<sub>3</sub> in presence of PBS at 37°C.

Wear tests on ZrO<sub>2</sub> and ZrO<sub>2</sub>-based composites samples processed by hot pressing will be performed by researcher Mihaela Buciumeanu. These results are not yet available in order to evaluate the behavior of these ZrO<sub>2</sub>-based composite samples in comparison with ZrO<sub>2</sub> ones.

Finally, wear tests on PEEK and PEEK-based composites samples were performed by researcher Mihaela Buciumeanu. Once again, the experimental procedure was very similar with the others described before. The alumina ball slides against the samples with the application of a vertical load of 30N. The sliding was carried out with a constant stroke length of 3 mm, with an oscillating frequency of 1Hz during 1h sliding time. The tests were lubricated with PBS at 37°C to mimic physiological conditions. The results of the specific wear rate of these samples are presented in figure 73. From this figure it is possible to conclude that the specific wear rate of Ti-based materials increases with the addition of a bioactive phase, being PEEK-10HAp sample the one that presents the highest value. Similarly to what was concluded in Ti6Al4V and Ti6Al4V-based composites wear tests, the wear resistance decrease with the addition of the bioactive material. Thus, this increase in wear rate on the composite samples could also be due to bioactive particles that were released from the samples that will act as abrasive particles and consequently, increases wear rate. In the same way, the difference between PEEK-10HAp and PEEK-10 $\beta$ TCP could be related with the particle size of the bioactive materials, once HAp has a higher particle size ( $d_{50}=10\mu\text{m}$ ) in comparison with  $\beta$ TCP ( $d_{50}=2.26\mu\text{m}$ ).

## Development of bioactive materials for dental implants using powder metallurgy

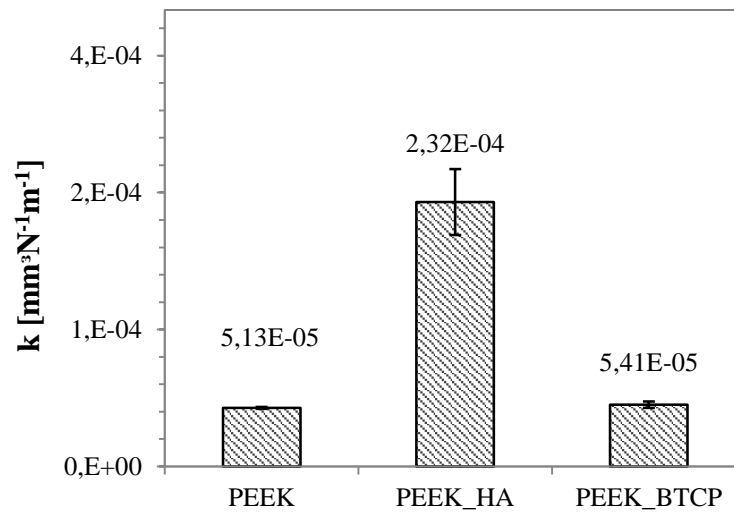


**Figure 73** - Specific wear rate for tested PEEK based materials processed by press-and-sintering against  $\text{Al}_2\text{O}_3$  in presence of PBS at  $37^\circ\text{C}$ .

Investigation on cellular viability, osteoblast cell function and cell morphology and adhesion are now being performed by researcher Gabriela Peñarrieta. Figure 74 shows preliminary results of osteoblast cellular viability acquired over 14 days. To accomplish these results a resazurin assay was used. Resazurin is a non-fluorescent blue dye that is reduced to a pink colored fluorescent resorufin. This reduction is correlated with the number of live organisms.

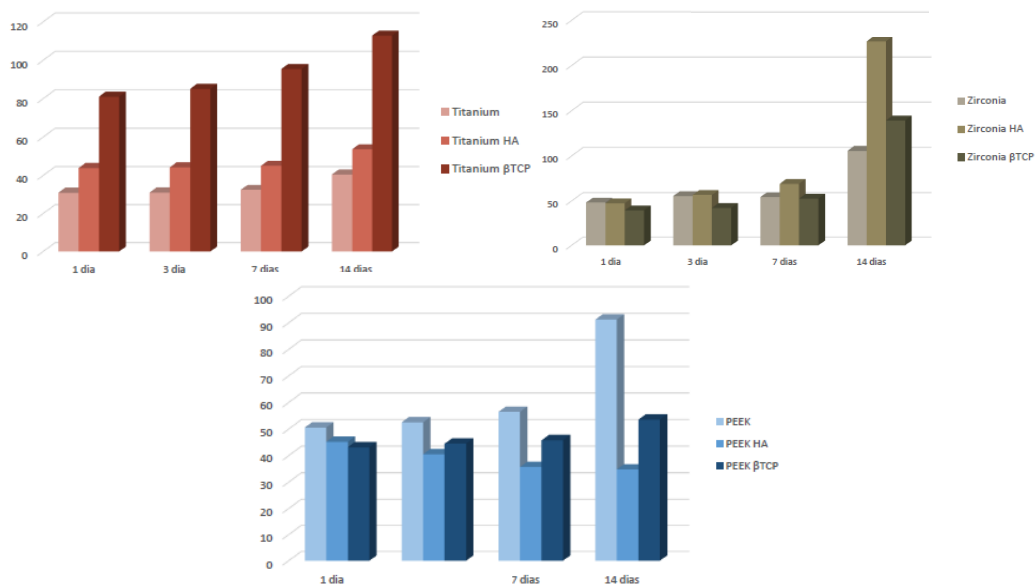


**Figure 74** – Cellular viability of osteoblast cells acquired over 14 days.

Development of bioactive materials for dental implants using powder metallurgy

Therefore, the results obtained in figure 74 allow concluding that, overall, the addition of bioactive materials presents beneficial results in respect of cellular viability, except for PEEK that presents higher values in comparison with PEEK-based composites. It is also observable an increase in viability from day 1 to day 14 in all tested samples, with exception of PEEK-10HAp samples, where cell viability decrease along the 14 days.

Overall, this subchapter allows presenting other tests that are being made by other researchers on the samples processed in this study. These tests are important once they allow the validation of the materials produced in the scope of this thesis. As mentioned, in addition to these tests, tribocorrosion, corrosion and fatigue tests are now on going. The results here presented are preliminary data acquired by the researchers. Although these results present lower wear resistance, the addition of bioactive materials has shown to increase cell viability.

As mentioned above, the idea of processing these composites would be to use them in the upper region of a FGM being the composite a thin layer on the surface of the material. In this FGM, the inner zone would be composed only by the matrix that presents good mechanical properties for load-bearing applications such as dental implants and the bioactive material will be gradually added towards the outer zone. Thus, the decrease of mechanical properties displayed in this study, becomes less significant once the mechanical properties will be guaranteed on the inner part of the sample, being the composite a thin layer on the outer part.



# CHAPTER 5

## CONCLUSIONS

---

Chapter 5 is devoted to the main conclusions drawn from this work presenting also some possible pathways for future work.

The present dissertation reports the behavior of different materials in order to improve the osseointegration process, for further application in dental implants. Therefore, it is possible to present the following conclusions:

- The optimization of the powder dispersion methods allowed to conclude that the best dispersion was achieved when using the ultrasonification method;
- The samples processing using powder metallurgy technologies (Hot Pressing and Press and Sintering) was successfully accomplished;
- Microstructural results showed that Ti6Al4V and Ti6Al4V-based composites presented a good densification due to the nonexistence of porosity. ZrO<sub>2</sub> and ZrO<sub>2</sub>-based composites processed by hot pressing and press and sintering revealed that the densification was not total due to the presence of porosity. Comparing both powder metallurgy techniques, HP samples presented a higher densification than PS ones, as predicted. Additionally, it is also possible to conclude that by comparing unreinforced ZrO<sub>2</sub> and ZrO<sub>2</sub>-based composites, the composites present, apparently, lower porosity. Finally, microstructural results of PEEK and PEEK-based composites showed also a good densification with an effective distribution of the bioactive materials in the PEEK matrix. This absence of porosity, related to a good densification, was proven to enhance the mechanical properties of the samples.
- Hardness results of Ti6Al4V and Ti6Al4V-based composites showed that the addition of bioactive materials to the matrix increased their hardness. Hardness results of ZrO<sub>2</sub> and ZrO<sub>2</sub>-based composites revealed higher values on ZrO<sub>2</sub>-10βTCP samples and lower on ZrO<sub>2</sub>-10HAp when compared with ZrO<sub>2</sub> samples. Similar results were verified for PEEK and PEEK-based composites, which are related to the stiffness of the bioactive materials, that enhance their hardness.
- Shear tests revealed that Ti6Al4V has a higher shear strength than Ti6Al4V-based composites due to the addition of the bioactive phase. On the other hand, the results obtained from ZrO<sub>2</sub> and ZrO<sub>2</sub>-based composites revealed that the addition of bioactive material also decrease the shear strength but not as significantly as on Ti6Al4V-based composites. As expected, all HP samples exhibited higher shear strength than PS ones. Finally, PEEK and PEEK-based composites shear tests results also showed a decrease of shear strength when adding the bioactive reinforcement.

Development of bioactive materials for dental implants using powder metallurgy

- As already mentioned, despite the slight decrease of the mechanical properties of the composite samples, as the shear strength values, the addition of bioactive materials to the samples brings advantages for dental implantology once these materials promote a higher osseointegration.

With these findings, the future work should focus on the following aspects:

- XRD characterization on all samples to confirm the values obtained in EDS analysis;
- Development of functionally graded materials based on these composites, to produce materials where the inner zone is composed by either of the matrix materials (Ti6Al4V, ZrO<sub>2</sub> or PEEK) which ensures the necessary strength for load-bearing applications and the use of a composite on the outer zone to promote bioactive properties and therefore enhance osseointegration.
- Production of a HAp/ $\beta$ -TCP composite, instead of using HAp or  $\beta$ -TCP as a reinforcement, once these two materials have different degradation rates therefore adapting to bone regeneration.
- Explore the use of alternative materials such as bioglass which improves surface bioactivity and silver nanoparticles which have antibacterial properties preventing dental implant infections.





## 6. REFERENCES

- [1] P. Pachauri, L. R. Bathala, and R. Sangur, "Techniques for dental implant nanosurface modifications," *J. Advance Prosthodontics*, vol. 6, pp. 498–504, 2014.
- [2] H. Kenar, E. Akman, E. Kacar, A. Demir, H. Park, H. Abdul-Khaliq, C. Aktas, and E. Karaoz, "Femtosecond laser treatment of 316L improves its surface nanoroughness and carbon content and promotes osseointegration: An in vitro evaluation," *Colloids Surfaces B Biointerfaces*, vol. 108, pp. 305–312, 2013.
- [3] R. Depprich, H. Zipprich, M. Ommerborn, E. Mahn, L. Lammers, J. Handschel, C. Naujoks, H.-P. Wiesmann, N. R. Kübler, and U. Meyer, "Osseointegration of zirconia implants: an SEM observation of the bone-implant interface," *Head Face Med.*, vol. 4, no. 1, p. 25, 2008.
- [4] C. Massaro, P. Rotolo, F. De Riccardis, E. Milella, a. Napoli, M. Wieland, M. Textor, N. D. Spencer, and D. M. Brunette, "Comparative investigation of the surface properties of commercial titanium dental implants. Part I: Chemical composition," *J. Mater. Sci. Mater. Med.*, vol. 13, pp. 535–548, 2002.
- [5] A. Schwitalla and W.-D. Müller, "PEEK dental implants: a review of the literature.," *J. Oral Implantol.*, vol. 39, no. 6, pp. 743–9, 2013.
- [6] C. Aparicio, A. Padrós, and F. J. Gil, "In vivo evaluation of micro-rough and bioactive titanium dental implants using histometry and pull-out tests," *J. Mech. Behav. Biomed. Mater.*, vol. 4, no. 8, pp. 1672–1682, 2011.
- [7] B. L. Pereira, P. Tummler, C. E. B. Marino, P. C. Soares, and N. K. Kuromoto, "Titanium bioactivity surfaces obtained by chemical/electrochemical treatments," *Rev. Mater.*, vol. 19, no. 1, pp. 16–23, 2014.
- [8] M. Araújo, M. Miola, A. Venturello, G. Baldi, J. Pérez, and E. Verné, "Glass coatings on zirconia with enhanced bioactivity," *J. Eur. Ceram. Soc.*, vol. 36, no. 13, pp. 3201–3210, 2016.
- [9] L. Guo, J. Zhao, X. Wang, R. Xu, Z. Lu, and Y. Li, "Bioactivity of zirconia nanotube arrays fabricated by electrochemical anodization," *Mater. Sci. Eng. C*, vol. 29, no. 4, pp. 1174–1177, 2009.
- [10] R. Ma and T. Tang, "Current strategies to improve the bioactivity of PEEK," *Int. J. Mol. Sci.*, vol. 15, no. 4, pp. 5426–5445, 2014.
- [11] D. M. Dohan Ehrenfest, P. G. Coelho, B.-S. Kang, Y.-T. Sul, and T. Albrektsson, "Classification of osseointegrated implant surfaces: materials, chemistry and topography," *Trends Biotechnol.*, vol. 28, no. 4, pp. 198–206, 2010.
- [12] T. J. Gao, T. S. Lindholm, B. Kommonen, P. Ragni, a. Paronzini, and T. C. Lindholm, "Microscopic evaluation of bone-implant contact between hydroxyapatite, bioactive glass and tricalcium phosphate implanted in sheep diaphyseal defects," *Biomaterials*, vol. 16, no. 15, pp. 1175–1179, 1995.
- [13] a. Shahrjerdi, F. Mustapha, M. Bayat, S. M. Sapuan, and D. L. a. Majid, "Fabrication of functionally graded Hydroxyapatite- Titanium by applying optimal sintering procedure and powder metallurgy," *Int. J. Phys. Sci.*, vol. 6, no. 9, pp. 2258–2267, 2011.
- [14] L. J. J. Hobkirk, John A.; Watson, Roger M.; Searson, *Introducing Dental Implants*. London, 2003.
- [15] A. K. Singh, *Clinical Implantology*. Chennai, 2013.

- [16] M. Mehrali, F. S. Shirazi, M. Mehrali, H. S. C. Metselaar, N. A. Bin Kadri, and N. A. A. Osman, "Dental implants from functionally graded materials," *J. Biomed. Mater. Res. - Part A*, vol. 101, no. 10, pp. 3046–3057, 2013.
- [17] Y. Liu, C. Bao, D. Wismeijer, and G. Wu, "The physicochemical/biological properties of porous tantalum and the potential surface modification techniques to improve its clinical application in dental implantology," *Mater. Sci. Eng. C*, vol. 49, no. 14, pp. 323–329, 2015.
- [18] Nobel Biocare, "Missing teeth." [Online]. Available: <https://www.nobelbiocare.com/content/patient/uk/en/home/missing-teeth.html>.
- [19] Y. S. C H, "Soft Tissue Biology and Management in Implant Dentistry," in *Implant Dentistry - A Rapidly Evolving Practice*, InTech, 2011.
- [20] L. Gaviria, J. P. Salcido, T. Guda, and J. L. Ong, "Current trends in dental implants.," *J. Korean Assoc. Oral Maxillofac. Surg.*, vol. 40, no. 2, pp. 50–60, 2014.
- [21] K. J. Anusavice, *Phillips' Science of Dental Materials*. Florida: Saunders, 2003.
- [22] M. Albertini, M. Fernandez-Yague, P. Lázaro, M. Herrero-Climent, J. V. Rios-Santos, P. Bullon, and F. J. Gil, "Advances in surfaces and osseointegration in implantology. Biomimetic surfaces," *Med. Oral Patol. Oral Cir. Bucal*, vol. 20, no. 3, pp. e316–e325, 2015.
- [23] J. Junqueira, Luiz C.; Carneiro, *Histologia Básica*, 11<sup>o</sup> Editio. Rio de Janeiro: Guanabara Koogan S.A., 2008.
- [24] E. Kuzyk, Paul RT; Schemitsch, "The basic science of peri-implant bone healing," *Indian J. Orthop.*, vol. 45, no. 2, pp. 108–115, 2011.
- [25] V. A. O. Toledo, "Dental Implant Surface Modifications and Osseointegration," Portuguese Catholic University, 2013.
- [26] S. Anil, P. S. Anand, H. Alghamdi, and J. a Jansen, "Dental Implant Surface Enhancement and Osseointegration," *Implant Dent. - A Rapidly Evol. Pract.*, pp. 83–108, 2011.
- [27] P. M. Burgos, "On the influence of Micro- and Macroscopic Surface Modification on Bone Integration of Titanium Implants," Göteborg University and Lund University Hospital, 2006.
- [28] OpenStax College, "Anatomy and Physiology," *OpenStax CNX*. [Online]. Available: <http://cnx.org/contents/14fb4ad7-39a1-4eee-ab6e-3ef2482e3e22@8.24>.
- [29] Y.-W. Kim, "Surface Modification of Ti Dental Implants by Grit-Blasting and Micro-Arc Oxidation," *Mater. Manuf. Process.*, vol. 25, no. 5, pp. 307–310, 2010.
- [30] Y. Dai, M. Xu, J. Wei, H. Zhang, and Y. Chen, "Surface modification of hydroxyapatite nanoparticles by poly(L-phenylalanine) via ROP of L-phenylalanine N-carboxyanhydride (Pha-NCA)," *Appl. Surf. Sci.*, vol. 258, no. 7, pp. 2850–2855, Jan. 2012.
- [31] C. Q. Ning and Y. Zhou, "In vitro bioactivity of a biocomposite fabricated from HA and Ti powders by powder metallurgy method," *Biomaterials*, vol. 23, no. 14, pp. 2909–2915, Jul. 2002.
- [32] K.-H. Kim and N. Ramaswamy, "Electrochemical surface modification of titanium in dentistry.," *Dent. Mater. J.*, vol. 28, no. 1, pp. 20–36, 2009.
- [33] F. Mangano, L. Chambrone, R. Van Noort, C. Miller, P. Hatton, and C. Mangano, "Direct metal laser

- sintering titanium dental implants: A review of the current literature," *Int. J. Biomater.*, vol. 2014, 2014.
- [34] S. Ferraris, A. Venturello, M. Miola, A. Cochis, L. Rimondini, and S. Spriano, "Antibacterial and bioactive nanostructured titanium surfaces for bone integration," *Appl. Surf. Sci.*, vol. 311, pp. 279–291, 2014.
- [35] R. A. Gittens, L. Scheideler, F. Rupp, S. L. Hyzy, J. Geis-Gerstorfer, Z. Schwartz, and B. D. Boyan, "A review on the wettability of dental implant surfaces II: Biological and clinical aspects," *Acta Biomater.*, vol. 10, no. 7, pp. 2907–2918, 2014.
- [36] J. I. Rosales-Leal, M. A. Rodr??guez-Valverde, G. Mazzaglia, P. J. Ram??n-Torregrosa, L. D??az-Rodr??guez, O. Garc??a-Mart??nez, M. Vallecillo-Capilla, C. Ruiz, and M. A. Cabrerizo-V??lchez, "Effect of roughness, wettability and morphology of engineered titanium surfaces on osteoblast-like cell adhesion," *Colloids Surfaces A Physicochem. Eng. Asp.*, vol. 365, no. 1–3, pp. 222–229, 2010.
- [37] J. Hu, Z. Wang, T. Guan, Y. Gao, X. Lv, X. Lin, C. yin Tang, and B. Gao, "In situ synthesis and fabrication of tricalcium phosphate bioceramic coating on commercially pure titanium by laser rapid forming," *Surf. Coatings Technol.*, vol. 204, no. 23, pp. 3833–3837, 2010.
- [38] G. Schmalz and D. Arenholt-bindslev, "Biocompatibility of Dental Materials," vol. 51, pp. 747–760, 2007.
- [39] D. W. Grainger, *The Williams dictionary of biomaterials*, vol. 2, no. 3. Liverpool: Liverpool University Press, 1999.
- [40] R. L. Sakaguchi and J. M. Powers, *Craig's Restorative Dental Materials*. Philadelphia: Elsevier, 2012.
- [41] "Biological evaluation of medical devices - Part 1: Evaluation and testing within a risk management process," *ISO 10993-1*, 2009.
- [42] B. Uzer, S. M. Toker, A. Cingoz, T. Bagci-onder, G. Gerstein, and H. J. Maier, "An exploration of plastic deformation dependence of cell viability and adhesion in metallic implant materials," *J. Mech. Behav. Biomed. Mater.*, vol. 60, pp. 177–186, 2016.
- [43] J. Chen, Q. Zhang, Q. Li, S. Fu, and J. Wang, "Corrosion and tribocorrosion behaviors of AISI 316 stainless steel and Ti6Al4V alloys in artificial seawater," vol. 24, pp. 1022–1031, 2014.
- [44] Y. Li, C. Yang, H. Zhao, S. Qu, X. Li, and Y. Li, "New Developments of Ti-Based Alloys for Biomedical Applications," pp. 1709–1800, 2014.
- [45] Shammy Raj, "Processing and Characterization of Titanium-Hydroxyapatite Metal Matrix Composite for Biomedical Applications," National Institute of Technology Rourkela, 2013.
- [46] G. F. J.P. Simon, "An Overview of Implant Materials," *Acta Orthop. Belg.*, vol. 57, no. 1, 1991.
- [47] M. Niinomi, M. Nakai, and J. Hieda, "Development of new metallic alloys for biomedical applications," *Acta Biomater.*, vol. 8, no. 11, pp. 3888–3903, 2012.
- [48] M. Sampaio, "Wear of PEEK / Ti6Al4V systems under micro-abrasion and linear sliding conditions," University of Minho, 2015.
- [49] F. H. Jones, "Teeth and bones : applications of surface science to dental materials and related biomaterials," *Surf. Sci. Rep.*, vol. 42, pp. 75–205, 2001.
- [50] M. Souza, C M;Tajiri, Henrique A; Morsch, Carolina S; Buciumeanu, "Tribocorrosion Behavior of Ti6Al4V Coated with a Bio-absorbable Polymer for Biomedical Applications," *J. Bio- Tribo-corrosion*, vol. 27, no.

- 1, pp. 1–6, 2015.
- [51] M. Sampaio, M. Buciumeanu, B. Henriques, F. S. Silva, J. C. M. Souza, and J. R. Gomes, “Tribocorrosion behavior of veneering biomedical PEEK to Ti6Al4V structures,” *J. Mech. Behav. Biomed. Mater.*, vol. 54, pp. 123–130, 2016.
- [52] A. Arifin, A. B. Sulong, N. Muhamad, J. Syarif, and M. I. Ramli, “Material processing of hydroxyapatite and titanium alloy ( HA / Ti ) composite as implant materials using powder metallurgy : A review,” *Mater. Des.*, vol. 55, pp. 165–175, 2014.
- [53] R. Osman and M. Swain, “A Critical Review of Dental Implant Materials with an Emphasis on Titanium versus Zirconia,” *Materials (Basel)*, vol. 8, no. 3, pp. 932–958, 2015.
- [54] M. Özcan and C. Hämmerle, “Titanium as a reconstruction and implant material in dentistry: Advantages and pitfalls,” *Materials (Basel)*, vol. 5, no. 9, pp. 1528–1545, 2012.
- [55] Y. Li, C. Yang, H. Zhao, S. Qu, X. Li, and Y. Li, “New developments of ti-based alloys for biomedical applications,” *Materials (Basel)*, vol. 7, no. 3, pp. 1709–1800, 2014.
- [56] C. Oldani and A. Dominguez, “Titanium as a Biomaterial for Implants,” *Intechopen.Com*, pp. 149– 162, 2012.
- [57] B. Ali, E. B. Ould Chikh, H. M. Meddah, A. Merdji, and B. abbes Bachir Bouiadjra, “Effects of overloading in mastication on the mechanical behaviour of dental implants,” *Mater. Des.*, vol. 47, pp. 210–217, 2013.
- [58] J. E. Ratner, Dubby D.; Hoffman, Allan S.; Schoen, Frederick J. Schoen; Lemons, *Biomaterials Science- An Introduction to Materials in Medicine*. Academic Press, 1996.
- [59] C. Massaro, P. Rotolo, F. De Riccardis, E. Milella, A. Napoli, M. Wieland, M. Textor, N. D. Spencer, and D. M. Brunette, “Comparative investigation of the surface properties of commercial titanium dental implants. Part I: Chemical composition,” *J. Mater. Sci. Mater. Med.*, vol. 13, pp. 535–548, 2002.
- [60] J. C. M. Souza, S. L. Barbosa, E. Ariza, J. P. Celis, and L. A. Rocha, “Simultaneous degradation by corrosion and wear of titanium in artificial saliva containing fluorides,” *Wear*, vol. 292–293, pp. 82–88, 2012.
- [61] M. Sampaio, M. Buciumeanu, B. Henriques, F. S. Silva, J. C. M. Souza, and J. R. Gomes, “Tribocorrosion behavior of veneering biomedical PEEK to Ti6Al4V structures,” *J. Mech. Behav. Biomed. Mater.*, vol. 54, pp. 123–130, 2016.
- [62] Z. Özkurt and E. Kazazoğlu, “Zirconia dental implants: a literature review.,” *J. Oral Implantol.*, vol. 37, no. 3, pp. 367–76, 2011.
- [63] M. Santin and G. J. Phillips, *Biomimetic, Bioresponsive, and Bioactive Materials - An introduction to Integrating Materials with Tissues*. Brighton: John Wiley & Sons, 2012.
- [64] R. Depprich, H. Zipprich, M. Ommerborn, E. Mahn, L. Lammers, J. Handschel, C. Naujoks, H.-P. Wiesmann, N. R. Kübler, and U. Meyer, “Osseointegration of zirconia implants: an SEM observation of the bone-implant interface.,” *Head Face Med.*, vol. 4, p. 25, 2008.
- [65] M. Moraes and C. Elias, “Mechanical properties of alumina-zirconia composites for ceramic abutments,” *Mater. ...*, vol. 7, no. 4, pp. 643–649, 2004.
- [66] P. Sevilla, C. Sandino, M. Arciniegas, J. Mart??nez-Gomis, M. Peraire, and F. J. Gil, “Evaluating

- mechanical properties and degradation of YTZP dental implants," *Mater. Sci. Eng. C*, vol. 30, no. 1, pp. 14–19, 2010.
- [67] R. Depprich, H. Zipprich, M. Ommerborn, C. Naujoks, H.-P. Wiesmann, S. Kiattavorncharoen, H.-C. Lauer, U. Meyer, N. R. Kübler, and J. Handschel, "Osseointegration of zirconia implants compared with titanium: an in vivo study.," *Head Face Med.*, vol. 4, no. 1, p. 30, 2008.
- [68] C. Bergemann, K. Duske, J. B. Nebe, A. Schöne, U. Bulnheim, H. Seitz, and J. Fischer, "Microstructured zirconia surfaces modulate osteogenic marker genes in human primary osteoblasts," *J. Mater. Sci. Mater. Med.*, vol. 26, no. 1, p. 5350, 2015.
- [69] P. Assal, "The Osseointegration of Zirconia Dental Implants," *Res. Sci.*, vol. 123, pp. 644–654, 2013.
- [70] C. Sanon, J. Chevalier, T. Douillard, M. Cattani-Lorente, S. S. Scherrer, and L. Gremillard, "A new testing protocol for zirconia dental implants.," *Dent. Mater.*, vol. 5510, no. 1, pp. 1–11, 2014.
- [71] R. L. Sakaguchi and J. M. Powers, *Craig's Restorative Dental Materials*, vol. 71, no. 2. Philadelphia: Elsevier, 1977.
- [72] E. Camposilvan, Q. Flamant, and M. Anglada, "Surface roughened zirconia: Towards hydrothermal stability," *J. Mech. Behav. Biomed. Mater.*, vol. 47, pp. 95–106, 2015.
- [73] J. Chevalier, "What future for zirconia as a biomaterial?," *Biomaterials*, vol. 27, no. 4, pp. 535–543, 2006.
- [74] W. T. Lee, J. Y. Koak, Y. J. Lim, S. K. Kim, H. B. Kwon, and M. J. Kim, "Stress shielding and fatigue limits of poly-ether-ether-ketone dental implants," *J. Biomed. Mater. Res. - Part B Appl. Biomater.*, vol. 100 B, no. 4, pp. 1044–1052, 2012.
- [75] A. R. Rashidi, M. U. Wahit, M. R. Abdullah, and M. R. Abdul Kadir, "The Effect of Silane on the Biomechanical Properties of PEEK/HA Composite," *Adv. Mater. Res.*, vol. 1125, no. February 2016, pp. 426–431, 2015.
- [76] J. Simsiriwong, R. Shrestha, N. Shamsaei, M. Lugo, and R. D. Moser, "Effects of microstructural inclusions on fatigue life of polyether ether ketone (PEEK)," *J. Mech. Behav. Biomed. Mater.*, vol. 51, pp. 388–397, 2015.
- [77] K. B. Sagomonyants, M. L. Jarman-Smith, J. N. Devine, M. S. Aronow, and G. A. Gronowicz, "The in vitro response of human osteoblasts to polyetheretherketone (PEEK) substrates compared to commercially pure titanium," *Biomaterials*, vol. 29, no. 11, pp. 1563–1572, 2008.
- [78] S. M. Kurtz, *PEEK Biomaterials Handbook*, vol. 53, no. 9. Oxford: Elsevier, 2012.
- [79] F. Chen, H. Ou, B. Lu, and H. Long, "A constitutive model of polyether-ether-ketone (PEEK)," *J. Mech. Behav. Biomed. Mater.*, vol. 53, pp. 427–433, 2016.
- [80] A. D. Schwitalla, T. Spintig, I. Kallage, and W. D. Müller, "Flexural behavior of PEEK materials for dental application," *Dent. Mater.*, vol. 31, no. 11, pp. 1377–1384, 2015.
- [81] S. M. Kurtz and J. N. Devine, "PEEK Biomaterials in Trauma, Orthopedic, and Spinal Implants," *Biomaterials*, vol. 28, no. 32, pp. 4845–4869, 2007.
- [82] S. Najeeb, M. S. Zafar, Z. Khurshid, and F. Siddiqui, "Applications of polyetheretherketone (PEEK) in oral implantology and prosthodontics," *J. Prosthodont. Res.*, vol. 60, no. 1, pp. 12–19, 2016.

- [83] A. D. Schwitalla, M. Abou-Emara, T. Spintig, J. Lackmann, and W. D. Müller, "Finite element analysis of the biomechanical effects of PEEK dental implants on the peri-implant bone," *J. Biomech.*, vol. 48, no. 1, pp. 1–7, 2015.
- [84] D. Briem, S. Strametz, K. Schröder, N. M. Meenen, W. Lehmann, W. Linhart, A. Ohl, and J. M. Rueger, "Response of primary fibroblasts and osteoblasts to plasma treated polyetheretherketone (PEEK) surfaces," *J. Mater. Sci. Mater. Med.*, vol. 16, no. 7, pp. 671–677, 2005.
- [85] A. H. C. Poulsson, D. Eglin, S. Zeiter, K. Camenisch, C. Sprecher, Y. Agarwal, D. Nehrbass, J. Wilson, and R. G. Richards, "Osseointegration of machined, injection moulded and oxygen plasma modified PEEK implants in a sheep model," *Biomaterials*, vol. 35, no. 12, pp. 3717–3728, 2014.
- [86] D. Garcia-Gonzalez, M. Rodriguez-Millan, A. Rusinek, and A. Arias, "Low temperature effect on impact energy absorption capability of PEEK composites," *Compos. Struct.*, vol. 134, pp. 440–449, 2015.
- [87] J. Black, *Biological Performance of Materials - Fundamentals of Biocompatibility*, vol. 53, no. 9. Taylor & Francis, 2006.
- [88] Y. Deng, X. Liu, A. Xu, L. Wang, Z. Luo, Y. Zheng, F. Deng, J. Wei, Z. Tang, and S. Wei, "Effect of surface roughness on osteogenesis in vitro and osseointegration in vivo of carbon fiber-reinforced polyetheretherketone– Nanohydroxyapatite composite," *Int. J. Nanomedicine*, vol. 10, pp. 1425–1447, 2015.
- [89] L. Wang, L. Weng, S. Song, Z. Zhang, S. Tian, and R. Ma, "Characterization of polyetheretherketone-hydroxyapatite nanocomposite materials," *Mater. Sci. Eng. A*, vol. 528, no. 10–11, pp. 3689–3696, 2011.
- [90] C. Chu, X. Xue, J. Zhu, and Z. Yin, "Fabrication and characterization of titanium-matrix composite with 20 vol% hydroxyapatite for use as heavy load-bearing hard tissue replacement," *J. Mater. Sci. Mater. Med.*, vol. 17, no. 3, pp. 245–251, 2006.
- [91] D. Shi, *Introduction to Biomaterials*. China: Tsinghua University Press, 2006.
- [92] X. Zhao, J. Courtney, and H. Qian, *Bioactive Materials in Medicine*. Woodhead Publishing Limited, 2011.
- [93] C. B. Carter and M. G. Norton, *Ceramic Materials Science and Engineering*. Springer, 2007.
- [94] R. a Horowitz, D. D. S. Ziv, M. Dmd, C. Foitzik, H. Prasad, M. D. T. M. Rohrer, and M. S. A. Palti, "β-Tricalcium Phosphate as Bone Substitute Material : Properties and Clinical Applications," *Int. J. Dent. Implant. Biomater.*, vol. 1, no. 2, pp. 2–11, 2009.
- [95] S. C. V. Rodrigues, "Preparation of Collagen-Hydroxyapatite Biocomposite Scaffolds by Cryogelation Method for Tissue Engineering Applications," Universidade do Porto, 2011.
- [96] C. F. Koch, S. Johnson, D. Kumar, M. Jelinek, D. B. Chrisey, A. Doraiswamy, C. Jin, R. J. Narayan, and I. N. Mihailescu, "Pulsed laser deposition of hydroxyapatite thin films," *Mater. Sci. Eng. C*, vol. 27, no. 3, pp. 484–494, 2007.
- [97] D. Suárez-González, J. S. Lee, S. K. Lan Levengood, R. Vanderby, and W. L. Murphy, "Mineral coatings modulate β-TCP stability and enable growth factor binding and release," *Acta Biomater.*, vol. 8, no. 3, pp. 1117–1124, 2012.
- [98] A. C. Queiroz, J. D. Santos, R. Vilar, S. Eugênio, and F. J. Monteiro, "Laser surface modification of hydroxyapatite and glass-reinforced hydroxyapatite," *Biomaterials*, vol. 25, no. 19, pp. 4607–4614, 2004.

- [99] G. Grandi, C. Heitz, L. A. Dos Santos, M. L. Silva, M. Sant'Ana Filho, R. M. Pagnocelli, and D. N. Silva, "Comparative histomorphometric analysis between  $\alpha$ -Tcp cement and  $\beta$ -Tcp/Ha granules in the bone repair of rat calvaria," *Mater. Res.*, vol. 14, no. 1, pp. 11–16, 2011.
- [100] D. Smolen, T. Chudoba, I. Malka, A. Kedzierska, W. Lojkowski, W. Swieszkowski, K. J. Kurzydowski, M. Kolodziejczyk-Mierzynska, and M. Lewandowska-Szumiel, "Highly biocompatible, nanocrystalline hydroxyapatite synthesized in a solvothermal process driven by high energy density microwave radiation," *Int. J. Nanomedicine*, vol. 8, pp. 653–668, 2013.
- [101] M. A. Cunha, "Síntese e caracterização de Hidroxiapatita nanoestruturada obtidos por aspersão de solução em chama," Universidade Federal do Rio Grande do Sul, 2010.
- [102] A. C. F. M. Costa, M. G. Lima, L. H. M. A. Lima, V. V. Cordeiro, and K. M. S. Viana, "Hidroxiapatita: Obtenção, caracterização e aplicações," *Rev. Eletronica Mater. e Process.*, vol. 4, no. 3, pp. 29–38, 2009.
- [103] X. Yin, M. J. Stott, and A. Rubio, " $\alpha$ - and  $\beta$ -tricalcium phosphate: A density functional study," *Phys. Rev. B*, vol. 68, no. 20, p. 205205, 2003.
- [104] M. Yashima, A. Sakai, T. Kamiyama, and A. Hoshikawa, "Crystal structure analysis of  $\beta$ -tricalcium phosphate  $\text{Ca}_3(\text{PO}_4)_2$  by neutron powder diffraction," *J. Solid State Chem.*, vol. 175, no. 2, pp. 272–277, 2003.
- [105] M. N. A. Salimi, "Systematic investigations of calcium phosphates produced by wet chemistry method and supercritical processing techniques," University of Birmingham, 2013.
- [106] C. Wang, R. Quan, H. Wang, X. Wei, and Z. Zhao, "Investigation on high-temperature decomposition characteristic of hydroxyapatite," *2009 IEEE 3rd Int. Conf. Nano/Molecular Med. Eng. NANOMED 2009*, pp. 65–70, 2009.
- [107] G. Muralithran and S. Ramesh, "The effects of sintering temperature on the properties of hydroxyapatite," *Ceram. Int.*, vol. 26, pp. 221–230, 2000.
- [108] H. Khandelwal, G. Singh, K. Agrawal, S. Prakash, and R. D. Agarwal, "Characterization of hydroxyapatite coating by pulse laser deposition technique on stainless steel 316 L by varying laser energy," *Appl. Surf. Sci.*, vol. 265, pp. 30–35, 2013.
- [109] O. Blind, L. H. Klein, B. Dailey, and L. Jordan, "Characterization of hydroxyapatite films obtained by pulsed-laser deposition on Ti and Ti-6AL-4v substrates," *Dent. Mater.*, vol. 21, no. 11, pp. 1017–1024, 2005.
- [110] Z. Evis and A. E. R. H. Doremus, "Hot-pressed hydroxylapatite / monoclinic zirconia composites with improved mechanical properties," *J. Mater. Sci.*, vol. 42, pp. 2426–2431, 2007.
- [111] W. Zheng, "Preparation and Characterisation of Tricalcium Phosphate Scaffolds With Tunnel-Like Macro-Pores for Bone Tissue," Queensland University of Technology, 2011.
- [112] F. C. Campbell, *Structural Composite Materials*. ASM International, 2010.
- [113] X. Zhou, "Hydroxyapatite/Titanium Composite Coating For Biomedical Application," 2012.
- [114] E. Karamian, A. Khandan, M. R. Kalantar Motamedi, and H. Mirmohammadi, "Surface characteristics and bioactivity of a novel natural HA/zircon nanocomposite coated on dental implants," *Biomed Res. Int.*, vol. 2014, 2014.

- [115] A. Kuwabara, N. Hori, T. Sawada, N. Hoshi, A. Watazu, and K. Kimoto, "Enhanced biological responses of a hydroxyapatite/TiO<sub>2</sub> hybrid structure when surface electric charge is controlled using radiofrequency sputtering," *Dent. Mater. J.*, vol. 31, no. 3, pp. 368–376, 2012.
- [116] S. Ligot, T. Godfroid, D. Music, E. Bousser, J. M. Schneider, and R. Snyders, "Tantalum-doped hydroxyapatite thin films: Synthesis and characterization," *Acta Mater.*, vol. 60, no. 8, pp. 3435–3443, 2012.
- [117] S. Gräf and F. a Müller, "CO<sub>2</sub>-Laser-Assisted Surface Modification of Titanium Alloys for Biomedical Applications," vol. 286, pp. 281–286, 2014.
- [118] Y. C. Tsui, C. Doyle, and T. W. Clyne, "Plasma sprayed hydroxyapatite coatings on titanium substrates. Part 1: Mechanical properties and residual stress levels," *Biomaterials*, vol. 19, no. 22, pp. 2015–2029, 1998.
- [119] L. Le Guéhennec, A. Soueidan, P. Layrolle, and Y. Amouriq, "Surface treatments of titanium dental implants for rapid osseointegration," *Dent. Mater.*, vol. 23, pp. 844–854, 2007.
- [120] S. Allegrini, E. Rumpel, E. Kauschke, J. Fanghanel, and B. König, "Hydroxyapatite grafting promotes new bone formation and osseointegration of smooth titanium implants," *Ann. Anat.*, vol. 188, no. 2, pp. 143–151, 2006.
- [121] P.-C. Chang, N. P. Lang, and W. V. Giannobile, "Evaluation of Functional Dynamics during Osseointegration and Regeneration Associated with Oral Implants: A Review," *Clin. Oral Implants Res.*, vol. 21, no. 1, pp. 1–12, 2011.
- [122] Y. In-Sung, M. Seung-Ki, and A. Youngbai, "Influence of Bioactive Material Coating of Ti Dental Implant Surfaces on Early Healing and Osseointegration of Bone," *J. Korean Phys. Soc.*, vol. 57, no. 61, p. 1717, 2010.
- [123] G. Miranda, A. Araújo, F. Bartolomeu, M. Buciumeanu, O. Carvalho, J. C. M. Souza, F. S. Silva, and B. Henriques, "Design of Ti6Al4V-HA composites produced by hot pressing for biomedical applications," *Mater. Des.*, vol. 108, pp. 488–493, 2016.
- [124] A. R. Ribeiro, F. Oliveira, L. C. Boldrini, P. E. Leite, P. Falagan-Lotsch, A. B. R. Linhares, W. F. Zambuzzi, B. Fragneaud, A. P. C. Campos, C. P. Gouvêa, B. S. Archanjo, C. A. Achete, E. Marcantonio, L. A. Rocha, and J. M. Granjeiro, "Micro-arc oxidation as a tool to develop multifunctional calcium-rich surfaces for dental implant applications.," *Mater. Sci. Eng. C. Mater. Biol. Appl.*, vol. 54, pp. 196–206, 2015.
- [125] R. M. German, *Powder Metallurgy & Particulate Materials Processing*, Metal Powd. Princeton, 2005.
- [126] G. S. Upadhyaya, *Powder Metallurgy Technology*. Cambridge International Science Publishing, 1997.
- [127] P. Ramakrishnan, "History of powder metallurgy," in *Indian journal of history of science*, 1983, vol. 18, no. 1, pp. 109–114.
- [128] G. Miranda, "Development of aluminum based composites by pressure-assisted sintering," Universidade do Minho, 2015.
- [129] A. Bose and W. B. Eisen, *Hot Consolidation Of Powders And Particulates*. Metal Powder Industry, 2003.
- [130] F. Thummler and R. Oberacker, *Introduction to Powder Metallurgy*, vol. 34, no. 3. The Institute of Materials, 1995.



- [131] A. Shahrjerdi, F. Mustapha, M. Bayat, S. M. Sapuan, and D. L. A. Majid, "Fabrication of functionally graded Hydroxyapatite- Titanium by applying optimal sintering procedure and powder metallurgy," *Int. J. Phys. Sci.*, vol. 6, no. 9, pp. 2258–2267, 2011.
- [132] B. Henriques, S. Gonçalves, D. Soares, and F. S. Silva, "Shear bond strength comparison between conventional porcelain fused to metal and new functionally graded dental restorations after thermal-mechanical cycling," *J. Mech. Behav. Biomed. Mater.*, vol. 13, pp. 194–205, 2012.
- [133] O. Carvalho, G. Miranda, D. Soares, and F. S. Silva, "Carbon nanotube dispersion in aluminum matrix composites – quantification and influence on strength," *Mech. Adv. Mater. Struct.*, vol. 23, no. 1, pp. 66–73, 2016.
- [134] O. Carvalho, M. Buciumeanu, D. Soares, F. S. Silva, and G. Miranda, "Evaluation of CNT Dispersion Methodology Effect on Mechanical Properties of an AlSi Composite," *Journal of Materials Engineering and Performance*, vol. 24, no. 6. pp. 2535–2545, 2015.
- [135] J. Fruhstorfer, S. Schaffner, and C. G. Aneziris, "Dry ball mixing and deagglomeration of alumina and zirconia composite fine powders using a bimodal ball size distribution," *Ceram. Int.*, vol. 40, no. 9 PART B, pp. 15293–15302, 2014.
- [136] Z. Y. Liu, S. J. Xu, B. L. Xiao, P. Xue, W. G. Wang, and Z. Y. Ma, "Effect of ball-milling time on mechanical properties of carbon nanotubes reinforced aluminum matrix composites," *Compos. Part A Appl. Sci. Manuf.*, vol. 43, no. 12, pp. 2161–2168, 2012.
- [137] P. C. Ma, N. a. Siddiqui, G. Marom, and J. K. Kim, "Dispersion and functionalization of carbon nanotubes for polymer-based nanocomposites: A review," *Compos. Part A Appl. Sci. Manuf.*, vol. 41, no. 10, pp. 1345–1367, 2010.
- [138] T. Hielscher, "Ultrasonic Production of Nano-Size Dispersions and Emulsions," *Ens'05*, no. December, pp. 14–16, 2005.
- [139] V. S. Nguyen, D. Rouxel, R. Hadji, B. Vincent, and Y. Fort, "Effect of ultrasonication and dispersion stability on the cluster size of alumina nanoscale particles in aqueous solutions," *Ultrason. Sonochem.*, vol. 18, no. 1, pp. 382–388, 2011.
- [140] F. Bartolomeu, M. Buciumeanu, E. Pinto, N. Alves, F. S. Silva, O. Carvalho, and G. Miranda, "Ti6Al4V biomedical alloy wear behavior - a comparison between selective laser melting, hot pressing and conventional casting," 2016.
- [141] G. Bernard-Granger, A. Addad, G. Fantozzi, G. Bonnefont, C. Guizard, and D. Vernat, "Spark plasma sintering of a commercially available granulated zirconia powder: Comparison with hot-pressing," *Acta Mater.*, vol. 58, no. 9, pp. 3390–3399, 2010.
- [142] J. Chevalier, B. Cales, and J. M. Drouin, "Low-Temperature Aging of Y-TZP Ceramics," *J. Am. Ceram. Soc.*, vol. 82, no. 8, pp. 2150–2154, 1999.
- [143] S. Brundle, S. Richard; Evans, Charles A.Jr.; Wilson, *Encyclopedia of Materials Characterization*. 1992.
- [144] ASM International Handbook Committee, "ASM Handbook: Materials Characterization," vol. 10, p. 1310, 1998.
- [145] S. S. Da Rocha, G. L. Adabo, G. E. P. Henriques, and M. A. D. A. Nóbilo, "Vickers hardness of cast commercially pure titanium and Ti-6Al-4V alloy submitted to heat treatments," *Braz. Dent. J.*, vol. 17, no. 2, pp. 126–129, 2006.

- [146] T. Palathai, J. Tharajak, and N. Sombatsompop, "Hardness, adhesion index and microstructure of PEEK coating on Al or Fe substrate by LVOF flame spray," *Mater. Sci. Eng. A*, vol. 485, no. 1–2, pp. 66–73, 2008.
- [147] L. Galea, M. Bohner, J. Thuering, N. Doebelin, C. G. Aneziris, and T. Graule, "Control of the size, shape and composition of highly uniform, non-agglomerated, sub-micrometer  $\beta$ -tricalcium phosphate and dicalcium phosphate platelets," *Biomaterials*, vol. 34, no. 27, pp. 6388–6401, 2013.
- [148] Y. Yang, K. H. Kim, C. M. Agrawal, and J. L. Ong, "Interaction of hydroxyapatite-titanium at elevated temperature in vacuum environment," *Biomaterials*, vol. 25, no. 15, pp. 2927–2932, 2004.
- [149] A. Arifin, A. B. Sulong, N. Muhamad, and S. Selatan, "Characterization of hydroxyapatite/Ti6Al4V composite powder under various sintering temperature," *J. Teknol. (Sciences Eng.)*, vol. 75, no. 7, pp. 27–31, 2015.
- [150] C. J. Liao, F. H. Lin, K. S. Chen, and J. S. Sun, "Thermal decomposition and reconstitution of hydroxyapatite in air atmosphere," *Biomaterials*, vol. 20, no. 19, pp. 1807–1813, 1999.
- [151] W.-G. Kim and H.-C. Choe, "Surface characteristics of hydroxyapatite/titanium composite layer on the Ti-35Ta-xZr surface by RF and DC sputtering," *Thin Solid Films*, vol. 519, no. 20, pp. 7045–7049, Aug. 2011.
- [152] B. Henriques, D. Soares, and F. S. Silva, "Microstructure, hardness, corrosion resistance and porcelain shear bond strength comparison between cast and hot pressed CoCrMo alloy for metal-ceramic dental restorations," *J. Mech. Behav. Biomed. Mater.*, vol. 12, pp. 83–92, 2012.
- [153] G.-J. Oh, K.-D. Yun, K.-M. Lee, H.-P. Lim, and S.-W. Park, "Sintering behavior and mechanical properties of zirconia compacts fabricated by uniaxial press forming," *J. Adv. Prosthodont.*, vol. 2, no. 3, pp. 81–7, 2010.
- [154] R. Ma, L. Fang, Z. Luo, R. Zheng, S. Song, L. Weng, and J. Lei, "Fabrication and characterization of modified-hydroxyapatite/polyetheretherketone coating materials," *Appl. Surf. Sci.*, vol. 314, pp. 341–347, 2014.
- [155] E. Chang, W. J. Chang, B. C. Wang, and C. Y. Yang, "Plasma spraying of zirconia-reinforced hydroxyapatite composite coatings on titanium: part I: phase, microstructure and bonding strength.," *J. Mater. Sci. Mater. Med.*, vol. 8, no. 4, pp. 193–200, 1997.
- [156] L. Fu, K. Aik Khor, and J. Peng Lim, "The evaluation of powder processing on microstructure and mechanical properties of hydroxyapatite (HA)/yttria stabilized zirconia (YSZ) composite coatings," *Surf. Coatings Technol.*, vol. 140, no. 3, pp. 263–268, 2001.